Effects of Look-Ahead Time in a Haptic Shared Controller for Preview Tracking

MSc Thesis Report

J.E. Span

March 12, 2021

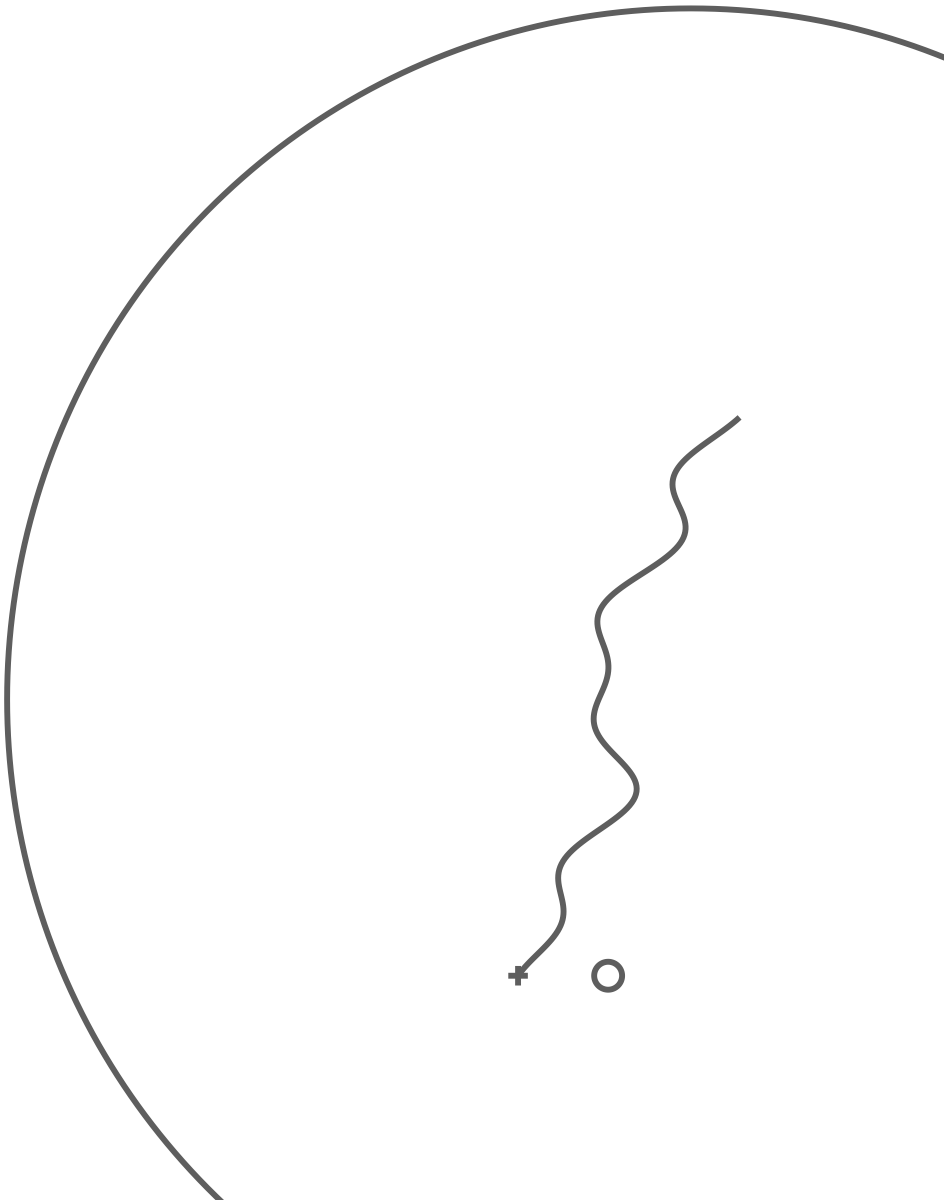

TU Delft

Effects of Look-Ahead Time in a Haptic Shared Controller for Preview Tracking

MSc Thesis Report

by

J.E Span

to obtain the degree of Master of Science

at the Delft University of Technology,

to be defended publicly on Thursday March 25, 2021 at 13:00

Student number:	4279603	
Project duration:	September 1, 2019 – March 25, 2021	
Thesis committee:	Prof. dr. ir. M. Mulder,	TU Delft, chair
	Dr. ir. D. M. Pool,	TU Delft, supervisor
	Dr. ir. K. van der El,	TU Delft, supervisor
	Dr. ir. M. M. van Paassen,	TU Delft, additional committee member
	Prof. dr. ir. D. A. Abbink,	examiner

An electronic version of this thesis is available at `http://repository.tudelft.nl/`.

TU Delft

Preface

This report contains my master thesis work, and includes the literature study and all results obtained in my research. It concludes my master Aerospace Engineering and with that almost eight years of studying at Delft University of Technology. For this research I investigated the effects of varying the look-ahead time of a haptic shared controller in a shared preview control task. I did a literature study, performed computer simulations and finally conducted a human-in-the-loop experiment with ten participants.

I could not have done this without the huge amount of help from several people. First of all, Daan, thank you for being my daily supervisor, for your valuable advice and expertise. Your experience in helping students shows, and somehow after each of our frequent meetings I was always more confident and happy about my work than I was beforehand. Kasper, as my second supervisor and expert on preview control you always added a lot of knowledge and good insights. I appreciate your involvement and help with my thesis project, thank your for that. Max, when I first came to your office in search of a graduation topic, I was overwhelmed by the multitude of ideas you had. Thank you for being so enthusiastic about your work, and being so involved with your students. René, of course your expertise could not be missed in a graduation project involving haptics. Thank you for your help in setting up my experiment, and for applying your Dueca wizardry to solve the problems I encountered.

It feels like ages ago, but at the start of my project, I was happy to share a room at the faculty with my fellow C&S students, appropriately named the 'Upper House'. Unfortunately we were not able to continue our daily coffee breaks, vrijmibo' and terrible jokes after having to work from home. Still, I would like to thank you for those first months, Simon, Peter, Michiel, Marc, Sven, Jesse, Jesse and Bas! On a similar note, back in the days of working at the faculty, we had the so-called 'preview' meetings with fellow students also working on the subject of preview control. Casper, Tjeerd, Pieter-Bas, it was nice to be able to share our work with each other and help each other during these meetings. Special thanks to Lorenzo, my housemate who is also passionately working on the topic of haptic shared control, thanks for all the interesting discussions and helping to set up my experiment.

Finally, to you, dear reader, thank you in advance for your interest in my thesis work. The first part is the scientific paper that resulted from the final phase of the project, which includes all results from the experiment and my main conclusions. The second part is the outcome of the preliminary phase of the project and includes the literature study, offline simulations and experiment proposal. In the back I included appendices with results from a pre-experiment, individual participants results, additional conflict analysis and the experiment briefing and consent forms.

Enjoy!

J.E Span
Delft, March 2021

Contents

I Scientific Paper **1**

II Preliminary Thesis Report **17**

1 Introduction **19**
1.1 Research objective . . . 19
1.2 Thesis outline . . . 21

2 Manual Preview Control **23**
2.1 Compensatory Control . . . 23
2.2 Preview Control . . . 24
2.2.1 Early Preview Models . . . 25
2.2.2 Van der El Model . . . 25
2.2.3 Effect of varying preview time . . . 26
2.3 Conclusion . . . 27

3 Haptic Shared Control **29**
3.1 Sharing Control: Keeping the Human in the Loop . . . 29
3.2 Haptic Shared Controllers . . . 30
3.2.1 Meshed HSC . . . 30
3.2.2 Four-Design-Choices HSC . . . 31
3.2.3 Integration of the Van der El Model . . . 32
3.3 Conclusion . . . 33

4 Offline Simulations **35**
4.1 Setup . . . 35
4.1.1 Control Task . . . 35
4.1.2 Human Operator Model . . . 36
4.1.3 Haptic Shared Controller . . . 37
4.2 Method . . . 38
4.3 Results: Meshed HSC . . . 39
4.3.1 HO and HSC solo performance . . . 39
4.3.2 Meshed HSC Simulation I: Varying $\tau_{f,HSC}$ . . . 40
4.3.3 Meshed HSC Simulation II: Varying $\tau_{f,HO}$ . . . 41
4.4 Results: FDC-HSC . . . 42
4.4.1 Tuning SoHF and LoHS gains . . . 42
4.4.2 FDC-HSC Simulation I: Varying $\tau_{f,HSC}$ . . . 43
4.4.3 FDC-HSC Simulation II: Varying $\tau_{f,HO}$ . . . 44
4.5 Discussion . . . 46
4.5.1 Effect of varying look-ahead time . . . 46
4.5.2 Comparison of Meshed HSC and FDC-HSC . . . 47
4.6 Conclusions . . . 48

5 Experiment Proposal **49**
5.1 Control Task . . . 49
5.2 Apparatus . . . 49
5.3 Experiment Design . . . 50

5.4 Metrics . . . 50
5.5 Hypotheses . . . 51

Bibliography **53**

A Pre-Experiment Results **57**
A.1 Conditions . . . 57
A.2 Experiment Design . . . 57
A.3 Results . . . 58
A.3.1 Measured Data . . . 58
A.3.2 Van der Laan questionnaire . . . 59
A.3.3 Discussion . . . 60

III Paper Appendices **61**

B Individual Experiment Results **63**
B.1 Subject 1 . . . 64
B.2 Subject 2 . . . 65
B.3 Subject 3 . . . 66
B.4 Subject 4 . . . 67
B.5 Subject 5 . . . 68
B.6 Subject 6 . . . 69
B.7 Subject 7 . . . 70
B.8 Subject 8 . . . 71
B.9 Subject 9 . . . 72
B.10 Subject 10 . . . 73

C Conflict Analysis **75**

D Experiment Briefing and Consent Form **77**

E Van Der Laan Questionnaire **81**

List of Abbreviations

CE	Controlled Element
DI	Double Integrator
FDC	Four Design Choices
HC	Human Controller
HO	Human Operator
HSC	Haptic Shared Controller
LoHS	Level of Haptic Support
LoHA	Level of Haptic Authority
NMS	Neuromuscular System
SI	Single Integrator
SoHF	Strength of Haptic Feedback

List of Symbols

δ_R	Reference stick deflection [rad]
τ_n	Near viewpoint [s]
τ_f	Far viewpoint [s]
$\tau_{f,HO}$	Human look-ahead time [s]
$\tau_{f,HSC}$	Haptic look-ahead time [s]
e	Tracking error [cm]
e^*	Internal error [cm]
F_{HO}	HO stick force [N]
F_{HSC}	HSC stick force [N]
F_R	Reference force [N]
f_d	Disturbance signal [cm]
f_t	Target signal [cm]
$f^*_{t,f}$	Filtered far viewpoint [cm]
H_{CE}	Controlled element dynamics
H^*_e	Internal error response
H_{nms}	Neuromuscular response
H_{of}	Far viewpoint filter
K_{e^*}	Error gain [-]
n	Remnant signal [cm]
t	Time [s]
t_{LH}	Look-ahead time [s]
T_f	Far viewpoint time constant [s]
$T_{L,e}$	Lead time constant [s]
$T_{l,e}$	Lag time constant [s]
u	Stick deflection, control input [rad]
x	System output [cm]
x_R	Reference output [cm]

I

Scientific Paper

Effects of Look-Ahead Time in a Haptic Shared Controller for Preview Tracking

Joeri Span

***Abstract*—In haptic shared control (HSC), an alternative to full automation, a human operator (HO) performs a steering task while being assisted by continuous force feedback on the control device. Human-haptic conflict, caused by misalignment of intentions or different use of reference information, is a source of annoyance and controllers should be designed to eliminate it as much as possible. One way to influence how a haptic shared controller uses reference information is by adjusting the look-ahead time. This paper describes a human-in-the-loop experiment that was conducted to investigate the effects of varying the haptic look-ahead time in a shared-control preview tracking task. A haptic shared controller was designed according to the Four Design Choices philosophy that uses an internal HO model to provide a human-compatible reference. Results show that the applied HO stick torques become lower with respect to the HSC torques for larger haptic look-ahead times, which shows how the HSC has a higher share in the control task as the look-ahead time is high. Conflict calculations reveal a region around 0.7-0.8 s haptic look-ahead time where conflict is minimal, and no significant change in conflict occurs. Subjective ratings by the participants show a similar yet larger region, from 0.5 to 0.9 s, for which no significant difference in usefulness and satisfaction is perceived. Meanwhile, despite showing a strong 'exchange' of authority through human-haptic forces around a look-ahead time of 0.7 s, the error remains low, indicating how the HO adapts to changes in the haptic controller to keep the tracking error satisfactory. The results of this paper highlight the importance of properly tuning the haptic look-ahead time, while also revealing a 'region of acceptance' for which participants are unlikely to notice any change in the haptic shared controller.**

I. Introduction

HAPTIC shared control (HSC) is gaining interest as an alternative to full automation of control tasks such as driving a car [1], [2]. In haptic shared control, a driver, or human operator (HO), is in control of a vehicle while being assisted by force feedback through the steering wheel, provided by a haptic shared controller [3], [4]. As a result, the human and the automation system can continuously communicate both ways and correct each other, benefiting from the strengths of both the HO and the HSC. By keeping the human "in-the-loop", haptic shared control has the potential to eliminate issues that often arise when automating a control task [5]. These issues include loss of situation awareness, over-reliance on the automation system, and increased complexity of the system [6]. Moreover, in its current state, autonomous driving may not be able to fully replace manual driving due to technical, ethical, and legal reasons.

Due to the complex nature and unpredictability of human control behavior, designing a well-functioning HSC is not straightforward. Misalignment between the human's and HSC's intentions can cause conflicting torques, leading to annoyance and increased control effort [7]. Reduced user acceptance may in turn lead to the system being turned off by the user, eliminating the potential benefits in terms of safety. A framework proposed by Van Paassen et al. [8], named the *Four Design Choices Architecture* (FDCA), has been successful in reducing human-haptic conflict [9]. The FDCA philosophy offers a control architecture that is designed to reduce conflicts, by making four explicit design choices. The first is to synthesize a human-compatible reference (HCR) trajectory for the HSC. This trajectory is followed by the controller using two paths: a feedback path reducing the error between the system output and the HCR, characterized by the *strength of haptic feedback* (SoHF) and a feedforward path providing an anticipatory guidance torque, named the *level of haptic support* (LoHS). These two paths are added up to yield the total haptic torque, after which the resulting authority on the task is determined by the *level of haptic authority* (LoHA).

Of the four design choices, the HCR offers a way to incorporate explicit knowledge of human control behavior in the haptic controller, by using driver models to generate the reference trajectory. Control-theoretic HO models have been developed for target-following tasks, describing how humans use reference information to come up with the desired control action [10], [11]. A recent example of such a model is the novel human controller model for preview control by Van der El et al. [11], which is an extension to established quasi-linear HO models for compensatory control [12].

Van der El's HO model provides knowledge on what portion of previewed information is used by an HO. The model splits the response to the previewed target in a *near-viewpoint*, characterized by a high-frequency feedforward response, and a *far-viewpoint*, characterized by a low-frequency feedback response. The far-viewpoint response, considered to be the main response, describes how humans use the available preview information in their control strategy. It has been known from early research that increased preview time leads to better tracking performance [13], [14], and recent experiments extend this knowledge by showing how humans adjust their far-viewpoint [15].

When designing an FDCA-type haptic shared controller and using the preview control HO model to define the HCR, the far-viewpoint parameter (often referred to as *look-ahead time* when considering HSC) becomes a key parameter. It determines the controller's timing and accuracy. A controller with a long look-ahead time can anticipate the target better and act earlier, possibly incorporating corner-cutting, while a controller with a short look-ahead time has to resort to more aggressive control to follow the target. Therefore, a poorly

chosen look-ahead time will likely be a source for human-haptic conflict and knowledge on the effect of various look-ahead times is required.

The goal of this paper is to analyze how various look-ahead times in a haptic controller affect performance and conflict in a shared preview tracking task. An experiment was conducted, in which ten participants were asked to track a target on a display with 1 second of preview using a side stick with haptic force feedback. Over nine haptic conditions that varied the HSC look-ahead time, the sensitivity to small changes in look-ahead time is investigated. One of the used metrics is human-haptic conflict, which occurs when the inputs of the HO and the HSC are opposite. Furthermore, participants were asked to rate the haptic support system during the experiment. The results of the experiment can improve knowledge on tuning haptic look-ahead times to decrease conflict in HSC.

The outline of the paper is as follows. First, the steps and results of preliminary research involving simulations are discussed in Section II. This section gives a thorough explanation of the control task considered throughout this paper and in the experiment. Section III then describes the setup for the experiment, including the hypotheses that are partially based on the outcome of the simulations. Then, Section IV presents an overview of the experiment results. These results are discussed thoroughly in Section V, after which this paper is concluded in Section VI.

II. Simulations

In this paper, the shared control task is first simulated to gain an understanding of the interaction between HO and HSC. The simulation setup uses the task parameters that will be used in the human-in-the-loop experiment: the controlled element, forcing functions, and HSC are identical. To simulate the HO, the Van der El human operator model is used [11].

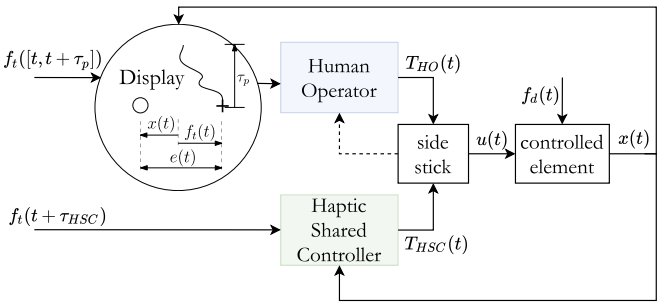

Fig. 1. The shared control task considered in this paper.

A. Control Task

Fig. 1 shows a block diagram of the control task. The HO performs the tracking task in a shared-control setting, together with the HSC. The forcing functions for the control task are two sum-of-sines, a target and a disturbance. The target $f_t(t)$ is tracked by the HO and the HSC, which both provide input torques to the side stick. The combined torques on the stick result in a control input $u(t)$ to the controlled element. The disturbance signal $f_d(t)$ is added to the controlled element output, making the task a target-following and disturbance-rejection task. The forcing functions are defined as the sums of 10 sinusoids, Eq. (1), with $A[i]$, $\omega[i]$ and $\phi[i]$ the amplitude, frequency and phase shift of the i^{th} frequency component, respectively. Both forcing functions have a bandwidth of approximately 1.5 rad/s [12], indicating that amplitudes of the sines with frequencies above 1.5 rad/s are attenuated with a factor 10. The forcing functions' spectra are shown in Fig. 2, the forcing function parameters are listed in Table I. Three realizations of the target function are shown, defined by different phase shifts, however, for the simulation, only the first realization is used. The standard deviation σ_{f_t} of the target function is 1.27 cm, the standard deviation σ_{f_d} of the disturbance function is 0.51 cm.

$$f_{t,d}(t) = \sum_{i=1}^{10} A_{t,d}[i] \sin\left(\omega_{t,d}[i]t + \phi_{t,d}[i]\right) \tag{1}$$

The controlled element is a single-integrator system expressed as $H_{CE}(j\omega) = K_{CE}/j\omega$, with a gain $K_{CE} = 1.5$. Inputs are given to the system by a side stick, included in the simulation, and modeled as H_{stick} (Eq. (2)). The stick is modeled as a mass-spring-damper system with inertia $I = 0.01$ kg/m^2, damping $b = 0.22$ Nms/rad, stiffness $k = 3.58$ Nm/rad, and stick gain $K_{stick} = 0.44$ cm/deg. The stick model describes the relation between input torques given by the HO and the HSC, T_{HO} and T_{HSC}, and the stick position which acts as the controlled element input $u(t)$.

$$H_{stick} = \frac{K_{stick}}{I(j\omega)^2 + bj\omega + k} \tag{2}$$

B. Human Operator model

The human operator in this control task is simulated as a quasi-linear controller: the responses to the target and system output are linear, and a randomly generated noise input is added to account for all non-linearities that characterize a human operator. The used model is by Van der El et al. [11] and predicts human tracking behavior in target-following tasks with preview information. A block diagram of the model is shown in Fig. 3. According to Van der El, the HO response to a previewed target $f_t([t, t+\tau_p])$ (with τ_p the preview time) can be characterized by a response function $H_{o_{f^*}}(j\omega)$ to a single *far-viewpoint* on the target, denoted τ_f. The transfer function $H_{o_{f^*}}(j\omega)$, shown in Eq. (3), is a low-pass filter with time constant $T_{l,f}$ and gain K_f. Subsequently, the filtered far-viewpoint $f^*_{t,f}(t)$ is used as the input to a compensatory control loop, where an 'internal' error $e^*(t)$ is minimized. Note that this is not the actual error between the target and the system output, but the error to a 'desired' path that ignores high frequencies of the target. The feedback control strategy that follows is essentially that of error-reducing compensatory control [12], where for a single integrator controlled element, the error response is described by a gain, K_{e^*}.

The physical limitations of the HO are modeled as a second-order neuromuscular system $H_{nms}(j\omega)$, shown in Eq. (4), and a pure time delay of τ_v seconds, $e^{-\tau_v j\omega}$. The output to the neuromuscular system is described in Van der El's model as

TABLE I
PARAMETERS FOR THE MULTISINE TARGET AND DISTURBANCE FUNCTIONS USED IN THE SIMULATIONS.

	target signal f_t						disturbance signal f_d			
i	k_t -	A_t cm	ω_t rad/s	$\phi_{t,1}$ rad	$\phi_{t,2}$ rad	$\phi_{t,3}$ rad	k_d -	A_d cm	ω_d rad/s	ϕ_d rad
1	3	0.731	0.157	4.488	4.578	1.620	4	0.292	0.209	0.241
2	5	0.731	0.262	5.699	2.459	5.502	7	0.292	0.367	1.669
3	8	0.731	0.419	1.373	0.980	4.688	9	0.292	0.471	1.899
4	11	0.731	0.576	5.472	0.889	1.675	13	0.292	0.681	1.295
5	19	0.731	0.995	1.331	5.683	2.283	22	0.292	1.152	3.982
6	29	0.731	1.518	5.257	2.214	4.867	31	0.292	1.623	4.496
7	47	0.073	2.461	5.399	1.002	5.342	51	0.029	2.670	3.365
8	77	0.073	4.032	3.289	5.478	4.198	79	0.029	4.136	0.469
9	143	0.073	7.488	2.999	5.050	1.738	147	0.029	7.697	0.964
10	263	0.073	13.77	5.591	4.613	1.349	267	0.029	13.98	4.296

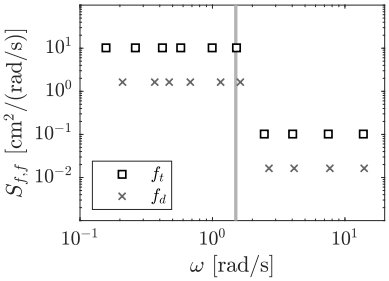

Fig. 2. Power spectra of target and disturbance

the control input $u(t)$ directly into the controlled element, meaning that the modeled dynamics include the physical stick as well. In the case of shared control, with both an HO and an HSC acting on the stick, we are interested in the torques. By passing the HO output $u(t)$ through an inverse stick model, H_{stick}^{-1} (see Fig. 3), we obtain the input torque T_{HO}.

The model parameters used for the simulated HO are displayed in Table II. These parameters are averaged fitted parameters from earlier human-in-the-loop experiments [15], making the HO model representative for real human control behavior in this type of control task. It was also found that above a certain *critical preview time*, humans on average no longer adjust their far-viewpoint τ_f. The far-viewpoint parameter shown in Table II is set to 0.6 s, which is the average critical preview time [15]. The other parameters correspond to realistic average control behavior with this far-viewpoint [15].

$$H_{o_f}(j\omega) = \frac{K_f}{1 + T_{l,f} j\omega} \tag{3}$$

$$H_{nms}(j\omega) = \frac{\omega_{nms}^2}{(j\omega)^2 + 2\xi_{nms}\omega_{nms} j\omega + \omega_{nms}^2} \tag{4}$$

Remnant noise is added to the HO input to simulate the stochastic human control behavior. The characteristics of this remnant noise are taken from earlier literature on similar preview control tasks [16]. According to this, remnant noise injected at the HO input can be modeled by applying a low-pass filter to a white noise source. For SI tasks, the filter has a break frequency $\omega_{b,n}$ of 3.5 rad/s. The noise gain is tuned such that the contribution of the noise to the total control input is given by $\sigma_{u_n}^2/\sigma_u^2 = 0.35$. Based on this, for remnant injected at the HO input torque, a noise gain K_n of 40 is used. In the simulations, 1,000 remnant realizations are used.

TABLE II
BASELINE MODEL PARAMETERS

τ_{HO} [s]	K_f [s]	$T_{l,f}$ [s]	K_{e^*} [-]	τ_v [s]	ω_{nms} [rad/s]	ξ_{nms} [-]	K_n [-]	$\omega_{b,n}$ [rad/s]
0.6	1.0	0.20	1.25	0.20	10.5	0.35	40	3.5

C. Haptic Shared Controller

In shared control, a haptic controller continuously exerts forces to the stick, providing guidance to the operator. The HSC considered in this paper implements the Four-Design-Choices Architecture (FDCA). In this controller, the reference (HCR) is provided by the Van der El HO model. The implementation of the FDC-HSC is shown in Fig. 4, and represents the haptic controller architecture for both the simulations and the experiment. The HCR, shown in the gray dashed area, simulates the HO model in tracking the target in a closed loop and provides a reference torque $T_R(t)$ and a reference path $x_R(t)$. The HCR model architecture is the same as used to simulate the HO, shown in Fig. 3. It includes a CE model, H_{ce}, in order to calculate the system output that is used as a reference path, $x_R(t)$. The HCR outputs do not depend on the outputs of the actual control task, but provide a desired input to the HSC, which consists of feedforward gain K_{LoHS} and feedback gain K_{SoHF}. The LoHS gain, K_{LoHS}, provides the direct feedthrough of the reference torque $T_R(t)$ to the stick, while the feedback gain K_{SoHF} acts on the error between the reference path $x_R(t)$ and the actual CE output $x(t)$.

The parameters for the FDC-HSC are the HO model parameters in the HCR and the gains K_{LoHS} and K_{SoHF}. The HCR parameters are chosen to be equal to the simulated HO, given in Table II. Thus, the assumption was made that the HSC uses fully accurate knowledge of the HO and that the HCR perfectly matches the HO. Also, by keeping all parameters constant, the effect of varying look-ahead time τ_{HSC}, the main interest in this research, can be isolated. This means the assumption is made that the HO does not adapt its control strategy under the influence of the HSC, even though this is to be expected in real-life situations. The LoHS and SoHF gains were chosen heuristically, setting the values such that the haptic guidance is felt sufficiently, but not considered annoying. The feedforward gain K_{LoHS} was then set to 0.6, meaning that 60% of the reference torque is provided by the HSC. The value was chosen such that the HSC does not execute the full control task. The feedback gain K_{SoHF} was set to 0.8, which was considered high enough to correct for control errors made by the HO. As mentioned earlier, the HO model parameters result in optimal performance with a look-ahead time of 0.6 seconds

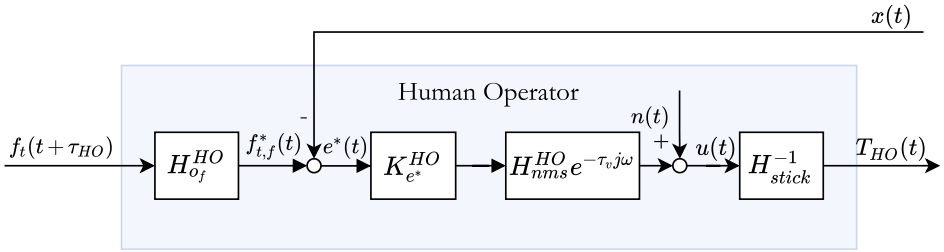

Fig. 3. The human operator model

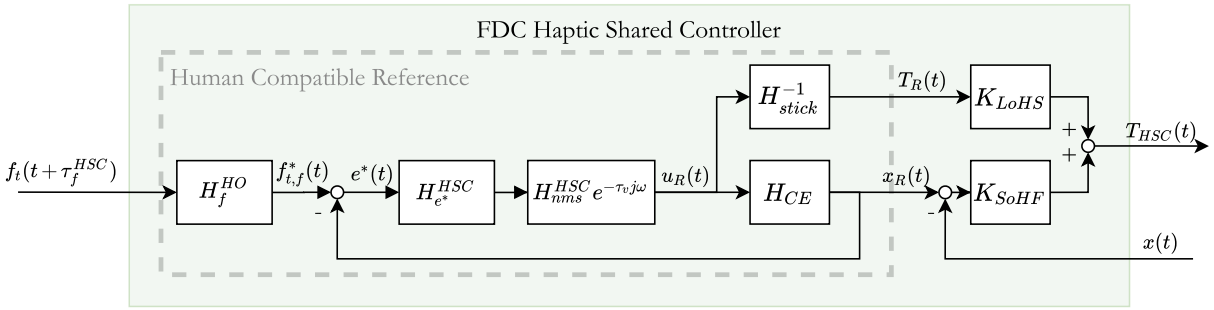

Fig. 4. The haptic shared controller

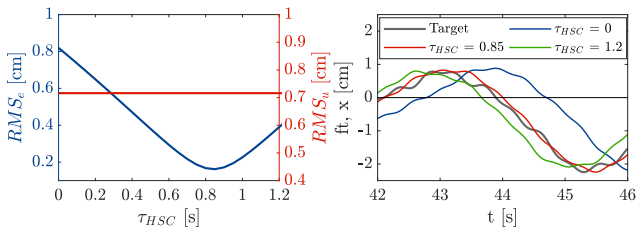

(a) Error and control activity (b) Target and output

Fig. 5. Simulation of the HSC executing the control task without the HO in the loop.

but are kept fixed as the look-ahead time is varied. Fig. 5a shows the performance of the tuned HSC without the HO in the loop, and reveals that optimal performance is achieved for a higher look-ahead time, τ_{HSC} = 0.85 s. This is because the controller's K_{LoHS} and K_{SoHF} gains are tuned for shared control *with* an HO in the loop, and thus the gains are too low for optimal performance at a look-ahead time of 0.6 seconds, and instead a higher look-ahead time is needed. In Fig. 5a, it is seen that the control activity, RMS_u, does not vary at all with the look-ahead time. This is reflected by Fig. 5b, where changes in look-ahead time appear as pure phase shifts of the CE output.

D. Metrics

Running simulations allows for analysis of the expected shared control task performance, the HO and HSC torques, and conflict. The performance can be described by several metrics that are often used in manual control experiments [11], [15]. The following metrics are of interest for the analysis:

1) Tracking error RMS: The error is given by $e(t) = f_t(t) - x(t)$ and indicates how well the HO and HSC together succeed in accurately following the target. As an overall metric for the error magnitude over time, RMS_e is used.

2) Control input RMS: Control activity is given by $u(t)$, the CE input which results from the combined HO and HSC torques on the stick. RMS_u is used as a metric for control activity over time.

3) Input torque RMS: By looking at the HO and HSC torques, T_{HO} and T_{HSC}, respectively, the individual contributions to the control task by the HO and HSC can be analyzed. Comparing the two torques quantifies how the HO and the HSC are sharing control. A large HO torque indicates a high control effort by the HO, which is not desirable [8]. Again, RMS_T is used as a metric for the torque over time.

4) Conflict time: In shared control, ideally, the HO agrees with the guidance given by the HSC, and their two torques complement each other. Therefore, human-haptic conflict is an important metric to analyze. Here, conflict is defined to occur when the signs of the HO and HSC input torques are opposite. (see Eq. (5)). Additionally, conflict occurs only when the magnitude of the HO torque is above a threshold c, such that conflicts that occur when the HO input is small are not counted.

$$O_{conf} = \begin{cases} 1, & \text{if } T_{HO} \cdot T_{HSC} < 0 \\ & \text{and } |T_{HO}| > c \cdot \max|T_{HSC}| \\ 0, & \text{otherwise} \end{cases} \tag{5}$$

5) Conflict torque RMS: The conflict time provides a measure of how often conflict occurs, but it offers no information on how large the conflict is. For this, the conflict torque ΔT is calculated as $\Delta T(t) = T_{HSC}(t) - T_{HO}(t)$. In order to have a metric that describes how large the conflict is over a

certain amount of time, the root mean squared conflict torque, $RMS_{\Delta T}$, is used.

E. Simulation Results

The computer simulations were performed with measurement runs lasting 120 seconds. The HO and HSC (HCR) used the same model parameters, listed in Table II. A set of three HO look-ahead times was used, τ_{HO} = [0.3, 0.6, 0.9] s. For haptic look-ahead times τ_{HSC} on the interval 0 to 1.2 seconds, 1,000 repetitions were simulated, each with a different remnant realization. Fig. 6 displays the resulting metrics for all runs, showing the effect of varying the look-ahead time. In each plot, the line represents the average value over 1,000 remnant realizations. For all simulations, the HO look-ahead time, τ_{HO} is indicated by the vertical line that matches the line for that look-ahead time (indicated in the legend).

1) Error: Fig. 6a reveals that the haptic look-ahead time has a strong effect on the error. For τ_{HO} = 0.6 s, the minimum RMS error is approximately 0.19 cm, achieved around τ_{HSC} = 0.65 s. Both an increase and a decrease of τ_{HSC} cause the error to increase steeply, up to 0.46 cm at both 0.0 and 1.2 seconds haptic look-ahead time. The effect of varying the human look-ahead time is a shift in the τ_{HSC} that results in the minimum RMS$_e$. If τ_{HO} is higher, the optimal error is achieved at a comparatively lower haptic look-ahead time, and vice versa. This shows how the HO and the HSC effectively compensate each other's look-ahead times.

2) Control activity: The control activity is represented by the CE input, $u(t)$, which is plotted in red alongside the error in Fig. 6a. The effect of τ_{HSC} on RMS$_u$ is small compared to the effect on the error. The control activity remains largely constant, with a small peak around τ_{HSC} = 0.75 s. This peak occurs where the human and haptic look-ahead times are equal, thus the control inputs given by the HO and HSC are perfectly in phase, and add up to a larger total.

3) Input torques: Fig. 6b shows the HO and HSC torques, breaking down the individual contributions to the control activity by the HO and the HSC. While Fig. 6a shows that the total control activity remains largely constant, the individual torque components may be much higher when there is a large difference between human and haptic look-ahead times. This hints at conflict, where both torques are opposite and cancel out. The HO and HSC torques are equal around a haptic look-ahead time that is higher than the HO look-ahead time.

4) Conflict: By looking at the conflict time (Fig. 6c) and the conflict torque (Fig. 6d) together, the cooperation between the HO and HSC can be analyzed. Conflict time is defined by Eq. (5), and describes how often the two torques are opposite. The conflict time is shown for a threshold of $c = 0$ (all conflicts are counted) and $c = 0.1$ (only conflicts where the HO torque magnitude is larger than 10% of the maximum HSC torque are counted). Comparing the percentage of conflict at $\tau_{HSC} = 0$ s with the conflict at $\tau_{HSC} = 1.2$ s reveals that applying a threshold causes a larger reduction of conflict time for the latter. In other words, for higher haptic look-ahead times, small conflicts make up a larger part of the total conflict time. Using this metric, occurrence of conflict is high, ranging from 40% to 80% of the time without a threshold, and from 10% to 60% with a threshold. The trends show clear conflict minima, which occur when the haptic look-ahead times are considerably higher than the human look-ahead times (i.e., for $\tau_{HO} = 0.6$ s, the minimum conflict occurs when $\tau_{HSC} = 0.8$ s without a threshold). When a threshold of 0.1 is applied, these minima are located at higher τ_{HSC}. On the interval [0,1.2] seconds, a human look-ahead time τ_{HO} of 0.3 seconds (the dotted line) results in the most conflicts when $\tau_{HSC} = 1.2$ s and when no threshold is applied. For the other human look-ahead times, the highest conflict times are achieved when $\tau_{HSC} = 0$ s. Fig. 6d shows the conflict torque RMS and reveals a similar trend as the conflict time without a threshold. The minima are around the same haptic look-ahead times. Note that $RMS_{\Delta T}$ is often much higher than the RMS values of the HO and HSC torques in Fig. 6b. This shows how the HO and HSC torques are often opposite in sign, which is reflected by the high conflict time.

Overall, the simulation results show a strong effect on the tracking error, the HO and HSC torques, and the conflict metrics, caused by varying only the haptic look-ahead time. However, since the HO parameters are kept constant, effects of HO adaptation for varying look-ahead times are not investigated.

III. Experiment

A. Control Task

The control task performed in the experiment is the same as performed in the simulations, as described in Section II-A. Additionally, three different realizations of the target function are used, to prevent participants from remembering the signal.

B. Apparatus

The experiment was conducted at the Human-Machine Interaction Lab at the faculty of Aerospace Engineering of TU Delft. Participants were seated in front of a display with a resolution of 1280 by 1024 pixels, a size of 36 by 29.5 cm, and a 100 Hz refresh rate. On the display (see Fig. 1), a one-second window of preview was shown of the target signal, $f_t([t, t+1])$, which participants were tasked to follow. For their control input, and the haptic force feedback, participants used an electro-hydraulic servo-controlled side-stick located on their right-hand side. The stick has a moment arm of 9 cm and can only rotate around its roll axis. The stick has a torsional stiffness of 3.58 Nm/rad, damping 0.22 Nm s/rad, and inertia 0.01 kg m^2. A stick gain of 0.44 cm/deg is used [11].

C. Conditions

One independent variable is varied in the experiment, the haptic look-ahead time τ_{HSC}. We are interested in showing the effect caused by changes in this parameter in detail, such as shown in Fig. 6. Therefore, the conditions were chosen such that a grid of look-ahead times is obtained with a relatively high resolution. The look-ahead times for each condition are listed in Table III. As a baseline, the average critical human

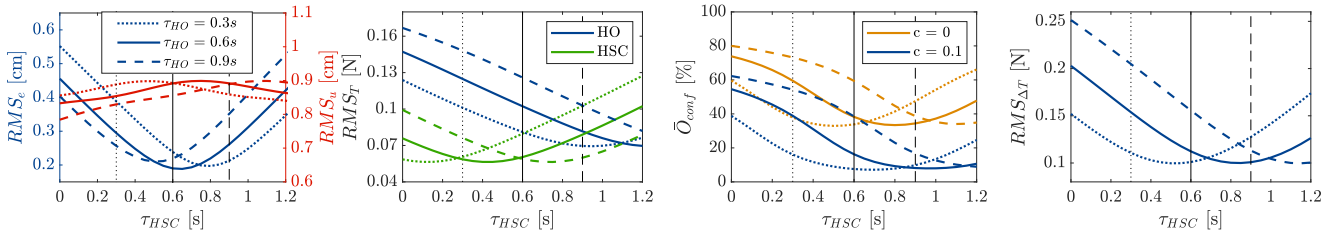

(a) Error and control activity (b) HO and HSC torque (c) Conflict time (d) Conflict torque

Fig. 6. Output metrics for the simulations, showing the effect of varying the haptic look-ahead time, showing the mean from 1000 remnant realizations.

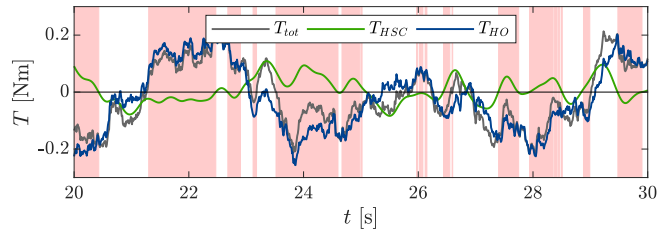

(a) Run with high conflict (τ_{HSC} = 0.0 s)

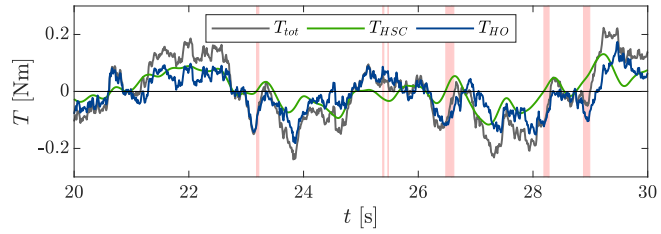

(b) Run with low conflict (τ_{HSC} = 0.8 s)

Fig. 7. Time traces of two simulated sample runs, plotting the HO and HSC torque along with the total torque. Conflict is marked with red areas.

preview time from earlier research [15], 0.6 seconds is used, as it is expected that the participants will use this as their look-ahead time (far-viewpoint). The total visual preview presented to the participant is kept fixed at 1 second. While the average viewpoint used is at 0.6 seconds, some participants may prefer a higher value. The range of chosen look-ahead times is centered around 0.6 seconds and ranges from 0 to 1.2 seconds. From 0.3 to 0.9 seconds, the look-ahead times close to the critical preview time, a high resolution is used, with increments of 0.1 seconds, to be able to investigate subtle differences in performance and acceptance. Additional to nine haptic conditions, a non-haptic condition is included for reference.

TABLE III
CONDITIONS FOR THE EXPERIMENT

	NH	H0	H03	H04	H05	H06	H07	H08	H09	H12
τ_{HSC} [s]	-	0.0	0.3	0.4	0.5	0.6	0.7	0.8	0.9	1.2

D. Experiment Procedure

Ten subjects participated, aged 22-26 years old. The participants performed a target-following and disturbance-rejection task with preview, supported by continuous haptic guidance. They were instructed to follow the previewed target as accurately as possible and to do so with the presence of haptic force feedback on the stick.

The experiment had a within-subjects design. The order of the 10 conditions was determined from a randomized balanced Latin square, such that each participant was presented with a unique order of conditions. The duration of a single run was 128 seconds, of which the first 8 seconds are considered run-in time, and were discarded. For each condition, the participants conducted a training run to get used to the haptic setting. After the training run, three repetitions were performed, resulting in a dataset of three runs per condition for each subject. At the start of the experiment, participants were trained for 4 repetitions of the non-haptic condition. Another set of 4 runs of the non-haptic condition was performed at the end of the experiment. Together with the training set, these data were used to identify HO behavior, with a special interest in the participants' look-ahead time, and possible adaptation between the start and the end of the experiment.

E. Metrics

1) Subjective Metrics: Participants were asked to fill out a Van der Laan questionnaire [17] throughout the experiment, after completing each condition. In the questionnaire, the haptic support system is rated based on properties related to usefulness and satisfaction. Subsequently, two output metrics are calculated, a *usefulness score* and a *satisfaction score* [17].

2) Objective Metrics: From measured time data from the control task, objective metrics were calculated. The time data include the error ($e(t)$), the control input ($u(t)$), the HO torque (T_{HO}) and the HSC torque (T_{HSC}). By taking the RMS of the time traces for these metrics, an overall 'score' can be accounted to a single run. Averaging the RMS values for all runs of a condition allows for a comparison between conditions. Additionally, two metrics are used for conflict, the conflict time (O_{conf}) and the conflict torque ($\text{RMS}_{\Delta T}$). All objective metrics are the same as those used for the simulations and are described in more detail in Section II-D.

F. Statistical Analysis

Statistical tests were performed on the subjective and objective output metrics. First, a Shapiro-Wilk normality test was performed on the output metrics. Then, the metrics were

TABLE IV
LATIN-SQUARE SHOWING THE ORDER OF THE EXPERIMENT CONDITIONS FOR TEN SUBJECTS.

Subject	*Training*	Conditions										*Reference*
1	NH	NH	H05	H0	H07	H12	H03	H09	H04	H08	H06	NH
2	NH	H05	H07	NH	H03	H0	H04	H12	H06	H09	H08	NH
3	NH	H07	H03	H05	H04	NH	H06	H0	H08	H12	H09	NH
4	NH	H03	H04	H07	H06	H05	H08	NH	H09	H0	H12	NH
5	NH	H04	H06	H03	H08	H07	H09	H05	H12	NH	H0	NH
6	NH	H06	H08	H04	H09	H03	H12	H07	H0	H05	NH	NH
7	NH	H08	H09	H06	H12	H04	H0	H03	NH	H07	H05	NH
8	NH	H09	H12	H08	H0	H06	NH	H04	H05	H03	H07	NH
9	NH	H12	H0	H09	NH	H08	H05	H06	H07	H04	H0	NH
10	NH	H0	NH	H12	H05	H09	H07	H08	H03	H06	H0	NH

tested for sphericity using Mauchly's test for sphericity. A Greenhouse-Geisser correction was applied for metrics that did not pass the sphericity test. After this, a repeated-measures ANOVA was performed to test for a significant effect of the independent variable, the haptic look-ahead time τ_{HSC}, on the metrics. Additionally, pairwise comparisons were used to find significant effects between the best performing condition (or one of the best) and other haptic conditions, as well as the non-haptic condition. For the normally distributed metrics, a t-test was used for the pairwise comparison. For non-normally-distributed metrics, a Wilcoxon signed-rank test was done.

G. Human Operator Model Identification

The measurements done for the non-haptic condition NH allow for HO system identification using the method in [11]. Since this method has not been used in haptic shared control before and an additional haptic response increases the complexity of the problem, identification for the haptic conditions is not considered here. The estimated HO model parameters will be used in two ways. First, the estimated viewpoint τ_{HO}, the human look-ahead times, can be compared to the optimal haptic look-ahead times, the time for which conflict is minimal, from the experiment. It will be investigated how individual differences between the participants during the non-haptic condition affect the results in the haptic conditions. Second, the other model parameters can be used to verify the parameters used in the HO model used to generate the HCR. This subsection will explain the steps taken to perform a HO system identification on the experiment data.

1) Model Structure: Fig. 8 shows the considered HO model, rewritten in two distinct operator responses, to the target (H_{o_t}) and to the output (H_{o_x}) [11]. Identification is done on the controlled element input signal $u(t)$, which is considered to be the HO control output. This means that stick dynamics are included in the HO response blocks. Since our main interest lies in the look-ahead parameter τ_{HO} and not in the neuromuscular parameters, a simplified version of the HO model is used. This version excludes the second-order neuromuscular dynamics and instead uses only a gain and a pure delay, as shown in Eq. (6) [12]. Leaving out these dynamics removes some accuracy in the high frequency range, but the presence of a low-pass filter in the target response makes this less of a problem. The phase delay normally caused by the second-order dynamics is captured in the time delay τ_v, which can be seen as an equivalent, lumped delay [12]. The target response consists of the low-pass 'far-viewpoint' response and the gain and delay, shown in Eqs. (7) and (8). From these HO describing functions, the parameter vector to be estimated follows as $\Theta = [\tau_{HO}, K_f, T_{l,f}, K_e, \tau_v]$.

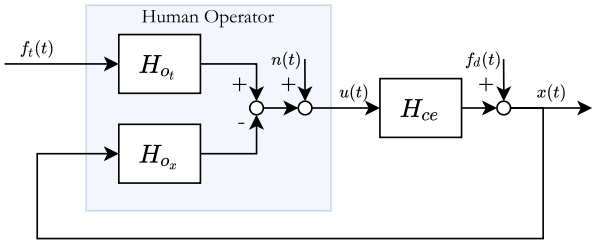

Fig. 8. Block diagram of the two-channel HO structure

$$H_{o_x}(j\omega) = K_e e^{-\tau_v j\omega} \tag{6}$$

$$H_{o_f}(j\omega) = K_f \frac{1}{T_{l,f} j\omega + 1} \tag{7}$$

$$H_{o_t}(j\omega) = H_{o_x} H_{o_f} e^{\tau_{HO} j\omega} \tag{8}$$

2) Parameter Estimation: The identification is done in the frequency domain. As per the diagram in Fig. 8, the control input given by the HO can be modeled by Eq. (9). Here, $F_t(j\omega)$ and $X(j\omega)$ are the Fourier transforms of the target signal $f_t(t)$ and the control output $x_t(t)$, respectively. $\hat{H_{o_t}}(j\omega_i|\Theta)$ and $\hat{H_{o_x}}(j\omega_i|\Theta)$ are the modeled human controller responses at frequency ω_i for a parameter set Θ. The cost function is obtained by taking the error between the Fourier transform of the measured control input, $U(j\omega)$, and the modeled control input $\hat{U}(j\omega)$, as defined by Eq. (10). The estimated parameter vector $\hat{\Theta}$ is then obtained by minimizing the squared error, described by Eq. (11).

$$\hat{U}(j\omega_i|\Theta) = \hat{H}_{o_t}(j\omega_i|\Theta) F_t(j\omega_i) - \hat{H}_{o_x}(j\omega_i|\Theta) X(j\omega_i) \tag{9}$$

$$\epsilon(j\omega_i|\Theta) = U(j\omega_i) - \hat{U}(j\omega_i|\Theta) \tag{10}$$

$$\hat{\Theta} = \underset{\Theta}{\operatorname{argmin}} \sum_{i=1}^{N_f} |\epsilon(j\omega_i|\Theta)|^2 \tag{11}$$

As a measure for the HO model's quality-of-fit, the Variance Accounted For (VAF) is used, Eq. (12). A VAF of 100% indicates that the measured data are fully described by the model.

$$\text{VAF} = \left(1 - \frac{\sigma_\epsilon^2}{\sigma_u^2}\right) \times 100\% \tag{12}$$

H. Hypotheses

The experiment was designed to test the following four hypotheses. These are formulated based on the results from the simulations, and findings from previous literature.

I. The tracking error reduces when sharing control with haptic feedback.
This hypothesis concerns the general effect of using haptic guidance in a preview tracking task. The error achieved by the participants in reference condition NH, manual control, can be compared to a haptic condition to show the advantage of using haptic shared control.

II. A range of haptic look-ahead times exists for which no significant change in the objective ratings, conflict time, and conflict torque is observed.
The calculated conflict in the simulations (Figs. 6c and 6d) shows a broad optimum around a look-ahead time of 0.8 seconds. Based on this, we expect that small increases and decreases in haptic look-ahead time around the minimum will not have a significant effect on the conflict time.

III. A range of haptic look-ahead times exists for which no significant change in the subjective ratings, usefulness and satisfaction is observed.
Similar to Hypothesis II, the same is the case for the subjective experience by the participants. It is expected that the scores calculated from the filled in Van der Laan questionnaires do not show any significant effects around the optimal look-ahead time.

IV. The haptic look-ahead time which results in the least conflict depends on the identified human look-ahead time of an individual in manual control.
The experiment data from the non-haptic condition will be used to estimate the human look-ahead time τ_{HO}. The look-ahead time for which conflict is at a minimum, the optimal look-ahead time, is considered as the 'desired' haptic setting. The simulations (see Fig. 6) predict how increasing τ_{HO} during shared control increases the optimal haptic look-ahead time. While the human look-ahead time during haptic shared control will be unknown, it is still expected that the human look-ahead time during manual control correlates with the desired haptic look-ahead time during shared control.

IV. Results

A. Subjective Results

Fig. 9 shows the subjective results based on the Van der Laan questionnaire filled out by the participants. Fig. 9a shows how each condition scores on both usefulness and satisfaction, showing the mean scores and the standard error. Conditions H0 and H12 are the least favorable, as expected, with H12 scoring the worst. The satisfaction scores for H0 and H12 are -0.65 and -1.23, respectively. This is much lower than the usefulness scores for these conditions, which are 0.08 for H0 and -0.28 for H12. The other conditions all have positive usefulness and satisfaction scores, with condition H03 having the lowest scores, a satisfaction score of 0.15 and a usefulness score of 0.30. The highest rated conditions are H06, H07, and H08, which have a satisfaction score of 1.20, 1.30, and 1.23, respectively, and a usefulness score of 1.02, 1.08, and 1.00, respectively. In Fig. 9b the score trends are plotted as a function of the haptic look-ahead time, τ_{HSC}, revealing a concave relationship with an optimum around τ_{HSC} = 0.7 s (H07). While this condition has the highest average score on both usefulness and satisfaction, the differences with the surrounding conditions are small.

B. Objective Results

The objective metrics calculated from the time data are plotted in Fig. 10. The graphs show the different output metrics as a function of the haptic look-ahead time, and include the experiment means across all subjects with standard error, as well as the simulation output. This subsection discusses the observed effects for each metric and compares it with the simulation predictions.

1) Error RMS: The experimental data for the error RMS are plotted in Fig. 10a. An overall significant effect of the haptic look-ahead time was found on the error RMS (Table V). Furthermore, the average error was significantly lower than the non-haptic condition for all haptic conditions except τ_{HSC} = 1.2 s, see Table VI. The average error that the participants achieved for the non-haptic condition is shown in the figure above 'NH' and is 0.31 cm. The simulated HO achieved a higher error with no HSC: RMS_e = 0.43 cm. The relationship between the haptic look-ahead time and the error is convex, with a minimum error of 0.19 cm in the experiment, matching the simulation predictions. However, the simulations predict an error of 0.45 cm for the haptic look-ahead times τ_{HSC} = 0 s and τ_{HSC} = 1.2 s, an increase of 137% with respect to the minimum. In the experiment, the error was 0.27 cm for τ_{HSC} = 0 s and 0.32 cm for τ_{HSC} = 1.2 s, an increase of only 42% and 65%, respectively. The difference between the simulation predictions and the experiment outcome indicates HO behavior adaptation in the experiment, which was not accounted for in the simulations. The experiment also reveals a difference in performance between the haptic conditions τ_{HSC} = 0 s and τ_{HSC} = 1.2 s, which was not predicted by the simulations. The standard error of the means is large, and between τ_{HSC} = 0.5 s and τ_{HSC} = 0.8 s it is not immediately clear which is the optimal condition, as no significant effect is found from pair-wise comparisons of condition H07 to H05, H06 and H08 (Table VI).

2) Control Activity: The control activity metric, RMS_u, is plotted in Fig. 10a and shows a clear downward trend with increasing τ_{HSC}. A significant effect of the haptic look-ahead time on RMS_u was found (see Table V). For the non-haptic condition, the control activity was RMS_u = 0.87 cm

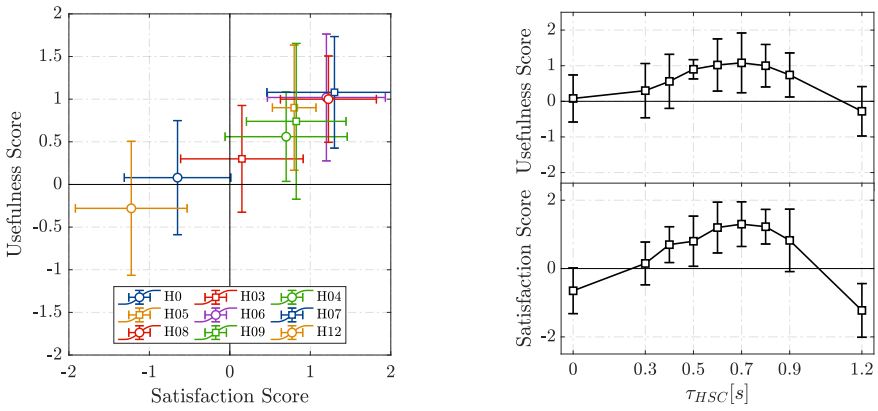

(a) Comparison of haptic conditions (b) Usefulness and satisfaction vs. τ_{HSC}

Fig. 9. Output of the subjective Van der Laan questionnaires: usefulness and satisfaction scores.

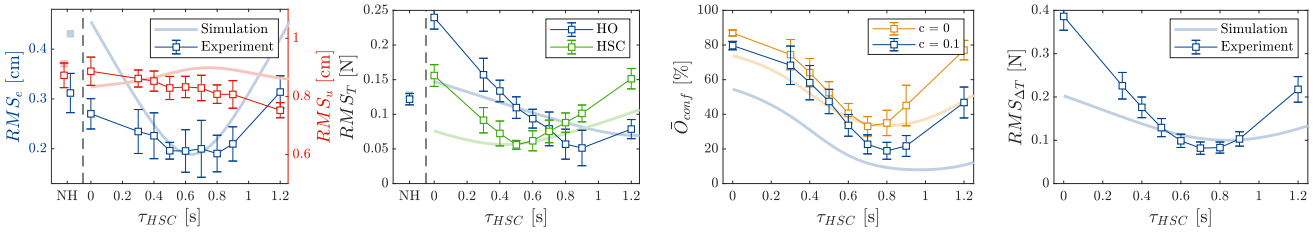

(a) Error and control activity (b) HO and HSC torque (c) Conflict time (d) Conflict torque

Fig. 10. Output metrics for the experiment, showing the effect of varying the haptic look-ahead time, including the predictions by the simulations.

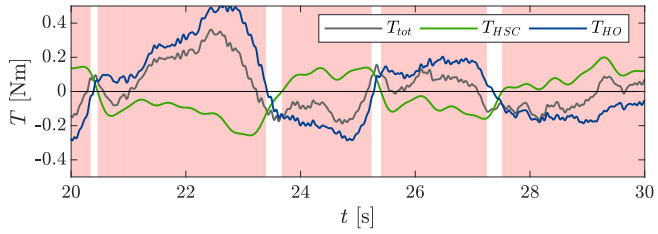

(a) Run with high conflict (τ_{HSC} = 0.0 s)

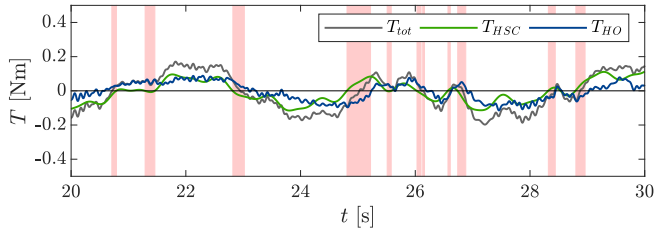

(b) Run with low conflict (τ_{HSC} = 0.7 s)

Fig. 11. Time traces of two typical experiment runs (subject 8), plotting the HO and HSC torque along with the total torque. Conflict is marked with red areas.

in the experiment, while the simulations predicted RMS_u = 0.91 cm, 4.6% higher. The control activity was found to be significantly lower than the non-haptic condition for haptic look-ahead times from 0.5 s to 1.2 s (see Table VI). As the haptic look-ahead time increases, the total control input decreases by approximately 20%. This is not in agreement with the simulation outcome, which shows an optimum of RMS_u = 0.89 at τ_{HSC} = 0.7 s. Fig. 5a showed how the HSC itself would not cause decreased control activity for higher look-ahead times, so this difference must be caused by the participants' control behavior adaptation. Overall, the control activity in shared control conditions was lower than in condition NH, except for the haptic condition τ_{HSC} = 0 s. As displayed in Table VI, pair-wise comparisons reveal that the control activity was significantly lower for condition H07 than conditions NH. Furthermore, no significant differences were found between H05, H06, and H07.

3) Input Torques: Fig. 10b shows the HO and HSC input torques as a function of the haptic look-ahead time. For the non-haptic condition, the HO input torque RMS is found to be $\text{RMS}_{T,HO}$ = 0.12 N, which was predicted by the simulations as $\text{RMS}_{T,HO}$ = 0.13 N. For a haptic look-ahead time of zero seconds, the HO and HSC torques are $\text{RMS}_{T,HO}$ = 0.24 N and $\text{RMS}_{T,HSC}$ = 0.16 N, respectively. Thus, when τ_{HSC} = 0 s, both the HO and HSC torque magnitudes are higher than the HO torque magnitude in manual control. As τ_{HSC} increases to 0.5 s, both the HO and HSC torque RMS decrease, to $\text{RMS}_{T,HO}$ = 0.11 N and $\text{RMS}_{T,HSC}$ = 0.06 N, respectively. For haptic look-ahead times between 0 s and 0.5 s, the HO torque RMS is between 50% and 85% higher than the HSC torque RMS, indicating that majority of the control task is executed by the HO. Additionally, for these conditions, the HO torque magnitude is larger than during manual control, and the achieved error is lower. This indicates that the HO collaborates

with the HSC to achieve a better performance than in manual control, but goes through a larger effort to achieve this. An example time trace of this is plotted in Fig. 11a, showing how the total stick torque, T_{tot} closely matches the HO torque, T_{HO}. Beyond 0.5 s, both torque magnitudes converge until they are equal at τ_{HSC} = 0.7 s. Fig. 11b shows an example time trace for this condition, showing how the input torques are evenly 'shared' between the HO and HSC.

For haptic look-ahead times higher than 0.7 s, the HSC torques increase with respect to the HO torques, and for τ_{HSC} = 1.2 s, the HSC torque RMS is twice as high as the HO torque RMS. Thus, for haptic look-ahead times higher than 0.7 s, the HSC provides the majority of the torque to the control task, whereas for haptic look-ahead times lower than 0.7 s, the HO provides the majority of the torque.

4) Conflict: The conflict time, given by Eq. (5), was calculated for two torque thresholds, $c = 0$ and $c = 0.1$. For both metrics, a statistically significant effect of the haptic look-ahead time was found (see Table V). Comparing the differences between these two results gives us information about the contribution of small conflicts, for which the HO torque is low.

The conflict time without a threshold, $\bar{O}_{conf,c=0}$, is at a minimum for τ_{HSC} = 0.7 s, while the conflict time with a 0.1 threshold, $\bar{O}_{conf,c=0.1}$, is at a minimum at τ_{HSC} = 0.8 s. The corresponding minimum conflict times are 33% and 19%, respectively. The conflict time at τ_{HSC} = 1.2 s is approximately 77% without a threshold, while applying the threshold lowers it to 46%. For τ_{HSC} = 0 s, the difference is much smaller: a decrease from 86% to 79% after the threshold is applied.

The simulations show a similar trend and are able to predict the conflict time well for the calculations with and without a threshold, up to a haptic look-ahead time of around 0.8 s. The discrepancy between the simulations and the experiment outcome is largest for τ_{HSC} = 1.2 s, for which the conflict without a threshold was predicted to be 48%, but was 77% in the experiment.

In Fig. 11, which shows the torques exerted by the HO and the HSC, conflict time (with threshold c = 0.1) is marked with red areas. When τ_{HSC} = 0.0 s, conflict occurs about 80% of the time and it is clear how the HO torques generally oppose the HSC torques. For τ_{HSC} = 0.7 s, the HO and HSC are seen to cooperate well, and conflict time is only around 22%. As displayed in Table VI, for the conflict time ($\bar{O}_{conf}$), no significant difference is observed between conditions H07 and H08. If a 10% threshold is added to the conflict time ($\bar{O}_{conf,c=0.1}$), no significant effect is found between conditions H07 and H09 as well.

The conflict torque RMS is shown in Fig. 10d, where it is also compared to the simulated conflict torque. For the experiment data, the minimum RMS$_{\Delta T}$ is approximately 0.08 N, and occurs for τ_{HSC} = 0.7 s. For the simulation data, the minimum conflict torque is 0.1 N, at τ_{HSC} = 0.85 s. The highest conflict torque, at τ_{HSC} = 0 s, is twice as high in the experiment data as predicted by simulations. This difference follows from the different magnitudes of the individual HO and HSC torques, as shown in Fig. 10b. For the conflict torque (RMS$_{\Delta T}$), no significant effect is observed between conditions H07 and H08 (see Table VI).

TABLE V
ANOVA RESULTS, SIGNIFICANCE OF HAPTIC LOOK-AHEAD TIME

*High significance ($p < 0.01$) indicated by **. Greenhouse-Geisser correction (GG) was applied when sphericity was not confirmed by Mauchly's test.*

	df	F	Sig.
RMS$_e$	2.785, 25.067 (GG)	24.86	**
RMS$_u$	8, 72	28.87	**
RMS$_{\Delta T}$	8, 72	260.17	**
$\bar{O}_{conf,c=0}$	3.267, 29.405 (GG)	110.29	**
$\bar{O}_{conf,c=0.1}$	3.113, 28.014 (GG)	141.89	**
Usefulness	3.773, 33.954 (GG)	16.15	**
Satisfaction	2.417, 21.752 (GG)	5.413	**

TABLE VI
PAIRWISE STATISTICAL TEST RESULTS

*Top rows: pair-wise test of RMS$_e$ and RMS$_u$ for the non-haptic condition NH to all haptic conditions. Bottom rows: comparison of all metrics for condition H07 to all other conditions. Significant effect ($p < 0.05$) indicated by *. For normally distributed metrics, a pairwise t-test was done (t), while for non-normally distributed metrics a Wilcoxon test was done (W)*

	NH	H0	H03	H04	H05	H06	H07	H08	H09	H12
τ_{HSC} [s]	-	0.0	0.3	0.4	0.5	0.6	0.7	0.8	0.9	1.2
RMS_e		*,t	*,W	*,W	*,t	*,W	*,W	*,W	*,W	-,t
RMS_u		-,W	-,t	-,t	*,t	*,t	*,t	*,t	*,t	*,t
RMS_e	*,W	*,t	*,W	*,W	-,t	-,W		-,W	-,W	*,t
RMS_u	*,W	*,W	*,t	*,t	-,t	-,t		*,t	*,t	*,t
$RMS_{\Delta T}$	*,W	*,t	*,t	*,t	*,t	*,W		-,t	*,t	*,t
$\bar{O}_{conf}0.0$	*,W	*,t	*,W	*,t	*,W	*,t		-,t	*,t	*,t
$\bar{O}_{conf}0.1$	*,W	*,W	*,W	*,t	*,W	*,t		-,W	-,t	*,t
Usefulness	*,W	*,t	*,t	*,t	-,t	-,t		-,t	-,t	*,t
Satisfaction	*,W	*,t	*,t	*,t	-,W	-,t		-,W	-,t	*,t

C. Parameter Estimation Results

The HO model parameters were estimated for the non-haptic conditions. Table VII summarizes the identified parameters for all experiment participants. The VAFs are high for each participant, ranging from 92% to 96%, indicating that the model is able to describe the data well, even without incorporating neuromuscular dynamics. The viewpoint parameter τ_{HO} varies from 0.61 to 0.96 seconds between participants.

TABLE VII
IDENTIFIED PARAMETERS FOR EACH PARTICIPANT

Subject	τ_{HO} [s]	K_f [-]	$T_{l,f}$ [s]	K_e [-]	τ_v [s]	VAF [%]
1	0.74	1.01	0.41	1.85	0.36	95.34
2	0.81	0.98	0.45	1.48	0.43	96.17
3	0.71	0.99	0.40	1.85	0.36	94.91
4	0.96	0.99	0.48	1.30	0.40	96.33
5	0.72	1.00	0.40	1.62	0.38	95.19
6	0.93	1.00	0.41	1.45	0.40	95.85
7	0.61	0.99	0.30	2.06	0.31	92.40
8	0.74	1.00	0.35	1.61	0.41	95.64
9	0.79	0.99	0.40	1.51	0.39	96.14
10	0.91	0.99	0.45	1.52	0.40	96.17

The resulting fitted target and output response bode plots are shown in Fig. 12 for Participant 1, which is representative for all other participants.

For the estimated HO parameters, a comparison can be made with the chosen human model parameters used to generate the HCR for the HSC (see Table II). In Fig. 13, the estimated parameters for each participant are plotted alongside the used HCR parameters. It is seen that the viewpoint parameter τ_{HO} used in the model is lower than the identified viewpoints for all participants. Only one participant has a viewpoint of around 0.6 s, and the majority of the participants have viewpoints between 0.7 s and 0.8 s. A weak correlation was found, with R^2 = 0.217 and an insignificant p-value, $p = 0.174 > 0.05$.

The viewpoint filter time constant, $T_{l,f}$ = 0.2 s for the HCR model, which is also lower than all participants, for which the identified time constant ranges from 0.3 s to 0.48 s. This indicates that the break frequency of the filter is lower, and thus more frequencies are filtered out by the HO. The time constant τ_v = 0.2 s for the HCR model, and between 0.31 s and 0.43 s for the participants. Since no neuromuscular dynamics are included, this time constant also includes the phase lag caused by the second-order dynamics as well, which is why it was expected to be higher than usual. The filter gain K_f = 1 for the HCR model, which is equal to the estimated filter gains for all participants. The equalization gain, K_{e^*} = 1.25 for the HCR model, while the estimated gains for the participants are higher, ranging from 1.3 to 2.06.

In Fig. 14, the identified human viewpoint parameters for the non-haptic conditions are plotted in comparison to the optimal haptic look-ahead time, the look-ahead time for which the conflict time with no threshold ($\bar{O}_{conf,c=0}$) is minimal. For seven participants, the optimal haptic look-ahead time was 0.7 s. For those participants, the estimated human look-ahead time τ_{HO} ranged from 0.61 to 0.96 s. Participant 10 had the highest optimal haptic look-ahead time of 0.9 s and had an estimated human look-ahead time of 0.91 s. The remaining participants, 1 and 6, had an optimal haptic look-ahead time of 0.8 s, and a human look-ahead time of 0.74 s and 0.93 s, respectively.

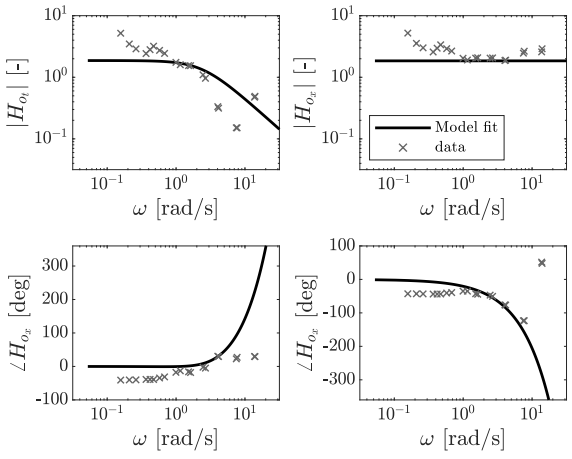

Fig. 12. Bode plots of the target and output responses for Participant 1

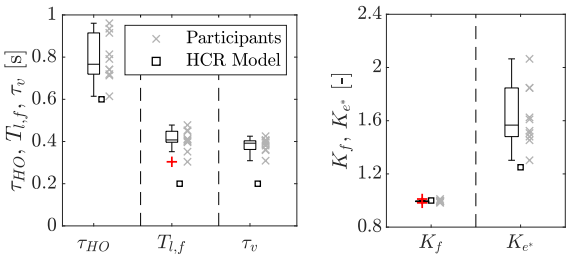

Fig. 13. Fitted human model parameters for all participants, including boxplots, compared to the parameters used in the HCR model. Outliers are marked with a red cross.

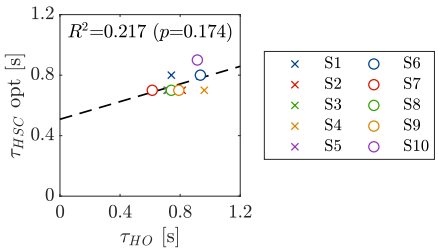

Fig. 14. Identified human viewpoints τ_{HO} for all participants versus optimal haptic look-ahead time τ_{HSC}, for which the conflict time is minimal

V. Discussion

This research was conducted to investigate the effects of varying the haptic look-ahead time in a shared preview control task. Four hypotheses were formulated to test in the experiment. In this section we discuss the main findings and whether these hypotheses can be confirmed.

Hypothesis I states that a human in cooperation with an HSC can achieve a lower tracking error than a human in manual control, which was predicted by the simulations. It was found by comparing the error in the non-haptic condition to the haptic conditions, that a lower error was achieved for all haptic conditions, except condition H12. Therefore, considering that of all haptic conditions, only a haptic look-ahead time of 1.2 seconds does not result in a lower error, Hypothesis I can be accepted.

No significant difference in conflict time and conflict torque was found between conditions H07 and H08. When considering the conflict time with an applied threshold of c = 0.1, this extends to condition H09. We consider this to be a range of haptic look-ahead times for which no change in measured conflict is observed. Based purely on the statistical results, we can therefore accept Hypothesis II. This result suggests that there is no clear preference between a haptic look-ahead time of 0.7 s and of 0.8 s.

For the subjective ratings for usefulness and satisfaction, a pairwise comparison to condition H07 showed no significant difference to conditions H05, H06, H08, and H09. Therefore, Hypothesis III is accepted as well. Hypotheses II and III suggest that there is a 'region' of look-ahead times acceptable for the user in shared control. Looking at the objective metrics for conflict, this region spans 0.2 seconds at most, but for the subjective ratings (usefulness and satisfaction), it could be

up to 0.4 seconds. Thus, a comparison between the objective conflict data (Figs. 10c and 10d) and the usefulness and satisfaction data Fig. 9b can be made. It shows that while a difference in conflict time between conditions is measurable, participants may not necessarily perceive this difference, or at least perceive it less strongly. It is possible that participants do notice conflict, but accept it as long as it is not too annoying, and helps in achieving the desired task performance. This notion is supported by the resulting errors, which reveal that HOs can still cooperate with the HSC to achieve a satisfactory task performance, even in the presence of conflicting torques.

The HO parameter estimation resulted in an identified human look-ahead time τ_{HO} for each participant in the non-haptic condition, which was compared to the optimal haptic look-ahead time τ_{HSC}. It was found that for 7 out of 10 participants the optimal haptic look-ahead time was τ_{HSC} = 0.7 s. For these participants, the estimated human look-ahead time ranged from 0.61 to 0.96 s, which means that the participant with the lowest τ_{HO} as well as the participant with the highest τ_{HO} both had an optimal τ_{HSC} of 0.7 s. It was thus difficult to identify a correlation between τ_{HO} and the optimal τ_{HSC}. Therefore, Hypothesis IV is not accepted. It is possible that a correlation exists, but that the variation in the optimal τ_{HSC} is smaller than can be shown with the current resolution of 0.1 s. To investigate this, an experiment can be conducted with a higher resolution, although the results of the subjective ratings suggest that participants will not notice such subtle differences in haptic feedback.

It is likely that HO control behavior changed substantially during haptic shared control. Therefore, future research can benefit from identification of the HO visual response in haptic shared control tasks, such that the effects on the HO viewpoint caused by varying haptic look-ahead times can be investigated. Knowledge on how humans use visual preview information when supported by haptic force feedback can be used to design haptic support for situations of reduced visibility, such as driving in bad weather. Furthermore, it remains unknown whether the haptic look-ahead time should be chosen to *complement* the human look-ahead time (i.e., the HO and the HSC each use a different portion of preview), or to be *aligned* to the human look-ahead time (i.e., the HO and HSC use the same portion of preview) in order to reduce conflict.

Identification of the human viewpoint can be done using Van der El's HO model [11]. However, as this model considers a manual control task with a visual response, the identification problem becomes more complicated when considering haptic shared control, and a separate tactile response might have to be incorporated to account for the response to haptic force feedback. Alternatively, experiments that force a different human look-ahead time can be conducted, for example by reducing or increasing the amount of available preview or by occluding specific parts of the previewed portion of the target [18]. A prediction of the effect of varying the human look-ahead time was made by the simulations in this paper, showing how reducing τ_{HO} by 0.3 s led to a reduction of the optimal τ_{HSC} for minimum conflict of approximately 0.3 s as well. However, as the simulations did not take into account any HO behavioral adaptation due to changing human and haptic look-ahead times, an experiment is needed to investigate this effect further.

The FDC-HSC used in this paper uses an HO model to generate the HCR, which ideally mirrors the actual HO in the loop. In this experiment, the HO model used empirical, averaged parameters. The parameter estimation on the manual control data has shown that the used empirical parameters differed from the identified HO parameters. Therefore, a more accurate representation of the HO's control behavior in this experiment was possible. This shows that HSC design can benefit from prior knowledge on the individual users of the system, by identifying manual control behavior in advance. Individual HO identification can account for individual preferences and different control behavior between users, potentially further reducing conflicts. Furthermore, the reduced model structure (e.g. without neuromuscular dynamics) used to identify the HO model was shown to be effective, with high VAF values (92-96%). Implementations of the HCR can therefore be simplified to a reduced model structure, to reduce the number of parameters used.

While a 'region of acceptance' of haptic look-ahead times has been found, the importance of properly tuning this look-ahead time was shown. It is evident that a deviation from the optimal look-ahead time, both shorter and longer, can lead to a conflict time twice as high, and conflict torques up to four times as high. In these cases, participants reported that they feel like they are 'fighting' the HSC, leading to an undesirable situation that was worse than with no HSC involved. This is reflected by the time traces showing the human-haptic torques applied to the stick, which show how the human essentially mirrors the haptic torques in the case of τ_{HSC} = 0 s. Choosing the proper haptic look-ahead time is therefore important when designing a well-functioning HSC.

VI. Conclusion

In this paper, the effects of varying the haptic look-ahead time in a shared control task were investigated. An experiment was conducted, in which participants tracked a previewed target in collaboration with a haptic shared controller through force feedback. Results show how setting the look-ahead time too high (τ_{HSC} = 1.2 s) or too low (τ_{HSC} = 0 s) leads to high conflict and error. For haptic look-ahead times from 0.5 to 0.9 seconds, no significant decrease in acceptance is indicated by the participants. On a smaller interval, this 'region of acceptance' is also visible in the objective conflict metric, for which no difference is observed between 0.7 and 0.8 seconds. This indicates a difference between perceived conflict and measured conflict. Substantial variations of human-haptic torques around the region of minimum conflict are observed, which suggests strong HO adaptation in this region. This research provides an example of how to implement a haptic shared controller which uses a human-compatible reference, and specifically shows the importance of tuning this reference properly in terms of look-ahead time. Its findings offer a step forward in knowledge on the design of conflict-reducing haptic shared controllers.

REFERENCES

[1] S. M. Petermeijer, D. A. Abbink, M. Mulder, and J. C. F. de Winter, "The Effect of Haptic Support Systems on Driver Performance: A Literature Survey," *IEEE Transactions on Haptics*, vol. 8, no. 4, pp. 467–479, 2015.

[2] M. Marcano, S. Diaz, J. Perez, and E. Irigoyen, "A Review of Shared Control for Automated Vehicles: Theory and Applications," *IEEE Transactions on Human-Machine Systems*, pp. 1–17, 2020.

[3] D. A. Abbink, M. Mulder, and E. R. Boer, "Haptic shared control: smoothly shifting control authority?" *Cognition, Technology & Work*, vol. 14, no. 1, pp. 19–28, mar 2012.

[4] D. A. Abbink, T. Carlson, M. Mulder, J. C. F. de Winter, F. Aminravan, T. L. Gibo, and E. R. Boer, "A Topology of Shared Control Systems—Finding Common Ground in Diversity," *IEEE Transactions on Human-Machine Systems*, vol. 48, no. 5, pp. 509–525, oct 2018.

[5] J. C. F. de Winter and D. Dodou, "Preparing drivers for dangerous situations: A critical reflection on continuous shared control," in *2011 IEEE International Conference on Systems, Man, and Cybernetics*. IEEE, oct 2011, pp. 1050–1056.

[6] L. Bainbridge, "Ironies of automation," *Automatica*, vol. 19, no. 6, pp. 775–779, nov 1983.

[7] R. P. Boink, M. M. Van Paassen, M. Mulder, and D. A. Abbink, "Understanding and reducing conflicts between driver and haptic shared control," in *2014 IEEE International Conference on Systems, Man, and Cybernetics (SMC)*, vol. 2014-Janua, no. January. IEEE, oct 2014, pp. 1510–1515.

[8] M. M. Van Paassen, R. P. Boink, D. A. Abbink, M. Mulder, and M. Mulder, "Four design choices for haptic shared control," in *Advances in Aviation Psychology, Volume 2*. Routledge, may 2017, pp. 237–254.

[9] W. Scholtens, S. Barendswaard, D. M. Pool, M. M. Van Paassen, and D. A. Abbink, "A New Haptic Shared Controller Reducing Steering Conflicts," in *2018 IEEE International Conference on Systems, Man, and Cybernetics (SMC)*. IEEE, oct 2018, pp. 2705–2710.

[10] D. T. McRuer, R. W. Allen, D. H. Weir, and R. H. Klein, "New Results in Driver Steering Control Models," *Human Factors: The Journal of Human Factors and Ergonomics Society*, vol. 19, no. 4, pp. 381–397, 1977.

[11] K. Van Der El, D. M. Pool, H. J. Damveld, M. M. Van Paassen, and M. Mulder, "An empirical human controller model for preview tracking tasks," *IEEE Transactions on Cybernetics*, vol. 46, no. 10, oct 2015.

[12] D. T. McRuer and H. R. Jex, "A Review of Quasi-Linear Pilot Models," *IEEE Transactions on Human Factors in Electronics*, vol. HFE-8, no. 3, pp. 231–249, sep 1967.

[13] T. B. Sheridan, "Three Models of Preview Control," *IEEE Transactions on Human Factors in Electronics*, vol. HFE-7, no. 2, pp. 91–102, 1966.

[14] K. Ito and M. Ito, "On tracking behaviors of the human operator in preview control systems," *Kybernetes*, vol. 4, no. 1, pp. 33–38, 1975.

[15] K. van der El, S. Padmos, D. M. Pool, M. M. Van Paassen, and M. Mulder, "Effects of Preview Time in Manual Tracking Tasks," *IEEE Transactions on Human-Machine Systems*, vol. 48, no. 5, pp. 486–495, oct 2018.

[16] K. van der El, D. M. Pool, and M. Mulder, "Measuring and modeling driver steering behavior: From compensatory tracking to curve driving," *Transportation Research Part F: Traffic Psychology and Behaviour*, vol. 61, no. October, pp. 337–346, 2019.

[17] J. D. Van Der Laan, A. Heino, and D. De Waard, "A simple procedure for the assessment of acceptance of advanced transport telematics," *Transportation Research Part C: Emerging Technologies*, vol. 5, no. 1, pp. 1–10, 1997.

[18] M. J. C. Kolff, "Effects of Visual Occlusion in Lane Keeping Tasks on Driver Model Identification and Gaze Behaviour," MSc Thesis, Delft University of Technology, 2019.

II

Preliminary Thesis Report

1 Introduction

Automation is making its way to the automotive industry. In modern cars, Advanced Driver Assistance Systems (ADAS) such as lane-keeping assist, adaptive cruise control and emergency braking are no longer an exception. Self-driving cars are no longer a dream of the future, but appear to be within reach. However, the majority of today's state-of-the-art of automation still requires the presence of a human operator. Self-driving cars do as their name suggests: they drive themselves, but only in a limited operational domain such as highways, where traffic complexity is predictable. And even still, a driver has to be present, either to perform part of the control task or to continuously monitor the system and intervene in case of failure. In other words, the role of the human operator has moved from manual controller to supervisor, a role in which humans are known to perform worse. This introduces new issues such as over-reliance, loss of situation awareness and loss of manual control skills [1].

Instead of fully automating a control task like driving a car, it is possible to have the driver and automation *share control*. A promising way to share control between human and automation is through continuous *haptic* (force) feedback on the control interface [2, 3]. The haptic support system essentially guides the driver through corners by moving the steering wheel. In this situation, the driver remains in the loop continuously and is able to communicate both ways with the automation system, benefiting from the automation's capabilities as well as the driver's.

Due to the complicated nature and unpredictability of human control behavior, designing a well-functioning haptic shared control system is not straightforward. User acceptance is of critical importance in a haptic support system, as bad functioning systems will be turned off by its user. Conflicts between the human operator and the automation system can occur because of differences in reference behavior or control strategy, and will have a negative impact on user acceptance. It is therefore important to include knowledge on human driving behavior in the design of haptic support systems, and design human-like support systems.

In the past decades, research efforts in the field of *manual control cybernetics* have been made to model the human controller using classical control theory. For a long time, this was only achieved for the highly limited *compensatory* control task, where a human operator follows a target using only the current deviation from it as an input [4]. More recently, progress was made on the topic of *preview* control, a type of task where the operator can see a portion of the future target, much like driving a car along a road. Research by Van der El [5] has resulted in a control-theoretic human controller model, which is able to replicate human steering behavior in such target following tasks with preview.

1.1. Research objective

An HSC should have a positive effect on performance and workload when sharing control with a driver. Its parameters should be tuned such that conflicts are minimized and the user experiences the haptic support as desirable. A key parameter is the look-ahead time in a preview control task. The input to the HSC is a point some time ahead on a reference trajectory, for instance the center of the road in case of a car driving task. In a similar way, a human driver uses the road ahead to determine their steering input. Changes in visibility due to fog, rain or objects blocking the view influence the available preview, and thus the look-ahead time.

In combination with haptic support, knowing the effect of changing visual preview can help determine the haptic controller setting.

In order to investigate this, this thesis research will implement Van der El's human controller model in a Haptic Shared Controller (HSC). This will result in an HSC that uses a future point on a reference for its control strategy, similar to the way humans do this. The haptic look-ahead time can be varied, which results in a different type of haptic guidance. For the human operator, the look-ahead time can be changed by enforcing a certain visual preview, for instance by shortening or blocking parts of the displayed reference signal.

Research objective

To implement a haptic shared controller based on a novel human controller model, and evaluate the effect of varying human and haptic look-ahead times on performance and conflict in the preview control task.

In addition to the main objective, four research questions were formulated.

Q1 *Is it possible to identify a region of acceptance in terms of haptic look-ahead times, in which performance and acceptance is not affected negatively?*

When implementing shared control in a real-life situation, it is impossible to exactly match the look-ahead parameter to the human's look-ahead time. Additionally, until driver individualization is possible, different persons may prefer different settings. It is therefore useful to know the acceptable margin in which the haptic look-ahead time can deviate from the human look-ahead time before annoyance occurs.

Q2 *If haptic look-ahead time does not match to human preview time, is it preferable to have a preview time that is too low, or too high?*

As an addition to Q1, it is useful to know whether this "region of acceptance" mainly lies below or above the human preview time. Perhaps it is preferable to the user to have a haptic support system that looks further away than the user, or perhaps it has to be closer.

Q3 *Does the measured 'conflict' correlate with the participants subjective perception of conflict?*

During the human-in-the-loop experiment, a measure of conflict will be calculated from the measured stick forces. Defining this conflict is not trivial, and it is valuable for future research to know how good this conflict metric is. Subjective questionnaires will be filled out by the participants after each run, in which they can indicate to what extent they experienced conflict.

Q4 *Can the novel human controller model be used for predicting performance in a target following task supported by haptic guidance?*

Before executing the experiment, offline simulations will be done. Here, the human controller model will be used to simulate human behavior in the shared control task. By comparing the outcome of this simulated experiment to the real experiment, this method of simulating a shared control task can be validated.

This research is intended to offer a general insight on the interaction between a human and haptic controller, and the effect of different look-ahead times.

1.2. Thesis outline

An overview of the project's subtasks is shown in Figure 1.1. The preliminary phase of the project is covered in this report, and contains the tasks shown in the top part. The literature review is split up in two main parts: manual preview control (Chapter 2) and haptic shared control (Chapter 3). These chapters provide the necessary background information of the two research topics, which are combined in the remainder of the thesis work. Starting out with simulations (Chapter 4), in order to predict how the combined human-haptic system performs while using different look-ahead times in a preview control task. The results of the simulations form the basis of the experiment plan (Chapter 5), detailing how the human-in-the-loop experiment will be performed, and which conditions will be used. The remainder of the project is still to be executed, and will be covered in the final thesis. In this part, the human-in-the-loop experiment will be conducted based on the simulations and experiment plan done in the preliminary part. This will be concluded by analyzing the measured data and concluding remarks.

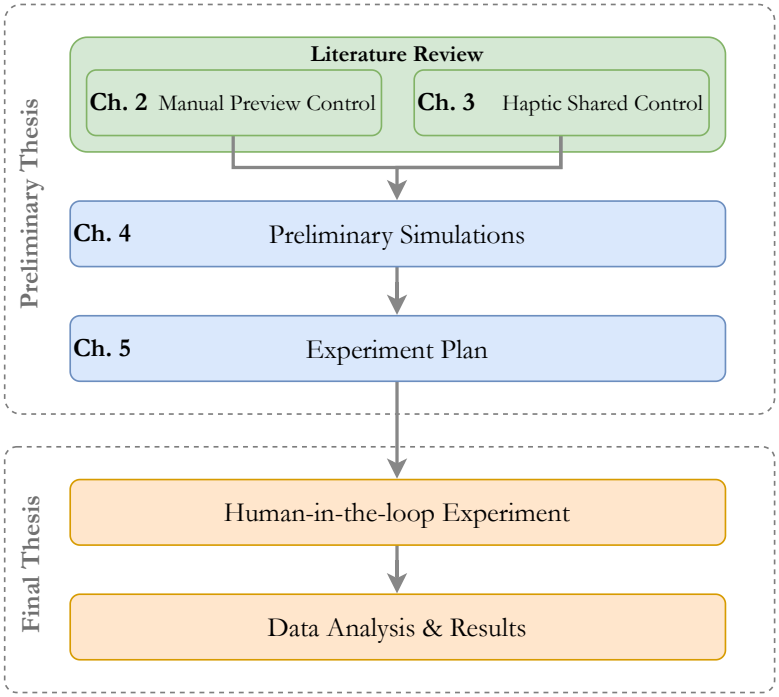

Figure 1.1: Outline of the thesis project, with the top section covered in this report.

2

Manual Preview Control

Manual control covers wide range of applications, including driving a car, flying an airplane and riding a bicycle. A good understanding of how humans manually control vehicles is essential when designing manual control interfaces or automation and support systems. The scientific field known as *manual control cybernetics* addresses this by mathematically modeling human control behavior using system identification and parameter estimation techniques. Cybernetics can come up with quantitative models that capture how humans apply low level control inputs and adapt to system dynamics.

During a manual control task, humans use various types of information as input. Figure 2.1 shows a schematic depiction of a driver in a car control task. Visual information, motion perception and touch are processed and used to identify the current state of the system and determine a control strategy. The human controller itself can be modeled as a combination of sensors (eyes, vestibular organs), internal processing (cortex) and actuators (neuromuscular system).

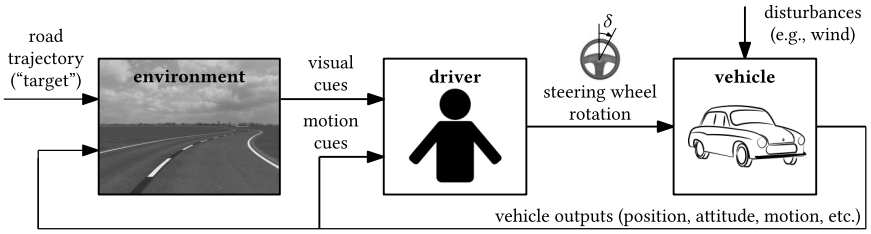

Figure 2.1: Overview of the manual control task of driving a car and the interaction of the (human) driver with the environment and vehicle (borrowed from [6]).

This chapter provides background information on the manual preview control task and efforts to model it. The focus of this thesis project is preview control, but at the basis of human controller models lies *compensatory* control, which will therefore be covered in Section 2.1. After this, the majority of the chapter will be dealing with *preview* control in Section 2.2, which is here also considered to include *pursuit*, as will be clarified later.

2.1. Compensatory Control

The human can be considered as a highly adaptive non-linear controller [4]. Pioneering research in the 1950's and 60's such as McRuer's work show the strength of modeling the human controller (HC) using a control theoretic framework [4, 7]. The goal was to define a control-theoretic model that could capture the way humans use information to come up with a control strategy during a manual control task. This resulted in McRuer's *crossover model*, which captures how humans adapt to the dynamics of the controlled element, or vehicle [4].

The control task considered by McRuer was a simple single-axis, *compensatory* target tracking task, which means that the HC only perceives the error between the target signal and the system output. A block diagram depicting this situation is shown in Figure 2.2. The control task consists of two forcing functions, a target

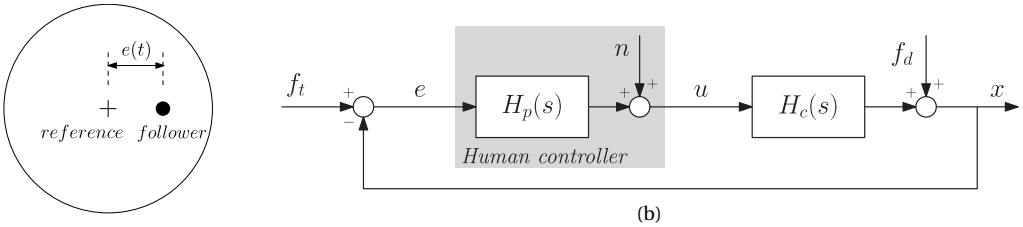

Figure 2.2: Depiction of the compensatory control display (a) [**?**] and block diagram (b) [8]

f_t and an added disturbance f_d. Often these forcing functions are a combination of multiple sines, such that power only exists at certain known frequencies, greatly aiding the model identification process. The HO controls a system $H_c(s)$ in order to achieve satisfactory tracking performance, which is a minimum error e, in a closed-loop fashion. Here, the HC is modeled as a quasi-linear controller in which $H_p(s)$ captures the linear part of human control behavior, and a remnant n captures the remaining non-linear part. The *crossover model*, shown in Equation (2.1), states that the open-loop response $H_p(s)H_c(s)$ always results in single-integrator behavior around the crossover frequency ω_c. This is invariant for different H_c dynamics, and thus shows how humans systematically adapt their control strategy (captured in H_p) to the controlled element (H_c) [4].

$$H_p(s)H_c(s) = \frac{\omega_c}{s}e^{-s\tau_e} \tag{2.1}$$

The most widely accepted linear model for HO dynamics is McRuer's *precision model* [4] (Equation (2.2)), containing three distinguishable parts. The equalization part contains a proportional gain and lead-lag terms, which capture how the HC adapts to controlled element dynamics. The order of the system dynamics determines how the input given by the HO is transferred to the output. For first-order or single integrator (SI) dynamics, also known as velocity control, the HO equalization part consists of only a gain term, as per the crossover model. Similarly, a gain (GN) controlled element or a double-integrator (DI) require a lead and or lag term, respectively. After the equalization part, a time delay is included to account to cover cognitive processing time. Finally, the neuromuscular system is modeled as an actuator using a second order system.

$$H_p(s) = \underbrace{K_p\left(\frac{T_L s+1}{T_I s+1}\right)}_{\text{Equalization}} \quad \underbrace{e^{-s\tau}}_{\text{Time delay}} \quad \underbrace{\frac{\omega_{nm}^2}{s^2+2\xi_{nm}\omega_{nms}s+\omega_{nm}^2}}_{\text{Neuromuscular dynamics}} \tag{2.2}$$

The model is successfully applicable, but only in the highly constrained case of compensatory control, that is, a case where the human controller acts only on the perceived error. This shows the limitation of the current state of cybernetic modeling, as "...we are currently able to model only the exception in manual control, and not the rule." [8].

2.2. Preview Control

Most real-life control tasks are much more complicated than a compensatory tracking task. A more widely applicable type of control task is *preview* control, which includes visual information of the current and part of the future of the target. Preview of future states adds a *feedforward* component to the control task and allows the human to anticipate, resulting in a better performance [9]. A prime example of preview control is steering a car along a road, where the road's center line might act as a target signal that one has to track. The driver perceives the car's current position on the road and uses visual information of the road ahead to determine their next steering input. A third type of tracking task is *pursuit control*, in which the HC perceives the controlled system output and the current target position. One can note that pursuit control is actually a special case of preview control, where the preview time is zero seconds [8]. Therefore, this section focuses on preview tracking, as this covers pursuit tracking as well.

2.2.1. Early Preview Models

After the success of the crossover model and the precision model for compensatory tracking [4], the search for a more general manual control model continued, including to pursuit and preview tasks. McRuer [10] proposed an architecture that includes three paths: the open-loop *precognitive* and *pursuit* level, and the closed-loop *compensatory* level. The compensatory level includes the error correcting response, whereas the pursuit path includes a visual response to the target signal. This covers previewed portions of the target as well. Finally, McRuer adds the precognitive path, which represents a fully feed-forward response based on full knowledge of the target.

Another driver model, proposed by Donges [11], presents the driver separated into two levels. The first is a "guidance" level, represented by a feed-forward open-loop response to the target and its future course, covering the preview aspect of control. The second level is a "stabilization" level, which is a compensatory closed-loop correcting the deviation from the target. The model is similar to the one by McRuer [10], except it leaves out precognitive control. Early theoretic preview control models proved difficult to validate due to their multi-channel nature [10–13].

While the mentioned models suggested the use of preview information [10, 11], it was not specified exactly *how* visual information is used in anticipatory control. In their experiment using partial occlusion of the visual field, Land & Horwood [14] showed that vision could be restricted to narrow near and far segments without loss in steering performance. They thus partially verified the use of a near and far viewpoint for steering, supporting the originally proposed model by Donges [11]. Points farther along the trajectory are used for information on road curvature, and points close to the vehicle are used for stabilization and more accurate information on road position. Figure 2.3 depicts this two-level architecture, which was established as a widely accepted approach of understanding visual control in curve driving [15].

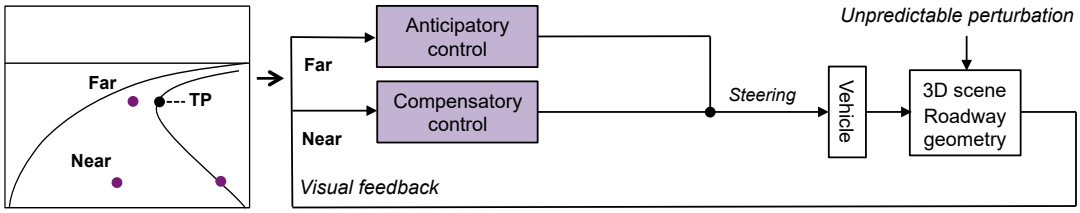

Figure 2.3: The two-point control architecture by Land & Horwood [14], as based on the two-level control architecture by Donges [11]. (Adapted from [15])

2.2.2. Van der El Model

One of the most recent studies to model the human controller was done by Van der El, who investigated how humans use preview information [6]. This has resulted in an empirical, quantitative human operator model for preview control. This model, shown in Figure 2.4, is the first preview control model to capture not only HO output, but also internal multi-loop responses [5]. Inspired by Land & Horwood and Donges' two-level control architectures, the model presents the HO to have two separate responses, to a near-viewpoint and a far-viewpoint on the target signal. The far-viewpoint response, which is the strongest of the two [16], consists of a low-pass filter (H_{o_f}), leading to a filtered version of the target signal ($f^*_{t,f}$). This captures how the HO might choose to ignore high frequencies and instead picking a 'corner-cutting' approach. The resulting control strategy can be described by an inner compensatory control loop on a *internal* error $e^*(t)$. This is not the actual error between the target and the system output, but is modeled to be a theoretical error from the HO's desired reference $f^*_{t,f}$. Since the resulting inner loop reflects the well-studied compensatory control task, the response $H_{O^*_e}$ is modeled as the equalization part of McRuer's precision model (Equation (2.2)). Similarly, the neuromuscular response and time-delay are included in the next block, keeping the same form as Equation (2.2). The near-viewpoint response H_{O_n} contains a high-pass filter and adds a feedforward open-loop response. Later experiments show, however, that the near-viewpoint response is so small compared to the far-viewpoint response that it may be neglected, leaving only a single feedforward component in the model [16].

Van der El's model has several strengths. First of all, it has successfully applied system identification methods

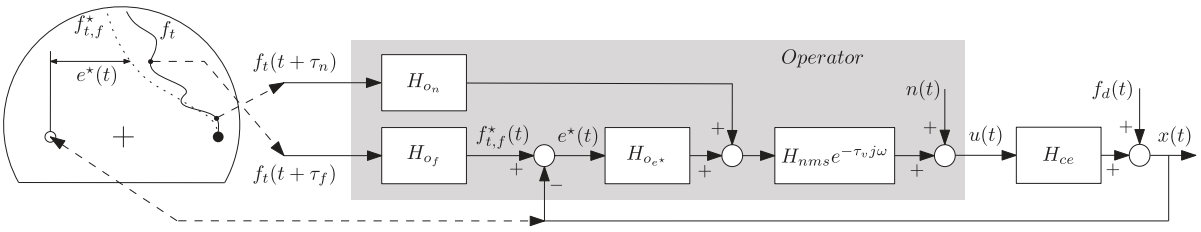

Figure 2.4: Van der El's human controller model, showing two different target responses, and compensatory control on a filtered target signal [17]

similar to McRuer's methods. Whereas for a long time a model of this sort was only available for compensatory tracking, it is now extended to preview control which covers a whole range of real-life applications, including car driving. Another strength is the use of physically meaningful parameters such as preview time, viewpoints, internal time delay and neuromuscular stiffness and damping [5].

Figure 2.4 shows the fundamental form of the Van der El model, as used in combination with abstract target tracking tasks. Later, this was extended to a driver model for application in car steering tasks. The three-level driver steering model proposed by Van der El [18] allowed for identification of three distinct internal driver responses, to the target, the heading error and the lateral position error. This driver model includes a single viewpoint response, as opposed to the earlier version of Van der El's preview control model [5], and other early driver models such as the one by Donges [11], which include two viewpoints. Kolff [19] used this three-level driver model in a recreation of Land & Horwood's 1995 experiment [14], and showed that steering behavior can be characterized by the use of a single optical cue, as opposed to Land & Horwood's results. For this reason, the fundamental form of the model will now also leave out the near viewpoint τ_n, which is still shown in Figure 2.4

2.2.3. Effect of varying preview time

The advantage of knowing a part of the future trajectory in a tracking task has been known for a while. Early studies have shown that performance increases as preview time becomes larger, up to a certain *critical preview* time, after which no notable performance improvement is observed [9]. The appearance of a *critical preview time* seems to suggest that a human operator adapts their control behavior to increase performance, but does so only up to this critical point. This effect was further investigated by Van der El and compared to earlier studies, shown in Figure 2.5a [17]. Here, the available preview time τ_p is shown on the x-axis. The resulting error power σ_e^2 as a fraction of the target and disturbance is shown for previous studies as well. Predictions are shown by simulating the Van der El model for the 'full model' (FMP) and 'reduced model' (RMP), for which the near-viewpoint τ_n is left out. Increasing the preview time results in a significantly lower error, up until a critical preview time. This critical preview time is around 0.5-0.75 s for single integrator dynamics, and 1-1.66 s for double integrator dynamics [17]. The differences between the RMP and FMP are considered to be minimal, which is why the remainder of this section will focus on the far viewpoint τ_f only.

The far-viewpoint parameter τ_f, from the Van der El model, indicates what point of the previewed target signal is used for the control strategy. The identified far-viewpoint depends on the provided preview time τ_p by the relation shown in Figure 2.5b [17]. Here, too, the presence of a critical preview time is visible. If the previewed target length is shorter than the critical preview time, HOs adjust their far viewpoint to the end of the previewed target. If it is higher, the far viewpoint remains at the critical preview time and the control behavior is no longer adapted. The same effect is present when controlling both SI and DI dynamics, but the critical preview time is longer for Di dynamics.

The relation between preview time τ_p and far viewpoint τ_f offers useful knowledge for human-in-the-loop experiments. Controlling the available preview time up to the critical preview time implicitly controls the human's chosen far viewpoint τ_f, making the far viewpoint an easily controllable parameter in experiments.

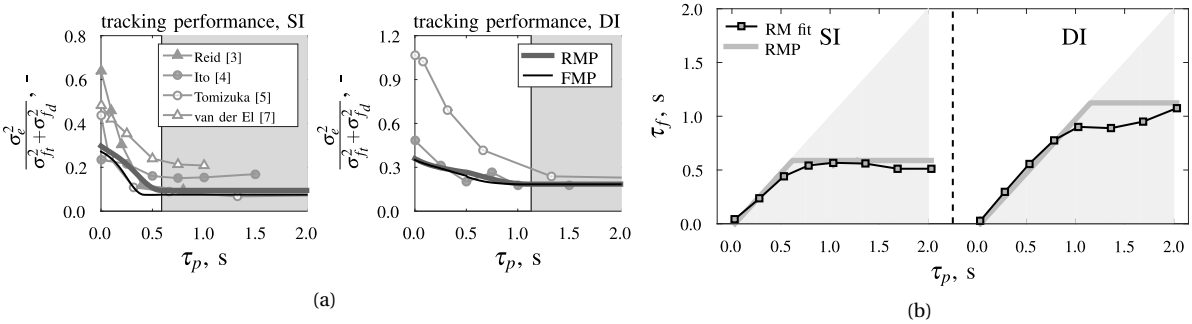

(a) (b)

Figure 2.5: The effects on varying preview time τ_p on tracking error (a) and identified far-viewpoint parameter τ_f (b) [17]

2.3. Conclusion

Studies into the manual control dynamics of the human have been done ever since the second half of the twentieth century. Today, manual control is still relevant and the results of early research is still useful. Even though a pure compensatory tracking task, modeled in McRuer's early work [4], is seldom found in real-life applications, parts of it can still be used in later iterations of driver models. Van der El's preview model [5] adds a response to the target signal, but inner loop dynamics are still based on McRuer's crossover and precision models.

Van der El's work shows how the successful model of one-dimensional tracking can be extended to curve driving, which makes it relevant for applications in driver support systems [16]. For implementation in actual haptic support systems, the model will need to be in this two-dimensional curve driving layout. However, for this thesis, the focus remains on abstract one-dimensional tracking tasks, for they are considered to be the first step in understanding the low-level interaction between a human controller and a haptic support system.

3

Haptic Shared Control

The future of transportation may very well be shaped by intelligent vehicles capable of moving through the environment on their own. Airline flights have already been largely automated, and the trend seems to continue as automation is becoming prevalent in cars as well. While automating control, these vehicles will still be designed for and occupied by humans, who are undeniably a crucial factor. In fact, in the current state of vehicle automation systems, human presence is required to take over where automation fails. But even in an ideal future where automation performs perfectly, humans may still be in control because regulations require it, or simply because we humans prefer to be in control. For this reason, an alternative form of automation has been getting increased attention in literature: sharing control between human and automation through haptic feedback on the control device [20].

This chapter provides a theoretical background on *haptic shared control*. Section 3.1 offers some background on the limitations of full automation and explains the concept of sharing control and how it is suitable for solving automation problems. Section 3.2 discusses two types of haptic shared controllers (Section 3.2.1 and Section 3.2.2), and compares how the novel Van der El human controller model can be integrated in these controllers Section 3.2.3.

3.1. Sharing Control: Keeping the Human in the Loop

The perceived benefits of automation are numerous: reduced physical workload, increased safety and improved performance. However, automation is not fully reliable, especially when unexpected changes in the environment occur. In contrast, the human operator is known to be good at learning and adapting, and their presence is required for monitoring the automation system. The human's supervisory role in the system gives rise to several human factors issues.

When a task is automated, the remaining tasks that are too difficult to automate remain the operator's responsibility. In other words, the system fails when it is most needed [1]. Adding to that, transitions of control from the automation to the human has to be done with limited information at hand, as a human supervisor has limited situation awareness due to not being in the loop [21]. Another issue of automation is the risk of losing manual control skills required to operate the system, because most of the tasks during normal operation are performed by the automation. Furthermore, actual workload might be increased instead of reduced, due to the higher cognitive demands of monitoring a system, and the fact that human intervention is needed at high-demanding critical situations [22]. Finally, as higher degrees of automation introduce more complexity in a system, transparency to the user is at risk [23]. In order to improve automation, a human-centered approach is needed [24, 25]. Keeping the human in the loop, both in the design and the use of automation systems, is essential in this approach.

It should not be forgotten that while the computer often beats the human when it comes to speed, predictability and reliability, it still lacks the adaptability, learning capabilities and intuition of a human operator. One way to combine the strengths of both, is by *sharing control* between human and automation [20]. Several definitions of shared control exist, however one clear definition is given by Abbink et al. [26]: *In shared control, human(s) and robot(s) are interacting congruently in a perception-action cycle to perform a dynamic task that*

either the human or the robot could execute individually under ideal circumstances. In human-automation interaction, feedback should be provided continuously and interaction with the user should be done effectively [25]. This is in line with the human-centered automation approach, which emphasizes that automation systems should provide adequate information and ensure active involvement of the human operator [24]. These criteria are summarized and reformulated as guidelines by Abbink et al. [3] and shown below.

Guidelines for sharing control [3]

The human operator should:

1. Always remain in control, but can experience or initiate smooth shifts between levels of automation;
2. Receive continuous feedback about the automation boundaries and functionality;
3. Continuously interact with the automation;
4. Benefit from increased performance and/or reduced workload.

Figure 3.1: Guidelines for human-automation interaction as proposed by Abbink et al. [3]

By allowing both the user and automation to exert forces on the control device, a two-way interaction between human and automation exists. This offers several benefits.

In a manual control task, information of the external environment (in car driving: the layout of the road that determines the steering input), is perceived mainly through vision. Adding information through touch, a different modality, may lead to reduced workload and increased performance [27]. Similarly, automation systems can provide more transparency and a more intuitive understanding of their intention by adding haptics as an information channel. This also uses the benefit of quick neuromuscular reflexes that allow for a faster and subconscious response to inputs [20].

When sharing control continuously, haptic feedback is useful for keeping the human operator aware of the system's functioning [26]. But the interaction is two-way, as it allows the user to give inputs to the system and correct it if needed. By applying less or more force to the control device, the human operator can continuously shift authority in favor of himself or the automation [3].

In car driving, possible applications of haptic shared control include haptic gas pedals for car following [28], or haptic guidance for steering [29, 30]. In aviation, haptic shared control can be applied in perspective flight-path displays [31], or in remote control of UAVs [32, 33]. Other possible applications or haptic shared control include robotic control [34, 35] and learning and skill transfer [36].

3.2. Haptic Shared Controllers

This section elaborates on two possible architectures for haptic guidance. The first one, a 'Meshed' Haptic Shared Controller (M-HSC), provides a simple control algorithm based on a look-ahead time and has been used by several studies in the past decade. The second one, the Four-Design-Choices Haptic Shared Controller (FDC-HSC), is a more recent development and is designed to contain a distinct feedforward and feedback component, meant to reduce human-haptic conflicts. Finally, usage of these two architectures with integration of the Van der El human controller, discussed in [Chapter **??**], is compared.

3.2.1. Meshed HSC

This section discusses a type of simple HSC that has been used frequently in recent research. First proposed by Mulder & Abbink [29], the controller was designed to provide haptic guidance for curve driving, in a continuous shared control task. The guidance was based on a future error between a reference trajectory (road center line) and the predicted position of the vehicle. Hence, the concept of a 'look-ahead time' is used here, which is one of the key parameters of the model. Scholtens [37] used the term 'Meshed' HSC (M-HSC) for this

type of controller, based on the fact that the haptic feedback is always dependent on the reference trajectory. This essentially means that any change in the reference trajectory will influence the given haptic feedback. The naming highlights the difference between the Meshed and Four-Design-Choices architecture, explained in Section 3.2.2.

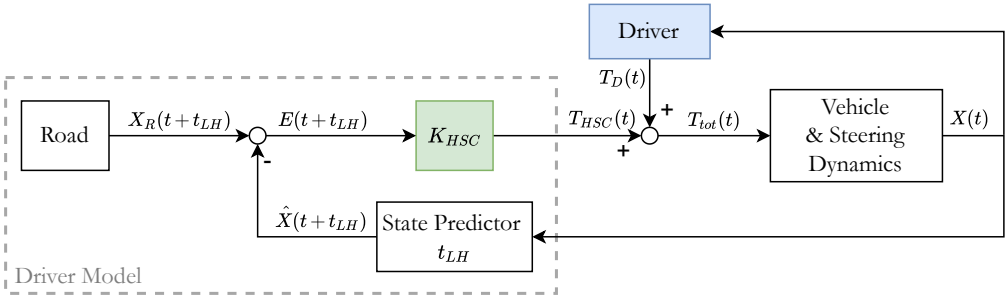

Figure 3.2: Meshed Haptic Shared Controller as developed by Mulder & Abbink [29], later used in [38] and [37]. (Recreated from [37])

The model architecture is shown in Figure 3.2. In this configuration, the haptic guidance is generated fully by a simple driver model. This model uses information from the road to generate a reference position located t_{LH} seconds away, denoted by $X_R(t+t_{LH})$. In a feedback path, it takes the current vehicle position $X(t)$ and predicts the future position at look-ahead time t_{LH}. Generally, this prediction is based on the current control torque given to the vehicle. A haptic control gain K_{HSC} is applied to the deviation of the predicted vehicle position from the reference, $E(t+t_{LH})$, to generate the haptic guidance torque T_{HSC}. Finally, the combined HSC and driver torque are added and fed to the steering wheel and vehicle, lumped in the Vehicle & Steering Dynamics block. The magnitude of the haptic guidance force is determined by K_{HSC}. Setting this parameter to a low value results in barely noticeable feedback torques, whereas choosing a high value can make a human driver unnecessary and result in full task automation [29]. Additionally, the look-ahead parameter t_{LH} can be tuned to include smoothing effects, as a longer look-ahead time results in starting the steering action earlier, and shorter times result in more aggressive steering [38].

The M-HSC was used by Boink [38], in an experiment focusing on human-haptic conflicts. As the haptic force feedback is generated from the error between target and vehicle output, the haptic guidance is fully dependent on the current driver's performance. The inherent linking of driver error and force feedback is believed to induce conflicts, as any deviation from the target results in a contradicting force. An additional effect is that when sharing control, the total torque applied to the steering wheel is always much higher than during manual control. Boink concluded that this type of 'simple' HSC algorithm is a source for conflict during curve driving, and a more sophisticated architecture was needed [38].

3.2.2. Four-Design-Choices HSC

A more elaborate haptic guidance design method is offered by Van Paassen's Four Design Choices [39]. These four independently designed choices are related to the *reference behavior*, *feedback control strategy*, *feedforward control strategy* and *level of authority*. Van Paassen suggests that in the design of HSC, following this philosophy can help reduce human-haptic conflict. The Four-Design-Choices HSC (FDC-HSC) is shown in Figure 3.3. Highlighted in the dotted boxes are the four design choices, which are explained below.

1. Human Compatible Reference (HCR) The first aspect is the reference trajectory, which should be aligned with the perception and strategy of the human operator. A Human-Compatible-Reference (HCR) is used as the target signal for the HSC, and can incorporate human-like behavior such as corner-cutting. The HCR often includes a driver model and the reference trajectory can be generated by fitting averaged trajectory data from earlier experiment runs to a driver model [37, 38]. The output of the driver model can contain the reference control input $\delta_R(t)$ and the reference output position $X_R(t)$.

2. Level of Haptic Support (LoHS) The applied control strategy that results from the HCR is split by two modes, of which the first one, named LoHS, is a pure feedforward path based on the desired steering input

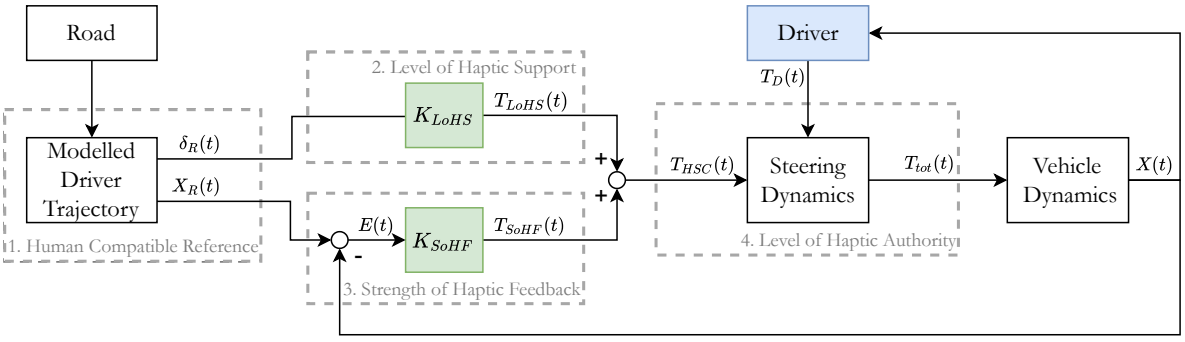

Figure 3.3: Four-Design-Choices Architecture in a shared control task. (Recreated from [39] and [37])

from the HCR. The portion of the guidance torque generated by the LoHS is independent from the current vehicle position, and is thus not affected by the driver's tracking performance. As such, the feedforward gain K_{LoHS} is separately tuneable and determines how much guidance towards the reference trajectory is given. For instance, a low LoHS would only provide haptic feedback when errors from the reference occur, such that a driver who is tracking the reference perfectly receives no force feedback. Conversely, a controller using a very high LoHS is able to track the reference without needing any driver inputs, based on the (future) reference trajectory. The input to the LoHS path can be the desired control input generated by the driver model, depicted by $\delta_R(t)$ in Figure 3.3.

3. Strength of Haptic Feedback (SoHF) The second portion of the haptic guidance is generated by a feedback component performing compensatory control, named Strength of Haptic Feedback (SoHF). The error $E(t)$ is calculated from the current vehicle position and the reference position $X_R(t)$ that is obtained from the HCR. The feedback gain K_{SoHF} determines how strongly the HSC corrects for deviations from the reference trajectory. A high SoHF gain compared to the LoHS gain results in a stronger haptic feedback when tracking performance is poor. Using a high haptic feedback gain is known to result in higher overall torque, and higher risk of conflicts [38].

4. Level of Haptic Authority (LoHA) Authority between driver and automation is determined by several factors, including the overall magnitude of the force feedback, and control device parameters such as damping, mass and stiffness. A higher stiffness of the steering wheel would require more effort for the driver to control. In turn, the driver can increase authority by applying more force to the control device and increasing stiffness of the muscles.

Scholtens [37] compared the F-HSC and M-HSC and revealed that conflict is greatly reduced when the F-HSC is used. Also, overall magnitude of torques during steering is reduced in the shared control task. It is suspected that both effects are mainly due to the separate feedforward path. The feedforward path provides constant guidance, which allows the driver to build trust in the system, and has a positive effect on the acceptance of the system.

3.2.3. Integration of the Van der El Model

Recent advances in modelling manual preview control have led to a better understanding of human behavior in tasks with preview. The human controller model developed by Van der El [5] is useful for identifying and simulating human control behavior, but this knowledge can also be used in the design of haptic shared controllers. The two different implementations of a shared control architecture, the M-HSC and the FDC-HSC, allow for integration of the Van der El model in two different ways, leading to two distinct controllers.

Integrating the Van der El model in the M-HSC architecture (Figure 3.2) can be achieved by replacing the simple driver model with the Van der El model. The resulting lay-out is shown in Figure 3.4, where the entire block diagram represents the dotted are in Figure 3.2. It involves replacing the original proportional feedback controller with the far-viewpoint filter, equalization and physical limitations blocks that model the inner hu-

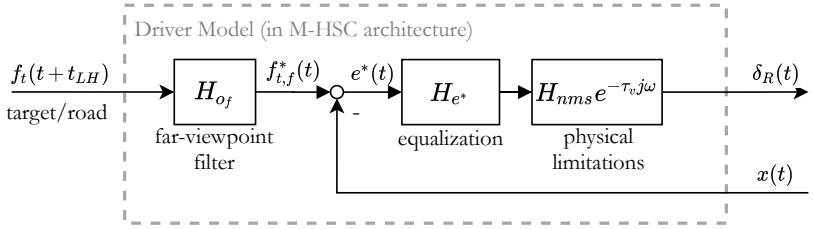

Figure 3.4: Integration of the Van der El human controller in the M-HSC architecture. This block corresponds to the "Driver Model" shown in Figure 3.2. in a shared control task. (Recreated from [39] and [37])

man control responses. The human controller model provides the haptic control input $\delta_R(t)$. This HSC still includes only a feedback path, and tuning the target response H_{o_f} cannot be done independently from the resulting haptic feedback. Thus, while including human control characteristics, the M-HSC with Van der El model integration still has the same limitations as the original M-HSC architecture.

In the FDC-HSC, the human compatible reference is provided by a driver model, which allows for integrating the Van der El model. In the resulting lay-out, shown in Figure 3.5, the dotted area represents the Human Compatible Reference area from Figure 3.3. A viewpoint t_{LH} seconds ahead on the outside environment or target signal is used as the input to the HCR. The outputs are the control input $\delta_R(t)$ and the position output $x_R(t)$, which are fed into the LoHS and SoHF paths, respectively. Note that the output signal, which is also fed into the feedback path, is generated by including a model of the controlled element dynamics H_{CE}. Furthermore, this implementation includes only the HCR, the outputs of which are fed into additional K_{LoHS} and K_{SoHF} gains as displayed in Figure 3.3, to be tuned separately. This allows for a proper application of the Four Design Choices philosophy, which includes a separately tuneable feedforward and feedback path.

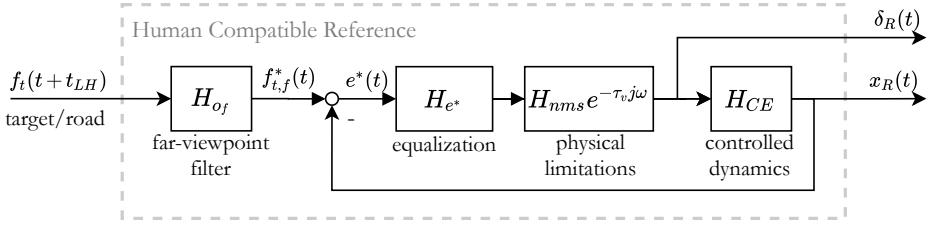

Figure 3.5: Integration of the Van der El human controller in the FDC-HSC architecture. This block corresponds to the "Human Compatible Reference" shown in Figure 3.3.

3.3. Conclusion

Haptic Shared Control is a promising method to combine manual driving and automation. This chapter provided the background information required for this thesis, and compared two relevant HSC models: the Meshed HSC and FDC-HSC. Whereas the Meshed HSC is a simple controller using only a feedback loop, the FDC-HSC improves human-haptic interaction by adding a separately tuneable feedforward path (LoHS) in addition to the feedback path (SoHF).

The remainder of this thesis will integrate the Van der El model (discussed in Chapter 2) with an HSC. In this chapter it was shown how this can be achieved for both the Meshed HSC and the FDC-HSC. The difference between the two types is that in the Meshed configuration, Van der El's human controller model fully describes the HSC, while in the FDC configuration, the model generates the human-compatible reference. It is expected that the FDC-HSC architecture will offer a better user experience and less conflict in a shared control task, as it both adds human-like steering through the HCR, and offers more tuning freedom by having the separate LoHS and SoHF gains. Simulations will be performed between both configurations, as covered in Chapter 4.

4

Offline Simulations

As an initial analysis, human-haptic performance in a preview tracking task will be simulated. The simulation considers a setup similar to the one that will be used in the human-in-the-loop experiment. Using Van der El's model for preview tracking [5], the human operator (HO) and a haptic shared controller (Meshed HSC) are simulated. In addition, simulation runs will be done using a Four Design Choices HSC (FDC-HSC). The goal of these simulations is to obtain initial knowledge on the effects of changing haptic *look-ahead time*, which is the key parameter of interest for this thesis work. These insights will form the basis of choosing the conditions for the human-in-the-loop experiment.

4.1. Setup

The simulations are run in MATLAB using the Simulink toolbox. The control task is a preview tracking task in which the HO and HSC, both modeled using the Van der El model, act on a controlled element (H_{CE}) through a stick (H_{stick}) in order to reduce the tracking error. A block diagram depicting the control task as implemented in the simulation is shown in Figure 4.1.

4.1.1. Control Task

The simulated HO and HSC share control by both applying input forces to a stick model H_{stick}, which is connected to the controlled element H_{CE}. The stick is modeled as a spring-damper system with $b = 0.20$ Nms/rad and $k = 3.58$ Nm/rad. The stick model outputs the stick deflection angle u in radians, which is the input to the controlled element H_{CE}. Two types of controlled element dynamics are tested: single integrator (SI) and double integrator (DI) dynamics. The respective transfer functions are shown in Table 4.2.

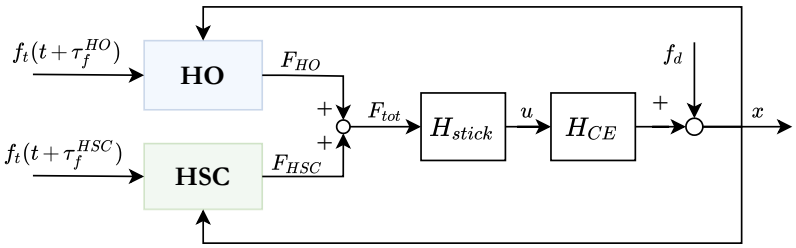

Figure 4.1: Block diagram of the simulated control task

The control task is simulated using two forcing functions: a target signal f_t that is tracked by the HO and HSC, and a disturbance function f_d that is added to the controlled element output. Often, human-in-the-loop experiments use two forcing functions in order to identify multi-loop human dynamics [5, 40]. Although human model identification is out of the scope of this preliminary thesis, the same familiar setup using two forcing functions is used in order to be consistent with earlier experiments. The forcing functions are multi-sine signals generated by Equation (4.1), where $N_f = 10$. The remaining function parameters are shown in

Table 4.1. The signals are periodical over a measurement time of 120 s. Both signals have a bandwidth of approximately 1.5 rad/s, above which the amplitudes are attenuated by 20 dB, such that higher frequencies are less dominantly present in the signal. The standard deviation of the target signal is $\sigma_t = 1.27$ cm. For the disturbance signal, $\sigma_d = 0.51$ cm. Figure 4.2 shows the forcing function spectra.

$$f(t) = \sum_{i=1}^{N_f} A_i \sin(\omega_i t + \phi_i) \tag{4.1}$$

Table 4.1: Parameters for the multisine target and disturbance functions used in the simulations.

target signal f_t				disturbance signal f_d			
k_t -	A_t cm	ω_t rad/s	ϕ_t rad	k_d -	A_d cm	ω_d rad/s	ϕ_d rad
3	0.731	0.157	4.488	4	0.292	0.209	0.241
5	0.731	0.262	5.699	7	0.292	0.367	1.669
8	0.731	0.419	1.373	9	0.292	0.471	1.899
11	0.731	0.576	5.472	13	0.292	0.681	1.295
19	0.731	0.995	1.331	22	0.292	1.152	3.982
29	0.731	1.518	5.257	31	0.292	1.623	4.496
47	0.731	2.461	5.399	51	0.292	2.670	3.365
77	0.731	4.032	3.289	79	0.292	4.136	0.469
143	0.731	7.488	2.999	147	0.292	7.697	0.964
263	0.731	13.77	5.591	267	0.292	13.98	4.296

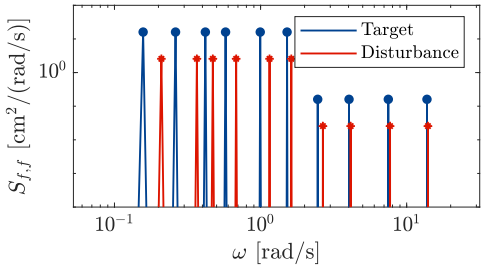

Figure 4.2: Power spectra of target and disturbance

4.1.2. Human Operator Model

The HO block in this control task, shown in Figure 4.3, is modeled using the Van der El human controller [5]. A more detailed explanation of this model can be found in Chapter 2. The model allows the implementation of a *far-viewpoint* τ_f^{HO} as the input, which is a future point on the target signal f_t. The response to this signal is modeled using a low-pass filter H_f^{HO} with gain K_f and time constant $T_{l,f}$. The resulting filtered signal $f_{t,f}^*$ is the input to a compensatory model structure, where the internal error e^* is to be minimized. This feedback loop is modeled by a human equalization function, which is McRuer's *precision model* [4]. For SI controlled element dynamics, $H_{e^*}^{HO} = K_{e^*}$ whereas for DI dynamics a lead term is included and $H_{e^*}^{HO} = K_{e^*}(T_{L,e}j\omega+1)$ as per McRuer's *crossover model*. The HO response includes neuromuscular limitations H_{nms}^{HO} and a time delay τ_v. In its original form, the HO model outputs a stick deflection u, but in the context of haptic force feedback, a force F is needed. To achieve this, the HO and HSC model outputs are multiplied by an inverse of the same stick model H_{stick}^{-1}. Finally, an overall HO gain, K_{HO} is added in order to determine the contribution of the HO in the HO-HSC shared control system. In this simulation, this is set to 0.5.

The baseline values for the model parameters are displayed in Table 4.2. The initial simulations use exactly the same model structure and parameters for the HSC as for the HO. The only parameter that is varied is the look-ahead time τ_f^{HO}.

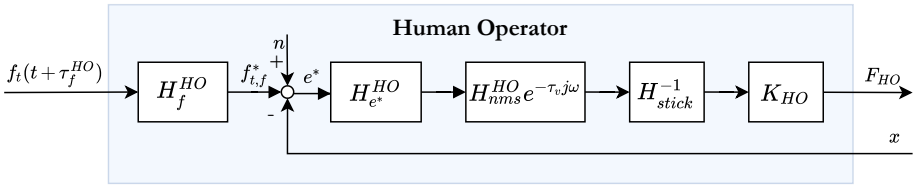

Figure 4.3: Block diagram of the HO model used in the simulation.

To simulate the inherently stochastic nature of human control behavior, remnant noise (n) is included. In order to create a noise signal that is representative, empirical results from [41] are used. These suggest that the portion of the control output power that is due to the remnant, expressed as $\sigma_{u_n}^2/\sigma_u^2$ should be approximately 0.35 for SI dynamics, and 0.5 for DI dynamics. Furthermore, the noise is filtered using a low-pass filter with a break frequency ω_b of 3.5 rad/s for SI dynamics and 0.5 rad/s for DI dynamics [41]. Consistent with the setup

Table 4.2: Baseline model parameters

	H_{CE}	τ_f [s]	K_f [-]	$T_{l,f}$ [s]	K_{e^*} [-]	T_{L,e^*} [s]	τ_v [s]	ω_{nm} [rad/s]	ξ_{nm} [-]
SI	$1.5/(j\omega)$	0.60	1.0	0.20	1.25	-	0.26	10.5	0.35
DI	$5/(j\omega)^2$	1.10	0.80	0.85	0.25	1.50	0.30	8.0	0.45

from [41], the remnant signal n is added to the output $x(t)$ in the HO feedback signal (shown at the top in Figure 4.1). The simulation is done with 100 remnant realizations. In order to obtain the correct $\sigma^2_{u_n}/\sigma^2_u$, a pre-simulation is done to determine the noise gain K_n. This was done with only human operator, so no HSC influence is included. The outcome of the pre-simulations resulted in a K_n of 3.4 for SI dynamics, and 9.5 for DI dynamics.

4.1.3. Haptic Shared Controller

The simulation is performed for two different HSC configurations. The Meshed-HSC, where the HSC is the Van der El human controller model and thus a mirror of the HO model, and the FDC-HSC, which implements the Van der El model as the human-compatible reference in a FDC type controller. These HSC setups are explained in this section.

Controller A: Meshed-HSC In the first setup, the HSC block is represented by the Meshed-HSC structure shown in Figure 4.4. The term 'meshed' refers to the fact that the HSC force feedback is coupled to the HO control output through the feedback path x. Therefore the haptic feedback that is provided is always dependent on the human's task performance. The controller is made out of the same human controller model that simulates the HO. This is done in order to simulate a shared control situation in which the HSC is capable of perfectly mirroring the HO's control behavior. The baseline parameters used are thus identical to the ones in the HO, shown in Table 4.2. The focus in the simulations is on look-ahead time τ_f^{HSC}, which is the only parameter that is varied. The overall haptic gain K_{HSC} is set to 0.5, equal to the HO gain, such that the combined gain is 1. This means that both HO and HSC contribute equally to the control task, if the other parameters are equal.

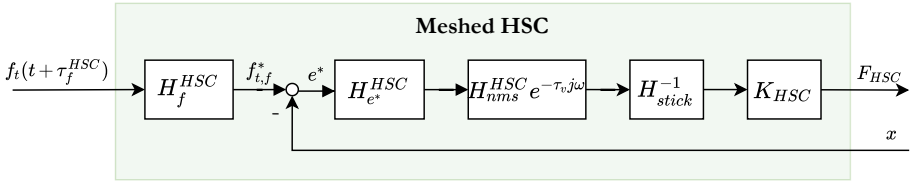

Figure 4.4: Block diagram of the Meshed HSC, with the same implementation of the HO model, but without remnant.

Controller B: FDC-HSC A limitation of the Meshed-HSC is that the haptic support cannot be tuned independently from the current output x. The FDC-HSC (Figure 4.5) addresses this problem by separating the haptic support in a feedforward path, denoted by level of haptic support (LoHS), and a feedback path, named strength of haptic feedback (SoHF). As opposed to the Meshed-HSC, which is fully described by the Van der El model, the FDC-HSC uses the Van der El model to generate a human-compatible reference (HCR). The model is simulated in a closed-loop setup using a model of the controlled element, H_{CE}, which is identical to the actual controlled element in the simulation. This way, the HCR outputs a reference stick force F_R and a reference output position x_R, which are fed into the LoHS and SoHF path, respectively. Tuning K_{LoHS} determines how much guidance is given independently from the current task output, while K_{SoHF} determines how strongly deviations from the reference are corrected. Finally, an overall gain K_{HSC} is used in the simulation to set the total contribution of the HSC to the combined HSC-HO controller. For the simulations in this chapter, this is set to 0.5.

Note that when H_{CE} has DI dynamics, the SoHF block should include a lead-term, in order to make the system controllable. This means that instead of a gain K_{SoHF}, the block will contain $K_{SoHF}(T_{SoHF}s+1)$. This

is identical to having an error gain $K_e = K_{SoHF}$ and error rate gain $K_{\dot{e}} = K_{SoHF} T_{SoHF}$, which will both be used in the remainder of this chapter. The HCR already incorporates the lead term for DI control tasks in $H_{e^*}^{HSC}$, the same way the Van der El model does in the HO and Meshed HSC configuration.

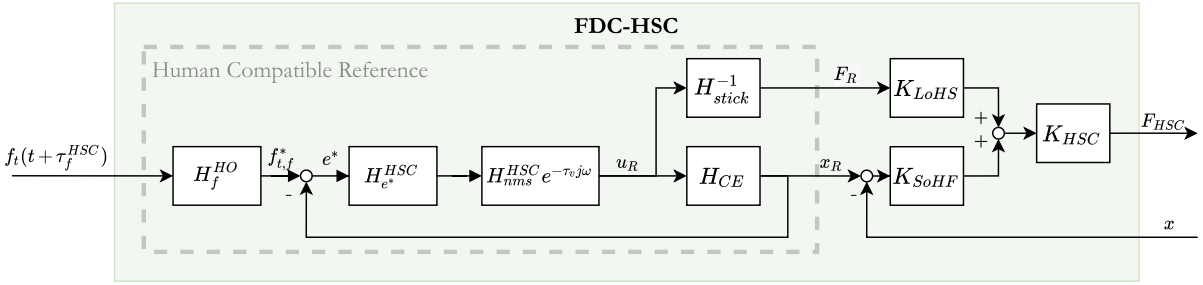

Figure 4.5: Block diagram of the FDC-HSC, with implementation of the Van der El model for the Human Compatible Reference portion of the FDC architecture.

4.2. Method

Using a baseline setup as described in Section 4.1, with two types of HSC, two sets of simulations are run. In the first simulation (**I**), the HO is kept constant while the HSC look-ahead time τ_{HSC} is varied between 0 and 2 seconds. In the second simulation (**II**), the HO look-ahead time τ_{HO} is varied for three HSC look-ahead times: the baseline value, a low look-ahead time and a high look-ahead time. An overview of the simulation settings is shown in Table 4.3, which will be executed for the Meshed HSC and the FDC-HSC.

Table 4.3: Overview of HO and HSC look-ahead time settings for simulation **I** and **II**.

	SI		**DI**	
	$\tau_{f,HO}$ (s)	$\tau_{f,HSC}$ (s)	$\tau_{f,HO}$ (s)	$\tau_{f,HSC}$ (s)
I	0.6	[0, 2]	1.1	[0, 2]
	[0, 2]	0.0	[0, 2]	0.0
II	[0, 2]	0.6	[0, 2]	1.1
	[0, 2]	1.2	[0, 2]	2.0

The simulation runs are done using SI and DI controlled element dynamics (H_{CE}). Typically, DI dynamics are more difficult to control and require a lower gain for a stable system. It is also expected that performance will be more sensitive to changing parameters, and possibly the effect of haptic support will be stronger. Comparison between two simulation outcomes will be taken into account in choosing the controlled element dynamics for the human-in-the-loop experiment.

The output of the simulation includes the controlled element output x, and separate input forces F_{HO} and F_{HSC}. In order to compare haptic-human performance for varying parameter settings, the variances of the input forces ($\sigma^2_{F,HO}$, $\sigma^2_{F,HSC}$) are considered. As a measure of overall performance, the tracking error (σ_e^2) is calculated. Finally, as a measure of total control activity, the variance of the stick deflection σ_u^2 is used. Conflict between human and haptic inputs is calculated by Equation (4.2), which defines occurrence of conflict where the directions of inputs are opposite. A conflict occurs when this is the case, and the magnitude of conflict relative to the total input magnitude is higher than a threshold c. Here, $c = 0.05$ which means that conflict is only counted when the difference between human and haptic inputs is larger than 5% of the combined input. The average $\bar{O}_{conf}$ is used as an indication of how often conflict occurred during a run, where a value of 1 indicates conflict during the entire run, and a value of 0 indicates no conflict at all. Finally, the integrated magnitude difference between haptic and human input, M_{conf} (Equation (4.3)), is used as an indication of severity of conflict. This is calculated by summing the force differences at the instances where conflict occurs.

$$O_{conf}[i] = \begin{cases} 1 & \text{if } F_{HO}[i] \cdot F_{HSC}[i] < 0 \text{ and } \frac{|F_{HO}[i] - F_{HSC}[i]|}{F[i]} > c \\ 0 & \text{otherwise} \end{cases} \tag{4.2}$$

$$M_{conf} = \sum_{i=1}^{N} O_{conf}[i] \cdot \left| F_{HO}[i] - F_{HSC}[i] \right| \cdot \mathrm{dt} \tag{4.3}$$

4.3. Results: Meshed HSC

This section discusses the results of the simulations with the Meshed HSC configuration. The shared control runs are split into simulation I (Section 4.3.2) and simulation II (Section 4.3.3). Before that, a brief analysis of the HO and HSC performance in 'solo' setup (not sharing control) under varying look-ahead times is provided here.

4.3.1. HO and HSC solo performance

For reference, the control task was first simulated with only the HO in the loop, to show control behavior without HSC influence. Then, the same was done with only the HSC in the loop. Note that the meshed HSC configuration is the same as the HO, so the only difference between the two is the added noise. The resulting plots, displayed in Figure 4.6, show the influence of look-ahead parameter τ_f ($\tau_{f,HO}$ and $\tau_{f,HSC}$, respectively) on tracking error e and HO and HSC control force F, and can also be used to show the effect of adding remnant noise. A sample run is plotted in Figure 4.8 for each of the simulations.

For both controllers, the error is minimal around $\tau_f = 0.6$ s and $\tau_f = 1.1$ s, for SI and DI dynamics respectively. Indeed these are equal to the baseline HO parameters displayed in Table 4.2, which have been chosen such that good stability and performance is achieved. These look-ahead times also match the critical preview times from previous experiments [17, 40], as discussed in Chapter 2 as well. The control force F stays constant for all τ_f, indicating that changing the look-ahead point does not require extra control activity to follow the target. The control output is lower for DI dynamics than for SI dynamics, as high control activity results in an unstable system. The error for the DI task is higher than the SI task, as expected due to the inherently less stable system that is more difficult to control. These results are thus fully consistent with literature [40].

Between the HO and HSC, there is a significant difference for the error and control force. For the HO, the added remnant noise appears to cause an increase in error and control force, by an absolute amount that is constant for every τ_f. Relatively, the HO's minimum error is more than twice as high for both SI and DI tasks. As τ_f moves away from the optimum in both directions and the error increases, the relative difference between HO and HSC error becomes less significant. The HO control force, invariant for τ_f, is twice as high in the SI task, and more than 4 times as high in the DI task. The HSC, steering without added noise, is able to achieve a lower minimum error using a much lower control force to achieve this. These differences can also clearly be observed in the time traces in Figure 4.8. Overall, while the effect of the remnant noise is large, it is not to such extent that the HO cannot successfully control the system anymore, as reasonable error scores are achieved.

The plots discussed here provide a good reference of how the respective controllers behave in solo setup.

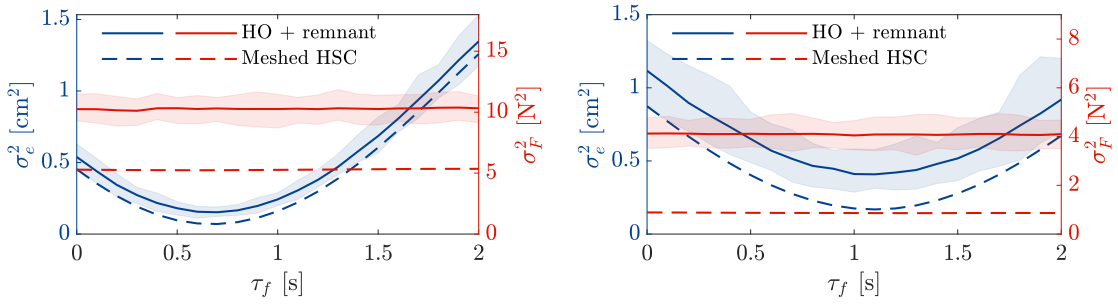

(a) SI, error and input

(b) DI, error and input

Figure 4.6: Outcome of simulation runs with HO and HSC separately. Influence of look-ahead time τ_{HO} on tracking error variance σ_e and control output variance σ_F

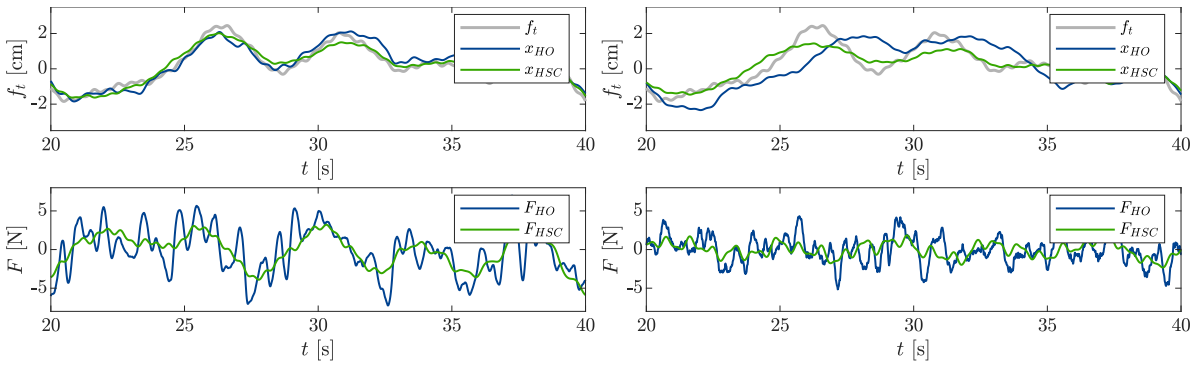

(a) SI, output and input, τ_f = 0.6 s

(b) DI, output and input, τ_f = 1.1 s

Figure 4.8: Partial time traces showing how the HO and Meshed HSC perform in solo setup. Single runs, using the baseline τ_f values.

These results will be referred to when analyzing the remainder of the simulations in this section, which are conducted in a shared control setup. Section 4.4.3, covering the FDC-HSC results, will also use these reference values to compare the FDC to the Meshed configuration.

4.3.2. Meshed HSC Simulation I: Varying $\tau_{f,HSC}$

In the first shared control simulation, the HSC look-ahead time is varied. Figure 4.9 shows the result of varying look-ahead time $\tau_{f,HSC}$ for 100 remnant realizations. For both the SI and DI control tasks, the achieved error is lower than in the simulations without HSC (Figure 4.6), at a cost of slightly higher control activity. The control output u is largely constant, similar to the HO reference behavior (Figure 4.6). For the SI task, minimum error is achieved around $\tau_{f,HSC}$ = 0.75 s, which is slightly higher than the baseline of $\tau_{f,HO}$ = 0.6 s (indicated by the dotted line). At the same point, with $\tau_{f,HSC}$ slightly higher than $\tau_{f,HSC}$, the applied forces F_{HO} and F_{HSC} are equal. The amount of conflict occurring ($\bar{O}_{conf}$) is at its minimum around $\tau_{f,HSC}$ = 0.55 s, and it is seen that the magnitude of conflict (M_{conf}) follows the same trend. As the haptic look-ahead time is increased, conflict and error increase. The distribution of control forces between HO and HSC changes such that the HSC applies more force to the stick. It thus be stated that the controller with a larger look-ahead time, applies more force in the shared control task.

Note that while all parameters are equal if $\tau_{f,HSC} = \tau_{f,HO}$, both controllers do not show equal behavior due to the added remnant noise, which is only added to the HO. Without remnant noise, conflict would be zero and $F_{HO} = F_{HSC}$ when $\tau_{f,HO} = \tau_{f,HSC}$. The added remnant noise makes these simulations interesting, because in real-life situations the HO would never show behavior equal to the HSC.

A comparison between the SI task and the DI task shows different results, however, the trends are similar. The differences occur mainly due to the added remnant that has a much higher contribution to the input for the DI task ($\sigma^2_{u_n}/\sigma^2_u$ = 0.5 versus $\sigma^2_{u_n}/\sigma^2_u$ = 0.35). This is reflected in the fact that the spread of values around the mean is much higher for all variables. The error is minimal around the baseline of $\tau_{f,HSC} = \tau_{f,HO}$ = 1.1 s. The same goes for the average amount of conflict and the magnitude of conflict, $\bar{O}_{conf}$ and M_{conf}, respectively. The human-haptic control forces are influenced less by changing look-ahead times for the DI task than for the SI task. On the 0-2 seconds domain, the noisy HO is always applying a higher control force than the HSC.

A sample output time series is plotted in Figure 4.11, for the SI task. In the sample shown here, $\tau_{f,HSC}$ = 1.7 s, which is much higher than $\tau_{f,HO}$, which is equal to 0.6 s. The different strategies between the two controllers can be clearly seen. The HSC, which uses a larger look-ahead time, applies more smoothing and responds to lower frequencies. The HO uses the signal closer ahead, and responds to higher frequencies. This causes conflict, marked in red, to occur at places where large low-frequency oscillations occur. Here the HSC tries to follow the lower frequency movement, while the HO still compensates for higher frequency oscillations.

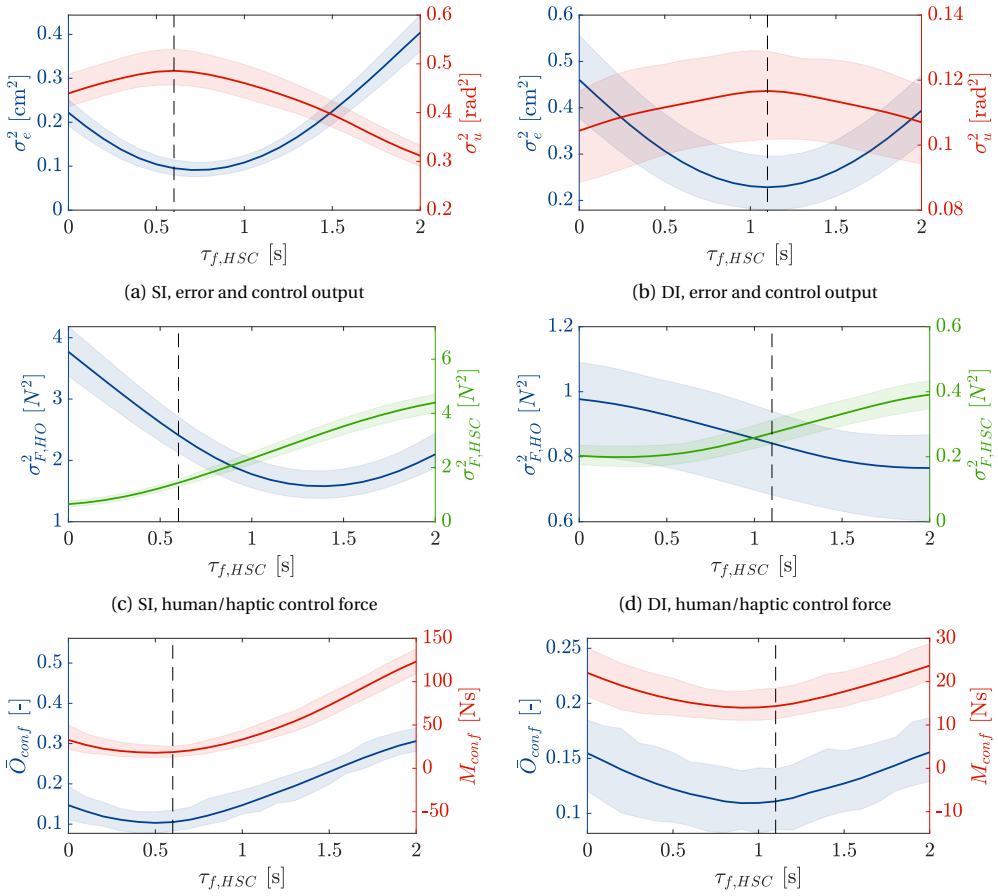

(a) SI, error and control output

(b) DI, error and control output

(c) SI, human/haptic control force

(d) DI, human/haptic control force

(e) SI, conflict

(f) DI, conflict

Figure 4.9: Effects of varying haptic look-ahead time $\tau_{f,HSC}$ on control input and error. The left hand-side shows results for SI dynamics, the right hand-side for DI dynamics. The dotted black line indicates the baseline value $\tau_{f,HO}$ = 0.6 (SI) and $\tau_{f,HO}$ = 1.1. The light areas include the results for 100 remnant realizations, with the line representing the mean result.

4.3.3. Meshed HSC Simulation II: Varying $\tau_{f,HO}$

Figure 4.10 shows the results of the second simulation, where HO look-ahead time $\tau_{f,HO}$ is varied. This was done for three HSC look-ahead times $\tau_{f,HSC}$ = 0, 0.6, 1.2 s for SI dynamics and $\tau_{f,HO}$ = 0, 1.1, 2.0 s for DI dynamics. These values cover the baseline value as well as two extreme values. The error plots show that for baseline parameter $\tau_{f,HO} = \tau_{f,HSC}$ = 0.6 s (SI) and 1.1 s (DI), the error is lowest, similar to the results from simulation I. These values are the optimal look-ahead times at which the HO achieves the lowest error. It thus follows that when the HSC look-ahead time is zero, the best performance is not achieved when HO look-ahead time is zero as well. In fact for the SI task at setting $\tau_{f,HSC}$ = 0 s, minimal error is achieved around $\tau_{f,HO}$ = 1.0 s. Here, as $\tau_{f,HSC}$ is much lower than the optimal value, $\tau_{f,HO}$ needs to be higher in order to compensate. Vice versa, for $\tau_{f,HSC}$ = 1.2 s, minimal error occurs around $\tau_{f,HO}$ = 0.4 s.

For each of the three $\tau_{f,HSC}$ settings, the control forces are equal at $\tau_{f,HO} = \tau_{f,HSC}$. This fact thus remains consistent even when changing the look-ahead times away from the optimal values. The same is valid for the amount of conflict, which is minimum when $\tau_{f,HO} = \tau_{f,HSC}$.

The differences between using SI and DI controlled element dynamics remain similar to the results of simulation I. Force inputs are influenced less by varying look-ahead times in the DI case than in the SI case.

A sample output time series is plotted in Figure 4.11, for the DI task. Compared to the output sample from SI dynamics, it is seen that the input forces are much lower. Here the HO has a higher look-ahead time than the HSC (1.7 s versus 1.1 s), which would mean the HO should respond to mainly low frequencies. However, due to the added remnant noise, high frequency oscillations remain present in the HO signal.

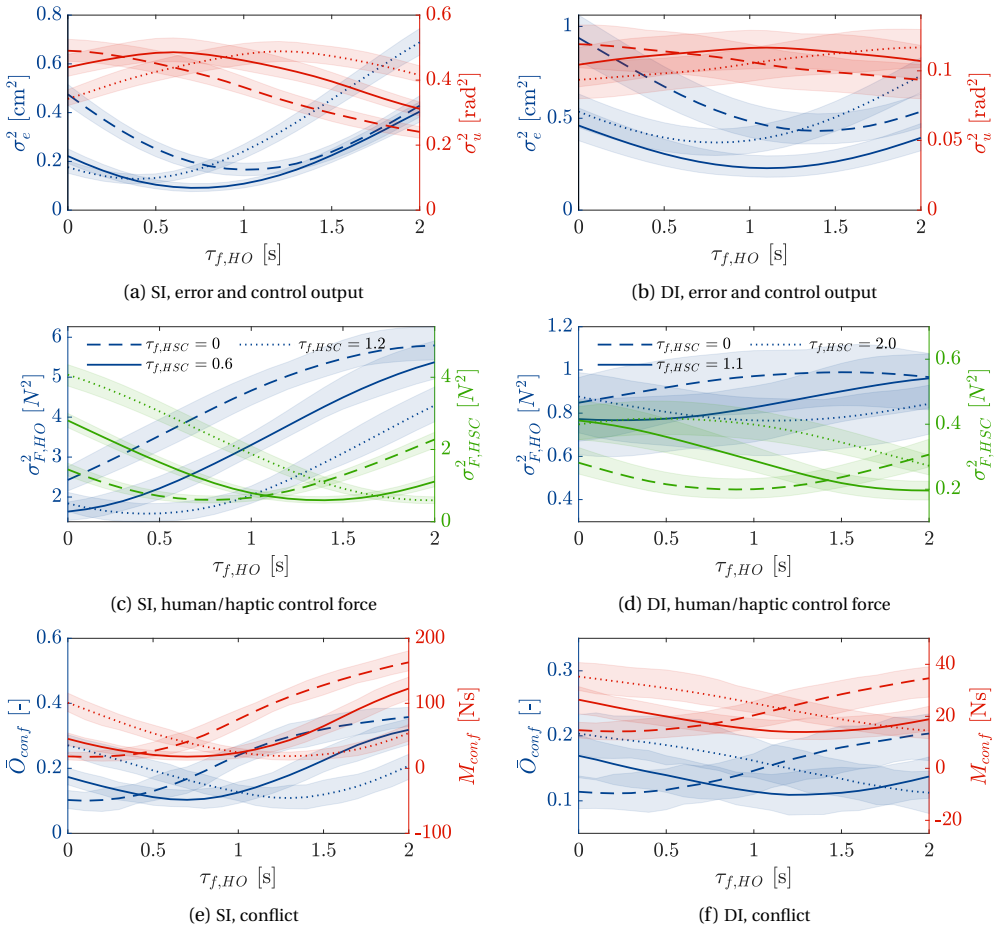

(a) SI, error and control output

(b) DI, error and control output

(c) SI, human/haptic control force

(d) DI, human/haptic control force

(e) SI, conflict

(f) DI, conflict

Figure 4.10: Effects of varying human look-ahead time $\tau_{f,HO}$ on control behavior. The left hand-side shows results for SI dynamics, the right hand-side for DI dynamics. The light areas include the results for 100 remnant realizations, with the line representing the mean result.

4.4. Results: FDC-HSC

In this section the second setup, in which the HO shares control with the FDC-HSC, is simulated. In the FDC configuration, the additional LoHS and SoHF gains need to be tuned, as opposed to the Van der El model parameters which are taken from literature. The tuning and analysis of the FDC gains is covered in Section 4.4.1. After this, Sections 4.4.2 and 4.4.3 discuss the results of simulations I and II.

4.4.1. Tuning SoHF and LoHS gains

For the SI control task, the SoHF is described by a single error gain K_{SoHF}, whereas for the DI task, two gains K_e and $K_{\dot{e}}$ are used (For an explanation, refer to Section 4.1.3). The feedforward gain K_{LoHS} is used in both SI and DI tasks. Given that the HCR model is simulated using the same controlled element dynamics (H_{CE} is equal in the HCR block and in the control task), the reference control force F_R is equal to the force required to successfully execute the control task *without disturbance*. Hence, if the LoHS gain is 1 and no disturbance signal is added to the output, technically no SoHF gain is needed. However, the task will be done with added disturbance, so for that the feedback gain K_{SoHF} will be tuned.

Tuning will be done by comparing the tracking error $\sigma_{e,HSC}$ (as a measure of task performance) and stick force $\sigma_{F,HSC}$ (as a measure of control effort) to the values achieved by the Meshed HSC. The FDC-HSC should perform at least as well as the Meshed HSC, which means that the error and control force should be lower.

First, the gain for the SI task is tuned. This is done for a feedforward gain of K_{LoHS} = 1, such that the task

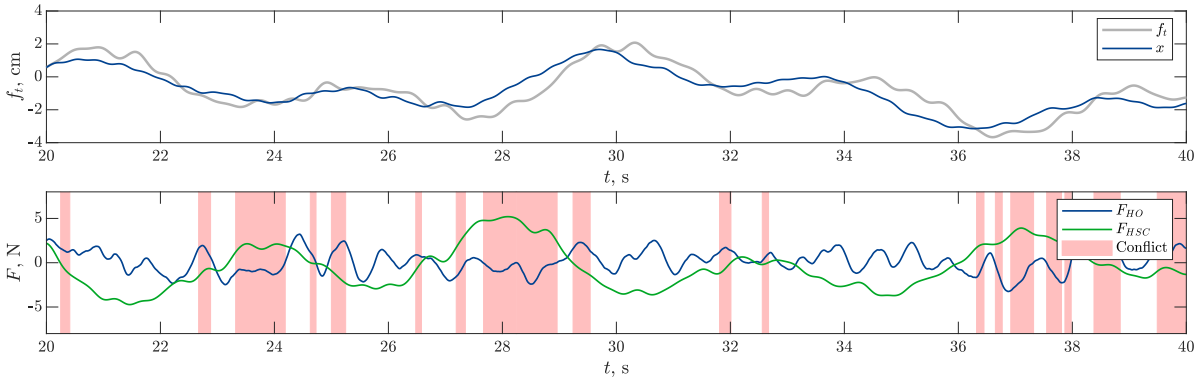

Figure 4.11: Example timeseries from simulation II for SI dynamics, with $\tau_{f,HSC}$ = 1.7, $\tau_{f,HO}$ = 0.6 s, and $\bar{O}_{conf}$ = 0.26. The top plot shows the output and the target function, the bottom shows the input forces given to the stick by the HO and HSC. Conflict is marked in red marked areas.

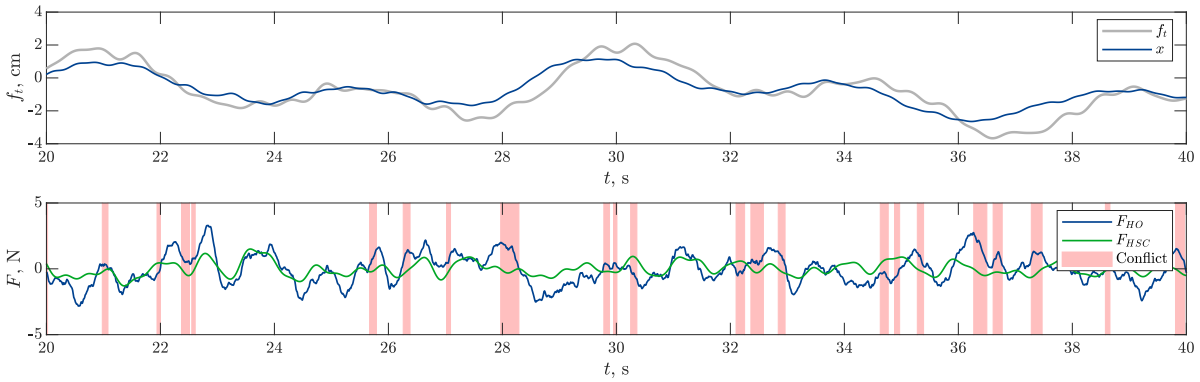

Figure 4.12: Example timeseries from simulation II for DI dynamics, with $\tau_{f,HSC}$ = 1.1, $\tau_{f,HO}$ = 1.7 s, and $\bar{O}_{conf}$ = 0.12. The top plot shows the output and the target function, the bottom shows the inputs given to the controlled element by the HO and HSC. Conflict is marked in red marked areas.

is fully automated by the HSC. Figure 4.13a shows how the error and control force are influenced by varying K_{SoHF}. The dotted horizontal lines indicate the minimum error and stick force achieved by the Meshed HSC. Taking into account these minimum requirements, the optimal K_{SoHF} is around 4.8.

The DI task uses the gains K_e and $K_{\dot{e}}$ instead of single SoHF gain. The effect of varying the error rate gain $K_{\dot{e}}$ is shown in Figure 4.13b for an error gain K_e of 1 and 0.5. For K_e = 0.5, the error and force requirement cannot be met for any $K_{\dot{e}}$. However, for $K_{\dot{e}}$ a notable improvement can be achieved by setting the error rate gain anywhere between 1.2 and 1.5. For the remainder of this section, the error rate gain is therefore set to $K_{\dot{e}}$ = 1.4. A summary of the chosen gains is shown in Table 4.4.

Table 4.4: Tuned FDC gains used in the simulations (as a result of Figure 4.13)

	K_{LoHS}			K_{SoHF}	
	C1	C2	C3		
SI	1.0	0.5	0.25	4.8	
				K_e	$K_{\dot{e}}$
DI	1.0	0.5	0.25	1.0	1.4

4.4.2. FDC-HSC Simulation I: Varying $\tau_{f,HSC}$

The first simulation is done by varying $\tau_{f,HSC}$, keeping $\tau_{f,HO}$ constant ($\tau_{f,HO}$ = 0.6 for SI, $\tau_{f,HO}$ = 1.1 for DI). As the extra feedforward path in the FDC-HSC, described by K_{LoHS}, is an important characteristic of this controller, three conditions regarding the LoHS are tested to investigate the effect. In conditions C1, C2 and

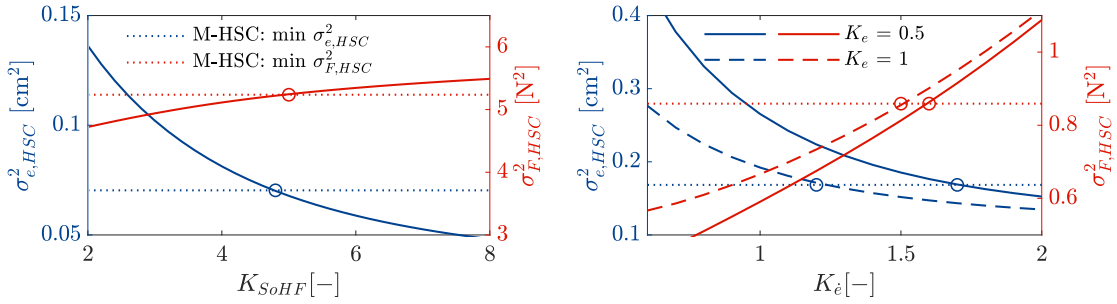

(a) SI, error and input

(b) DI, error and input

Figure 4.13: Resulting error and control force when varying SoHF gain, plotted for three different LoHS gains.

C3, the LoHS gain is set to a high (nominal), middle and low value, respectively. Table 4.4 shows the FDC gains as used in the simulations. Note that still, for the sake of the simulation, the additional HSC and HO gains of $K_{HSC} = K_{HO} = 0.5$ are included, because the outputs two individually tuned systems are added together. Keeping K_{HO} constant for all conditions also implies an important assumption, namely that the HO does not adapt to changing HSC settings, which is unlikely in real-life situations.

The simulation results are displayed in Figure 4.14. The baseline, fixed HO look-ahead time is indicated by the vertical striped line. Looking at the influence of changing $\tau_{f,HSC}$ on performance, the same trends can be recognized for the FDC-HSC as for the Meshed HSC. Figure 4.14a (SI) and Figure 4.14b (DI) reveal that a minimum error can be achieved, and it corresponds to a maximum control input σ^2_u given. The $\tau_{f,HSC}$ location where the minimum occurs, depends on the chosen K_{LoHS} condition. In the nominal condition ($K_{LoHS} = 1$), the minimum error occurs when the HSC look-ahead time is close to the HO look-ahead time, i.e $\tau_{f,HSC} \approx \tau_{f,HO}$. As K_{LoHS} is lowered, optima shift to a higher $\tau_{f,HSC}$. This suggests that the HSC needs to compensate a weaker gain by increasing the look-ahead time in order to achieve the best possible performance. Looking at Figure 4.14c and **??**, the largest part of the input force around this point is provided by the HO. This changes as the HSC look-ahead time increases, and the HSC control forces increases while the HO's decreases. Similar to the results from the Meshed HSC, the 'break-even' or 'equally' shared control ($\sigma^2_{f,HSC} = \sigma^2_{f,HO}$) occurs when the HSC look-ahead time is much higher than the HO's. This too, is dependent on the set LoHS gain. A lower K_{LoHS} is matched with the 'break-even' occurring at a higher $\tau_{f,HSC}$. For the SI, a nominal $K_{LoHS} = 1$ results in equally shared control around $\tau_{f,HSC} = 0.75$. For the DI task, the trend suggests that this point exists somewhere outside of the domain tested in this simulation, for a very high $\tau_{f,HSC}$. However, while results for higher look-ahead times exist in simulations, they have no real application in real-life situations as no significant HO adaptation occurs after a critical preview time [17].

Occurrence of conflict is shown in Figures 4.14e and 4.14f. Similar to the observed error, conflict is minimal around $\tau_{f,HSC} = \tau_{f,HO}$ for the nominal case of $K_{LoHS} = 1$. This minimum shifts to slightly higher HSC look-ahead times for the other, lower LoHS gain conditions. Overall it can be observed that to achieve a minimal conflict, the HSC look-ahead time should be closer to the HO look-ahead time than for achieving minimal error. The integrated magnitude of conflict, M_{conf}, increases along with an increasing occurrence of conflict $\bar{O}_{conf}$.

The differences between the SI and the DI task are as expected: when controlling a DI system, lower input forces and thus lower stick deflections are applied. Doing this, the minimum error that can be achieved is higher than for the SI task. Changing the look-ahead time in a DI task has a much lower impact on the control forces than in a SI task.

4.4.3. FDC-HSC Simulation II: Varying $\tau_{f,HO}$

Through simulation II a similar analysis is provided, but here the HO look-ahead time $\tau_{f,HO}$ is varied, while $\tau_{f,HSC}$ is kept constant at the same baseline values ($\tau_{f,HSC} = 0.6$ for SI, $\tau_{f,HSC} = 1.1$ for DI). The FDC gains and conditions are the same as for simulation I, and shown in Table 4.4. While simulation I and II are similar, due to a different approach slightly different results are expected, based on the difference between the HO and

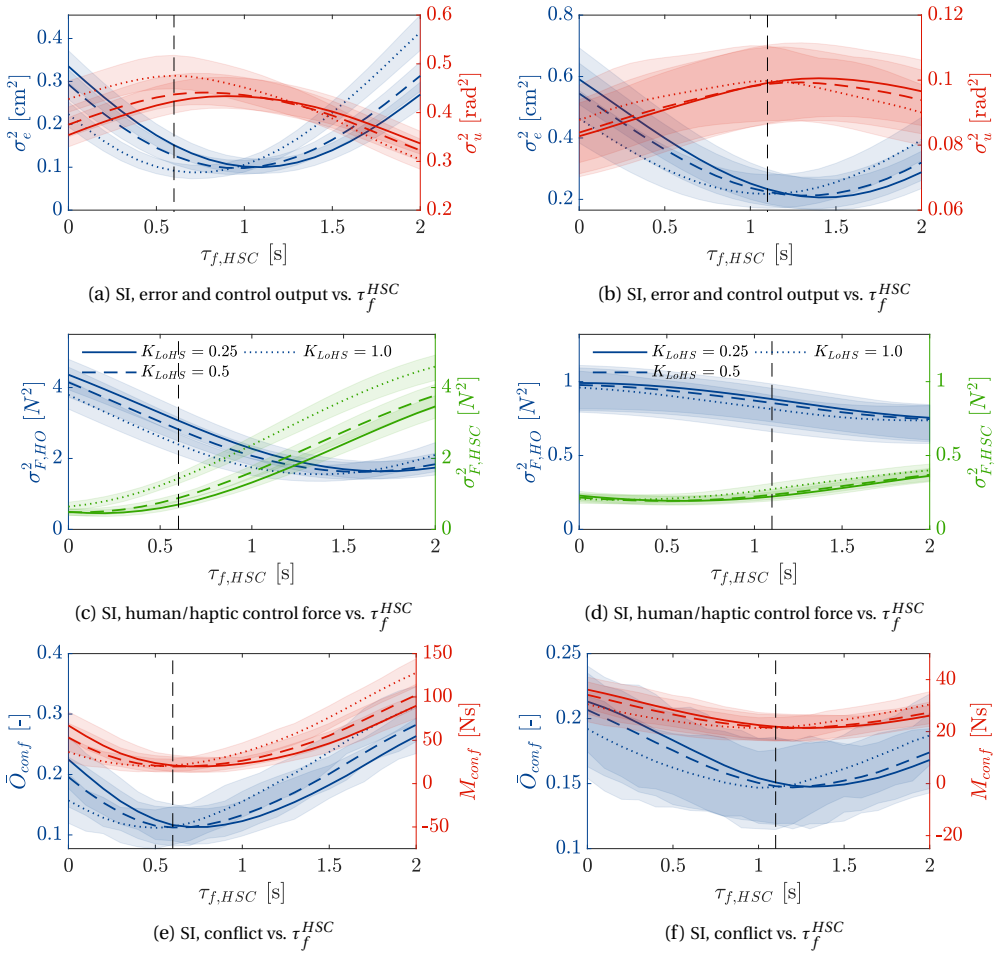

(a) SI, error and control output vs. τ_f^{HSC}

(b) SI, error and control output vs. τ_f^{HSC}

(c) SI, human/haptic control force vs. τ_f^{HSC}

(d) SI, human/haptic control force vs. τ_f^{HSC}

(e) SI, conflict vs. τ_f^{HSC}

(f) SI, conflict vs. τ_f^{HSC}

Figure 4.14: Results of simulation I, the effects of varying FDC-HSC look-ahead time τ_f^{HSC}, when sharing control with the HO. The left column shows the results from the SI task, and the right column shows the DI task. Each run is done for three LoHS settings: low ($K_{LoHS} = 0.25$), medium ($K_{LoHS} = 0.5$) and high ($K_{LoHS} = 1$). The light areas include the results for 100 remnant realizations, with the line representing the mean result.

HSC. The look-ahead time parameter is varied for the HO, which has added remnant noise, and an inherently different model structure than the FDC-HSC. In the Meshed HSC simulations, the only difference was the added remnant noise for the HO, as the HSC and HO model structure were the same.

The results of FDC-HSC simulation II are shown in Figure 4.15. Looking at the error σ_e^2 and stick deflection σ_u^2 (Figures 4.15a and 4.15b), similarities between both simulations are observed in the error trends: minima are achieved, its locations dependent on the LoHS condition. The difference is in the conformance of the minimum error with the maximum stick deflection. For this simulation, when $K_{LoHS} = 1$, minimum error is achieved when stick deflection is maximum. But when K_{LoHS} is lower, the minimum error can be achieved with a much lower stick deflection. For instance, for $K_{LoHS} = 0.25$, in the SI case the minimum error occurs for $\tau_{f,HO} \approx 0.9$, when $\sigma_u^2 = 0.38$, not near the maximum which occurs for $\tau_{f,HO} \approx 0.2$.

Figures 4.15c and 4.15d show how changing HO look-ahead time affects the shared control forces. Compared to simulation I, the plots appear mirrored around the $\tau_{f,HO} = \tau_{f,HSC}$ point, indicated with the vertical line. This point exists in both simulations and represents the exact same conditions, and thus results in the same outcome. Here, increasing $\tau_{f,HO}$ results in an increased HO force and a decreased HSC force, similar to how increasing $\tau_{f,HSC}$ would have the reversed effect.

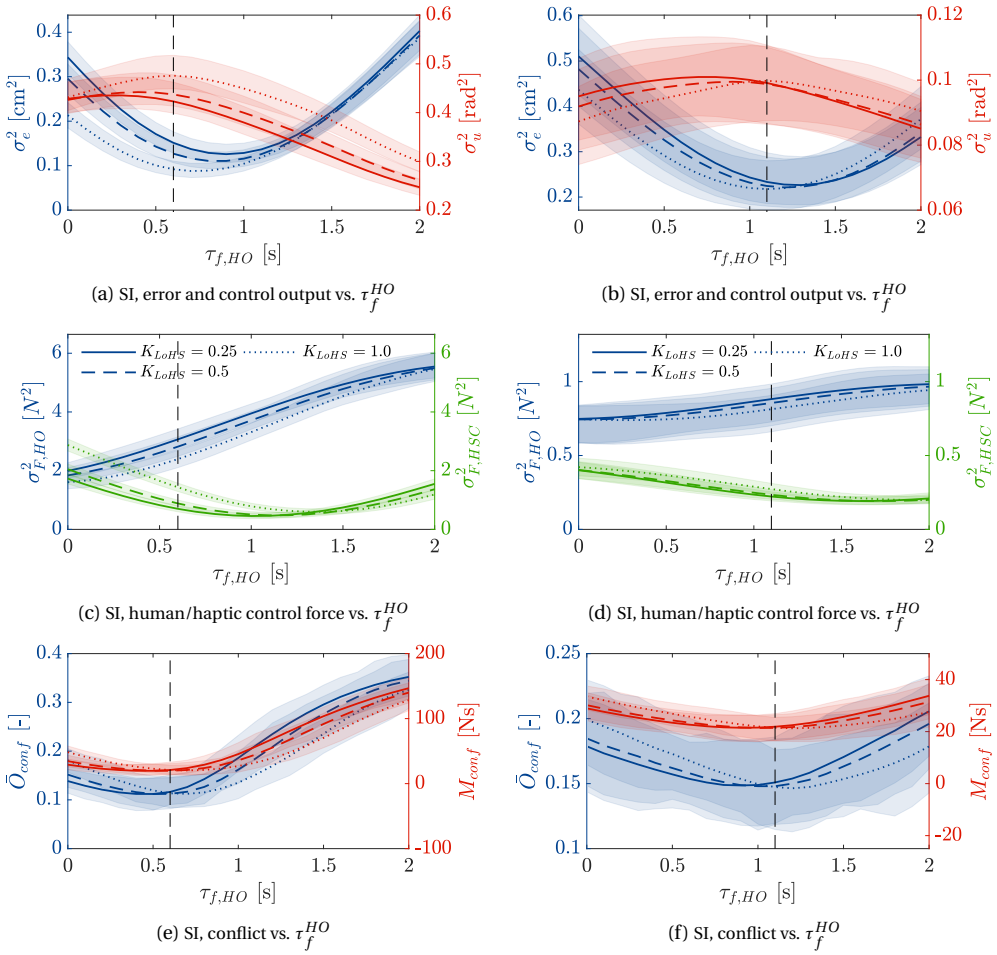

(a) SI, error and control output vs. τ_f^{HO}

(b) SI, error and control output vs. τ_f^{HO}

(c) SI, human/haptic control force vs. τ_f^{HO}

(d) SI, human/haptic control force vs. τ_f^{HO}

(e) SI, conflict vs. τ_f^{HO}

(f) SI, conflict vs. τ_f^{HO}

Figure 4.15: Results of simulation II, the effects of varying HO look-ahead time τ_f^{HO}, when sharing control with the FDC-HSC. The left column shows the results from the SI task, and the right column shows the DI task. Each run is done for three LoHS settings: low ($K_{LoHS} = 0.75$), nominal ($K_{LoHS} = 1$) and high ($K_{LoHS} = 1.25$). The light areas include the results for 100 remnant realizations, with the line representing the mean result.

4.5. Discussion

In previous sections Sections 4.3 and 4.4 the simulation results were shown and explained. This section provides a discussion of these results, in two subsections. Section 4.5.1 will discuss how varying look-ahead time affects performance and conflict in a shared control task, for both Meshed HSC and FDC-HSC. Section 4.5.2 provides a quantitative comparison of the Meshed HSC and FDC-HSC and discusses their differences.

4.5.1. Effect of varying look-ahead time

It appears that the optimal HSC look-ahead value depends on how the criterion for optimal performance is chosen. If a low error is desired, $\tau_{f,HSC}$ should be slightly higher than $\tau_{f,HO}$ when dealing with a SI task. However, when low conflict is deemed more important, $\tau_{f,HSC}$ should be equal to or slightly lower than $\tau_{f,HO}$. This is the case for both SI and DI dynamics tasks. Finally, if low control effort is desired, this can be achieved by having a $\tau_{f,HSC}$ that is significantly higher than $\tau_{f,HO}$, up to twice as high for a SI task.

The results from Meshed HSC simulation II reveal that the optimal $\tau_{f,HO}$ (at which a HO achieves the lowest error when no HSC is involved) is key in determining at what $\tau_{f,HSC}$ best tracking performance is achieved. When $\tau_{f,HSC}$ is too low, $\tau_{f,HO}$ must be much higher to compensate for the sub-optimal parameter value, and vice versa.

It is important to note that when aiming for the lowest conflict and equal HO and HSC behavior, the simula-

tion results suggest that approximately equal look-ahead times are desired. A deviation between look-ahead times, in either direction, results in an increase in conflict. This increase of conflict is both in terms of duration and magnitude, for both SI and DI controlled element dynamics. This suggests that the magnitude of conflict only depends on the duration of the conflict, and thus magnitude per time unit is not dependent on varying look-ahead times.

The simulations were done for both SI and DI controlled element dynamics. For the DI task, the inputs given by the HO and HSC models have lower magnitude than for the SI task as to achieve stability. This causes changing look-ahead times to have a lower relative impact for the DI task than for the SI task.

Finally, sample time series outputs from the simulations were analyzed. For the SI task, a clear distinction is seen between HO behavior with a short look-ahead time, and HSC behavior with a long look-ahead time. A controller with a longer look-ahead time will mainly follow low frequency oscillations, while a controller with a short look-ahead time will respond stronger to nearby high frequency oscillations. This difference in strategy is suspected to be a cause for conflict. For the DI task, this distinction is less visible. This can be attributed to the addition of strong remnant noise, and to the nature of the DI control task, which requires smaller and higher frequency inputs.

4.5.2. Comparison of Meshed HSC and FDC-HSC

For a comparison between the Meshed HSC and FDC-HSC performance, the 'baseline' situation of equal HSC and HO look-ahead times is taken, i.e. $\tau_{f,HSC} = \tau_{f,HO}$. Tables 4.5 and 4.6 provide and overview of the performance metrics at the baseline point. Note that this condition occurs and is the same in both simulations I (where $\tau_{f,HSC}$ is varied) and simulations II (where $\tau_{f,HO}$ is varied), so the content in the tables refers to both simulations.

The Meshed HSC baseline performance is shown in Table 4.5. The optimal error and conflict rates are achieved for the original baseline look-ahead times equal to 0.6 (SI) and 1.1 (DI). These are the optimal far-viewpoint parameters from the Van der El model, and all other model parameters are the ones originally identified by Van der El for that far-viewpoint. Since these model parameters are kept constant, the best performance is achieved for the same optimal far-viewpoint. The fact that the Meshed HSC and HO use the same parameters results in optimal performance for this look-ahead time in the shared control task.

The FDC-HSC baseline performance is shown in Table 4.6, with only one look-ahead time, the same as in the simulations. Here, the three LoHS conditions are shown. Using the nominal value $K_{LoHS} = 1$, a slightly but not substantially better tracking performance is achieved compared to the Meshed HSC. This comes at a cost of a higher stick deflection variance σ_u^2. Overall, the optimal performance of the FDC-HSC is not convincingly better than the optimal performance of the Meshed HSC.

In this chapter, the FDC-HSC was tuned in solo configuration only, and evaluated in shared control configuration. Optimizing the controller for a lowest error and conflict in a shared control task would likely result in a better performance.

Table 4.5: Meshed HSC summary of the performance for the baseline situation, $\tau_{f,HSC} = \tau_{f,HO}$.

		SI			**DI**		
$\boldsymbol{\tau_{f,HO} = \tau_{f,HSC}}$	**[s]**	**0.0**	**0.6**	**1.2**	**0.0**	**1.1**	**2.0**
σ_e^2	[cm^2]	0.22	0.10	0.14	0.46	0.23	0.39
σ_u^2	[rad^2]	0.44	0.49	0.44	0.10	0.12	0.11
$\sigma_{F,HO}^2$	[N^2]	3.77	2.41	1.62	0.98	0.84	0.77
$\sigma_{F,HSC}^2$	[N^2]	0.65	1.44	2.82	0.20	0.27	0.39
$\bar{O}_{conf}$	[-]	0.15	0.11	0.18	0.15	0.11	0.16
M_{conf}	[Ns]	32.71	18.70	46.43	22.03	14.35	23.71

Table 4.6: FDC-HSC summary of the performance for the baseline situation, $\tau_{f,HSC} = \tau_{f,HO}$.

		SI			**DI**		
$\boldsymbol{\tau_{f,HO} = \tau_{f,HSC}}$	**[s]**	**0.6**			**1.1**		
$\boldsymbol{K_{LoHS}}$	[-]	**0.25**	**0.5**	**1.0**	**0.25**	**0.5**	**1.0**
σ_e^2	[cm^2]	0.15	0.13	0.09	0.23	0.22	0.22
σ_u^2	[rad^2]	0.42	0.44	0.48	0.10	0.10	0.10
$\sigma_{F,HO}^2$	[N^2]	3.07	2.82	2.39	0.88	0.86	0.81
$\sigma_{F,HSC}^2$	[N^2]	0.70	0.88	1.43	0.22	0.23	0.27
$\tilde{O}_{conf}$	[-]	0.12	0.11	0.11	0.15	0.15	0.15
M_{conf}	[Ns]	20.93	19.72	20.86	21.88	21.43	21.48

4.6. Conclusions

In this chapter, initial simulations were done of a shared control task performed by a HO and HSC simultaneously. These simulations were focused on finding the influence of varying HSC look-ahead time $\tau_{f,HSC}$. In addition, this chapter provided a comparison between two types of HSC configurations: the Meshed HSC, and the FDC-HSC.

Apart from the look-ahead time, the simulations kept all HO parameters constant, since HO adaptation in shared control preview tasks is not well understood to implement it in simulations. This is a major assumption which will not hold up in real-life situations, where a HO is very likely to adapt to changes in the haptic support system.

With the simulations, the full strength of the FDC-HSC has not been shown. The ability to tune a separate feed-forward path, the LoHS, is considered to be the main strength of the FDC architecture. However, the resulting performance improvement is largely subjective and difficult to capture in a simulation. This will be investigated in the experiment phase.

The conclusions from this chapter partially form the basis for the human-in-the-loop experiment conditions, together with a few hands-on pre-experiments. After analyzing the SI and DI task outcomes, the human-in-the-loop experiment will be conducted with SI controlled element dynamics only. This type of tracking task is easier to learn and control for the participants, and results in less variation of outcomes. Additionally, the simulations suggest that varying look-ahead times have a much larger effect on SI task than on DI tasks.

Hands-on testing with various experiment conditions and the Meshed and FDC configurations will determine the full experiment plan. The experiment plan is covered in Chapter 5.

5

Experiment Proposal

In the final phase of this thesis project, a human-in-the-loop experiment will be conducted. In the experiment, participants perform a tracking task with visual preview, and are supported by continuous haptic force feedback. A pre-experiment was conducted to test the conditions, as discussed in Appendix A. The current chapter contains a detailed experiment proposal, designed using the results from the preliminary simulations. It discusses the used apparatus, the control task, the chosen conditions, the experiment design and the hypotheses.

5.1. Control Task

Participants will perform a target-following and disturbance-rejection task with preview, supported by continuous haptic guidance. The participants are instructed to follow the previewed target as accurately as possible. The forcing functions, a target and a disturbance, are the same multi-sine signals used in Chapter 4.

An overview of the control task is shown in Figure 5.1. The haptic shared controller (HSC) uses the Four-Design Choices architecture [39] (see Section 3.2.2 and Section 4.1.3). The human-compatible reference (HCR) is generated by simulating the HO model for preview control [5] in a closed-loop control task, and includes a model of the stick and the controlled element dynamics. The parameters are identical to the ones used in the preliminary simulations. The controlled element, denoted by H_{CE}, is a single-integrator system with a gain of 1.5. The side-stick, shown as H_{stick}, can be described as a mass-spring-damper system with a torsional stiffness of 3.58 Nm/rad, damping 0.22 Nm s/rad, and inertia 0.01 kg m^2. Additionally, a stick gain of 0.44 cm/deg is used.

In the experiment, different *haptic* look-ahead times are evaluated. The chosen look-ahead times are largely based on results of testing and a pre-experiment (Appendix A). The resulting nine haptic conditions shown in Table 5.1. The look-head times, τ_{HSC}, are chosen with small intervals of 0.1 seconds such that a detailed relation between haptic look-ahead time and task performance can be obtained.

Table 5.1: Conditions for the experiment

	NH	**H0**	**H03**	**H04**	**H05**	**H06**	**H07**	**H08**	**H09**	**H12**
τ_{HSC} (s)	-	0.0	0.3	0.4	0.5	0.6	0.7	0.8	0.9	1.2

5.2. Apparatus

The experiment will be conducted at the Human-Machine Lab at the faculty of Aerospace Engineering of TU Delft. Participants will be seated in front of a display with a resolution of 1280 by 1024 pixels, a size of 36 by 29.5 cm and a 100 Hz refresh rate. For their control input, and the haptic force feedback, participants use an electro-hydraulic servo-controlled side-stick located on their right-hand side. The stick has a moment arm of 9 cm and can only rotate around its roll axis.

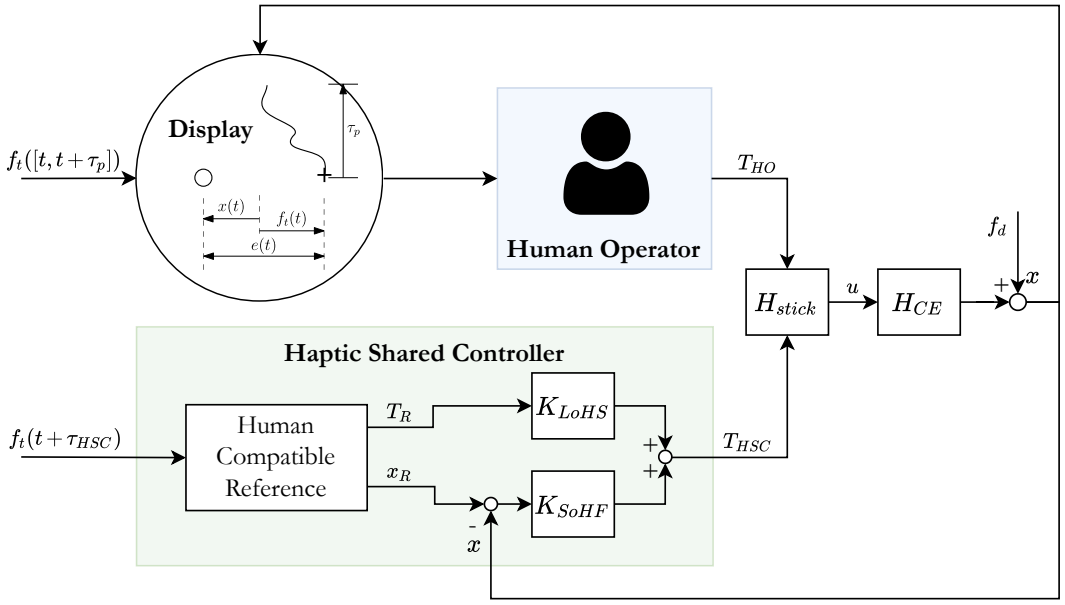

Figure 5.1: Schematic overview of the control task, showing the interaction between the human operator and the haptic shared controller.

5.3. Experiment Design

An experiment with 10 conditions was designed using a within-subjects design. The order of the conditions was determined by generating a randomized balanced Latin square, such that each participant is presented with a unique order of conditions. The duration of a single run is 128 seconds, of which the first 8 seconds are considered run-in time, and will be discarded. For each condition, the participants conduct a training run to get used to the haptic setting. After the training run, three repetitions are performed, resulting in a dataset of three runs per condition for each subject. At the start of the experiment, the participants will do a training containing 4 repetitions of the non-haptic condition. Another set of 4 runs of the non-haptic condition is done at the end of the experiment. Together with the training set, these data is used to identify HO behavior and adaptation between the start and the end of the experiment.

Table 5.2: Latin-Square showing the order of the experiment conditions for ten subjects.

Subject	*Training*	Conditions										*Reference*
1	NH	NH	H05	H0	H07	H12	H03	H09	H04	H08	H06	NH
2	NH	H05	H07	NH	H03	H0	H04	H12	H06	H09	H08	NH
3	NH	H07	H03	H05	H04	NH	H06	H0	H08	H12	H09	NH
4	NH	H03	H04	H07	H06	H05	H08	NH	H09	H0	H12	NH
5	NH	H04	H06	H03	H08	H07	H09	H05	H12	NH	H0	NH
6	NH	H06	H08	H04	H09	H03	H12	H07	H0	H05	NH	NH
7	NH	H08	H09	H06	H12	H04	H0	H03	NH	H07	H05	NH
8	NH	H09	H12	H08	H0	H06	NH	H04	H05	H03	H07	NH
9	NH	H12	H0	H09	NH	H08	H05	H06	H07	H04	H0	NH
10	NH	H0	NH	H12	H05	H09	H07	H08	H03	H06	H0	NH

5.4. Metrics

The experiment evaluates tracking performance in the shared control task. From measured data, several metrics can be obtained, which will be used in the post-experiment data analysis.

- *Tracking error*: The difference between the target and the system output, which is used as an indicator

for overall tracking performance.

- *HO torque*: The measured torque exerted on the stick by the participant. It can be used as an indicator for control effort, and to investigate how the HO responds to the haptic guidance.
- *HSC torque*: The torque that is provided by the haptic controller and applied to the stick. The HSC torque is a combination of the feedforward (LoHS) and feedback (SoHF) torques, which may also be analyzed separately.
- *Conflict time*: The amount of conflict between the HO and the HSC may indicate to what extent the HO agrees with the haptic guidance. Occurrence of conflict is defined as follows:

$$O_{conf} = \begin{cases} 1 & \text{if } T_{HO} \cdot T_{HSC} < 0 \text{ and } |T_{HO} - T_{HSC}| > 0.1 \cdot T \\ 0 & \text{otherwise} \end{cases} \tag{5.1}$$

- *Conflict torque*: The magnitude difference of opposing torques during conflict. The magnitude of conflict is defined as follows:

$$M_{conf} = O_{conf} \cdot \left| T_{HO} - T_{HSC} \right| \cdot \tag{5.2}$$

- *Van der Laan rating*: A Van der Laan questionnaire will be filled out by the participants after each condition, rating the haptic guidance system [42]. The questionnaires will result in a *usefulness score* and a *satisfaction score* for each condition. The ratings provide a subjective evaluation of the haptic conditions, and may be used as an indication for HO acceptance.

5.5. Hypotheses

The following hypotheses will be tested in the experiment. These are based on the preliminary simulations results and on the experience from pre-testing.

H1. In the shared control task, the lowest conflict is achieved when the HSC has a look-ahead time of 0.6 seconds (condition H06), which is an optimal HSC setting.
The HO model that is used in the HSC reference block uses empirical parameters, with an original look-ahead time (far-viewpoint) of 0.6 seconds. Upon changing the look-ahead time, no HO adaptation is taken into account in the model. Therefore, the remaining parameters (far-viewpoint filter, equalization gain and neuromuscular dynamics) are sub-optimal when responding to a different viewpoint than 0.6 seconds. In that case, the controller may be lagging or leading, causing more conflict with the HO.

H2. For conditions close to the optimal look-ahead time (H05, H06, H07), there is no significant increase in conflict time.
By looking at Figure A.2d, it might be possible to identify a 'region of acceptance' in which the amount of conflict does not increase substantially. The results of the pre-experiment show a steep increase of conflict beyond this region.

H3. The RMS of the added HO and HSC torque, and thus the control activity, is invariant with haptic look-ahead time.
This hypothesis is based on the assumption that the HO counters any undesired haptic guidance torques. For sub-optimal haptic look-ahead times, the HSC applies stronger undesirable torques, but these are countered by the HO, resulting in a net torque that is approximately the same magnitude.

H4. Conditions H03 to H09 will result in a lower tracking error than reference condition NH.
This hypothesis concerns the general effect of using haptic guidance in a preview tracking task. These conditions, while using different look-ahead times, are expected to result in a better task performance than the non-haptic conditions. Even with sub-optimal guidance, the HO can use the HSC to their advantage and achieve a lower tracking error. The remaining conditions H0 and H12 are considered extreme conditions, and expected to lead to a higher workload and worse performance.

Bibliography

[1] L. Bainbridge, "Ironies of automation," *Automatica*, vol. 19, no. 6, pp. 775–779, nov 1983.

[2] D. A. Abbink, E. R. Boer, and M. Mulder, "Motivation for continuous haptic gas pedal feedback to support car following," *IEEE Intelligent Vehicles Symposium, Proceedings*, pp. 283–290, 2008.

[3] D. A. Abbink, M. Mulder, and E. R. Boer, "Haptic shared control: smoothly shifting control authority?" *Cognition, Technology & Work*, vol. 14, no. 1, pp. 19–28, mar 2012.

[4] D. T. McRuer and H. R. Jex, "A Review of Quasi-Linear Pilot Models," *IEEE Transactions on Human Factors in Electronics*, vol. HFE-8, no. 3, pp. 231–249, sep 1967.

[5] K. Van Der El, D. M. Pool, H. J. Damveld, M. M. Van Paassen, and M. Mulder, "An empirical human controller model for preview tracking tasks," *IEEE Transactions on Cybernetics*, vol. 46, no. 10, oct 2015.

[6] K. van der El, "How humans use preview information in manual control," Ph.D. dissertation, 2018.

[7] D. T. McRuer and E. S. Krendel, "The human operator as a servo system element," *Journal of the Franklin Institute*, vol. 267, no. 5, pp. 381–403, 1959.

[8] M. Mulder, D. M. Pool, D. A. Abbink, E. R. Boer, P. M. Zaal, F. M. Drop, K. Van Der El, and M. M. Van Paassen, "Manual Control Cybernetics: State-of-the-Art and Current Trends," pp. 468–485, oct 2018.

[9] K. Ito and M. Ito, "On tracking behaviors of the human operator in preview control systems," *Kybernetes*, vol. 4, no. 1, pp. 33–38, 1975.

[10] D. T. McRuer, R. W. Allen, D. H. Weir, and R. H. Klein, "New Results in Driver Steering Control Models," *Human Factors: The Journal of Human Factors and Ergonomics Society*, vol. 19, no. 4, pp. 381–397, 1977.

[11] E. Donges, "A two-level model of driver steering behavior, Human Factors," *J Hum Factors Ergon Soc*, vol. 20, no. 6, p. 691, 1978.

[12] T. B. Sheridan, "Three Models of Preview Control," *IEEE Transactions on Human Factors in Electronics*, vol. HFE-7, no. 2, pp. 91–102, 1966.

[13] M. Kondo and A. Ajimine, "Driver's Sight Point and Dynamics of the Driver-Vehicle-System Related to It," in *Proceedings - SAE Automotive Engineering Congress*, Detroit, MI, 1968.

[14] M. Land and J. Horwood, "Which parts of the road guide steering?" *Nature*, vol. 377, no. 6547, pp. 339–340, sep 1995.

[15] O. Lappi and C. Mole, "Visuomotor control, eye movements, and steering: A unified approach for incorporating feedback, feedforward, and internal models," *Psychological Bulletin*, vol. 144, no. 10, pp. 981–1001, 2018.

[16] K. Van Der El, D. M. Pool, and M. Mulder, "Analysis of Human Remnant in Pursuit and Preview Tracking Tasks," *IFAC-PapersOnLine*, vol. 52, no. 19, pp. 145–150, 2019.

[17] K. van der El, S. Padmos, D. M. Pool, M. M. Van Paassen, and M. Mulder, "Effects of Preview Time in Manual Tracking Tasks," *IEEE Transactions on Human-Machine Systems*, vol. 48, no. 5, pp. 486–495, oct 2018.

[18] K. Van Der El, D. M. Pool, M. M. Van Paassen, and M. Mulder, "Identification and Modeling of Driver Multiloop Feedback and Preview Steering Control," in *2018 IEEE International Conference on Systems, Man, and Cybernetics (SMC)*, no. October. IEEE, oct 2018, pp. 1227–1232.

[19] M. J. C. Kolff, "Effects of Visual Occlusion in Lane Keeping Tasks on Driver Model Identification and Gaze Behaviour," MSc Thesis, Delft University of Technology, 2019.

[20] D. A. Abbink, D. Cleij, M. Mulder, and M. M. Van Paassen, "The importance of including knowledge of neuromuscular behaviour in haptic shared control," in *2012 IEEE International Conference on Systems, Man, and Cybernetics (SMC)*. IEEE, oct 2012, pp. 3350–3355.

[21] N. B. Sarter and D. D. Woods, "How in the world did we ever get into that mode? Mode error and awareness in supervisory control," *Human Factors*, vol. 37, no. 1, pp. 5–19, 1995.

[22] N. Sarter, D. D. Woods, and C. Billings, "Automation Surprises," in *Handbook of Human Factors & Ergonomics*, G. Salvendy, Ed. Wiley, 1997, pp. 1926– 1943.

[23] D. D. Woods, "Decomposing Automation: Apparent Simplicity, Real Complexity," in *Automation and Human Performance: Theory and Applications*. Routledge, jan 1996, pp. 3–17.

[24] C. E. Billings, "Human-Centered Aviation Automation: Principles and Guidelines (NASA Technical Memorandum 110381)," *NASA TechnicalMemorandum 110381*, no. February 1996, p. 222, 1996.

[25] D. A. Norman, "The 'problem' with automation: inappropriate feedback and interaction, not 'over-automation'." *Philosophical transactions of the Royal Society of London. Series B, Biological sciences*, vol. 327, no. 1241, pp. 585–593, 1990.

[26] D. A. Abbink, T. Carlson, M. Mulder, J. C. F. De Winter, F. Aminravan, T. L. Gibo, and E. R. Boer, "A Topology of Shared Control SystemsFinding Common Ground in Diversity," *IEEE Transactions on Human-Machine Systems*, vol. 48, no. 5, pp. 509–525, oct 2018.

[27] C. D. Wickens, "Multiple resources and performance prediction," *Theoretical Issues in Ergonomics Science*, vol. 3, no. 2, pp. 159–177, 2002.

[28] D. A. Abbink, "Neuromuscular analysis of haptic gas pedal feedback during car following," Ph.D. dissertation, Delft University of Technology, 2006.

[29] M. Mulder, D. A. Abbink, and E. R. Boer, "The effect of haptic guidance on curve negotiation behavior of young, experienced drivers," in *Conference Proceedings - IEEE International Conference on Systems, Man and Cybernetics*, 2008, pp. 804–809.

[30] L. Saleh, P. Chevrel, F. Claveau, J. F. Lafay, and F. Mars, "Shared steering control between a driver and an automation: Stability in the presence of driver behavior uncertainty," *IEEE Transactions on Intelligent Transportation Systems*, vol. 14, no. 2, pp. 974–983, 2013.

[31] D. G. Beeftink, C. Borst, D. Van Baelen, M. M. Van Paassen, and M. Mulder, "Haptic Support for Aircraft Approaches with a Perspective Flight-Path Display," in *2018 IEEE International Conference on Systems, Man, and Cybernetics (SMC)*. IEEE, oct 2018, pp. 3016–3021.

[32] T. M. Lam, M. Mulder, M. M. Van Paassen, J. A. Mulder, and F. C. T. Van der Helm, "Force-stiffness feedback in uninhabited aerial vehicle teleoperation with time delay," *Journal of Guidance, Control, and Dynamics*, vol. 32, no. 3, pp. 821–835, 2009.

[33] K. H. Goodrich, P. C. Schutte, and R. A. Williams, "Haptic-multimodal flight control system update," *11th AIAA Aviation Technology, Integration,and Operations (ATIO) Conference, including the AIAA Balloon Systems Conference and 19th AIAA Lighter-Than-Air Technology Conference*, no. September, pp. 1–17, 2011.

[34] L. B. Rosenberg, "Virtual fixtures: perceptual tools for telerobotic manipulation," *1993 IEEE Annual Virtual Reality International Symposium*, pp. 76–82, 1993.

[35] P. Marayong and A. M. Okamura, "Speed-Accuracy Characteristics of Human-Machine Cooperative Manipulation Using Virtual Fixtures With Variable Admittance," *Human Factors: The Journal of the Human Factors and Ergonomics Society*, vol. 46, no. 3, pp. 518–532, sep 2004.

[36] M. K. O'Malley, A. Gupta, M. Gen, and Y. Li, "Shared Control in Haptic Systems for Performance Enhancement and Training," *Journal of Dynamic Systems, Measurement, and Control*, vol. 128, no. 1, pp. 75–85, nov 2005.

[37] W. Scholtens, S. Barendswaard, D. M. Pool, M. M. Van Paassen, and D. A. Abbink, "A New Haptic Shared Controller Reducing Steering Conflicts," in *2018 IEEE International Conference on Systems, Man, and Cybernetics (SMC)*. IEEE, oct 2018, pp. 2705–2710.

[38] R. P. Boink, M. M. Van Paassen, M. Mulder, and D. A. Abbink, "Understanding and reducing conflicts between driver and haptic shared control," in *2014 IEEE International Conference on Systems, Man, and Cybernetics (SMC)*, vol. 2014-Janua, no. January. IEEE, oct 2014, pp. 1510–1515.

[39] M. M. Van Paassen, R. P. Boink, D. A. Abbink, M. Mulder, and M. Mulder, "Four design choices for haptic shared control," in *Advances in Aviation Psychology, Volume 2*. Routledge, may 2017, pp. 237–254.

[40] K. van der El, D. M. Pool, M. M. Van Paassen, and M. Mulder, "Effects of Preview on Human Control Behavior in Tracking Tasks With Various Controlled Elements," *IEEE Transactions on Cybernetics*, vol. 48, no. 4, pp. 1242–1252, 2017.

[41] K. Van Der El, D. M. Pool, M. M. Van Paassen, and M. Mulder, "Effects of Target Trajectory Bandwidth on Manual Control Behavior in Pursuit and Preview Tracking," *IEEE Transactions on Human-Machine Systems*, vol. 50, no. 1, pp. 68–78, 2020.

[42] J. D. Van Der Laan, A. Heino, and D. De Waard, "A simple procedure for the assessment of acceptance of advanced transport telematics," *Transportation Research Part C: Emerging Technologies*, vol. 5, no. 1, pp. 1–10, 1997.

A

Pre-Experiment Results

Before the final experiment, the experiment conditions were tested in a pre-experiment. The goal was to evaluate whether the chosen conditions are suitable for the final experiment. This appendix explains the used conditions and experiment design, and provides the results. It concludes with a discussion of the results.

A.1. Conditions

In earlier testing of the experiment setup with various haptic and visual preview times, when varying haptic preview time with steps of 0.3 seconds, the differences between haptic preview times 0.6 and 0.9 can be very subtle. It was decided to investigate these subtle differences by setting a higher resolution of 0.1 seconds, thus increasing the number of haptic conditions. Figure A.1 shows 9 haptic conditions, labeled as H followed by the corresponding haptic preview time, τ_{HSC}. For the human operator, the visual preview time will be set to a constant 1 second for all conditions. The length of 1 second is chosen as to provide sufficient preview for adequate tracking performance, based on the average critical preview time of 0.6 seconds. In addition to the 9 haptic conditions, a condition with no haptic support (NH) is added, resulting in a total of 10 conditions for the experiment.

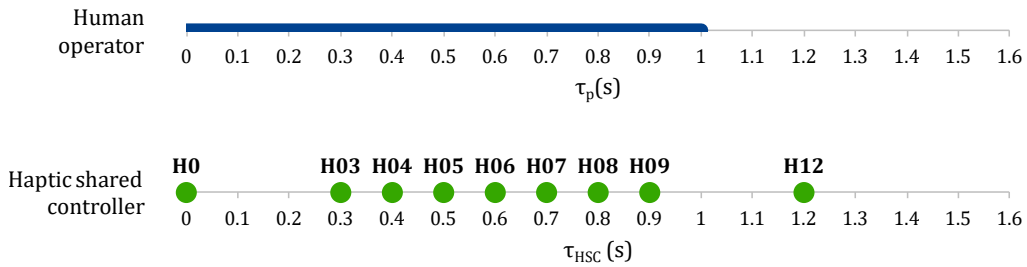

Figure A.1: Visualization of the preview times used in the experiment, showing the preview information used by the human operator and the haptic shared controller.

A.2. Experiment Design

An experiment with 10 conditions was designed using a within-subjects design. The order of the conditions was determined by generating a randomized balanced Latin square, such that each participant is presented with a unique order of conditions. For this pre-experiment, two participants participated, and were presented with the first two rows of the Latin square, shown in Table A.1. For participant 1, breaks were held after conditions H0, H03 and H04. Participant 2 also included 4 extra training runs for condition NH at the start, and at the end of the experiment for reference. Participant 2 therefore had breaks after conditions H07, H03, H04 and H06.

A run lasted 128 seconds, of which the first 8 seconds are considered run-in time, and are left out of the results. Per condition, 1 training run is done, followed by 3 measurement runs.

Table A.1: Order of conditions for two participants

Subject	Conditions									
1	NH	H05	H0	H07	H12	H03	H09	H04	H08	H06
2	H05	H07	NH	H03	H0	H04	H12	H06	H09	H08

A.3. Results

The output of the experiment contains all measured data, and the metrics that follow from it. The main variables of interest are the tracking error (e), control activity (u) and conflict time (T_{conf}). Additionally, the results of a Van der Laan questionnaire, filled in by the participants, are shown.

A.3.1. Measured Data

Figure A.2 shows the results of the pre-experiment for two participants. For both participants, the same relation between the haptic preview time and output variables are found. Participant 2 had an overall lower error (Figure A.2a), and appears to achieve this by exerting more control activity (Figure A.2b). Minimum error and control activity are found around τ_{HSC} = 0.7 and 0.8.

Figure A.2c shows the separated outputs of the FDC-HSC, consisting of the LoHS and SoHF paths, where $u_{HSC} = u_{HS} + u_{HF}$. For haptic preview times below 0.5 seconds, the haptic feedback (HF) portion (red) is dominant. Above 0.5 seconds, the haptic support (HS) portion, of which the RMS is invariant with τ_{HSC}, becomes dominant. For the highest condition (τ_{HSC} = 1.2 s), the RMS of the HF path is higher than the HS path again.

Figure A.2d shows the total occurrence of conflict (T_{conf}) as a percentage of run time. Conflict is defined as occurring when the signs of u_{HO} and u_{HSC} are opposite.

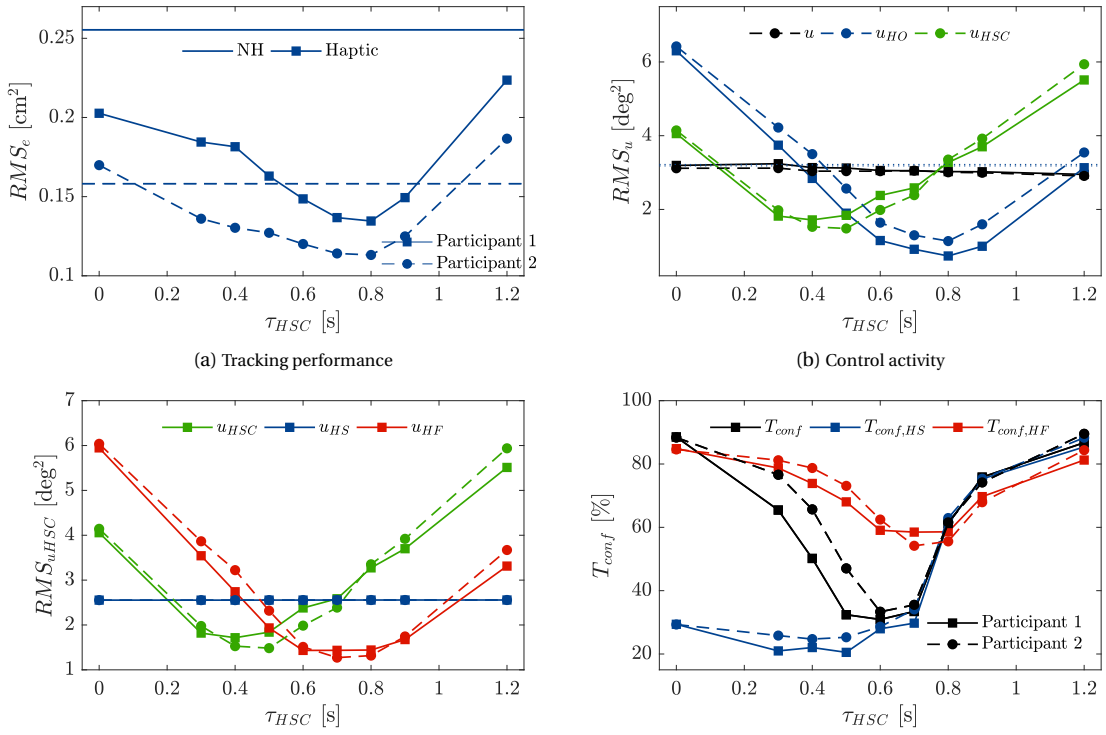

(a) Tracking performance

(b) Control activity

(c) LoHS and SoHF paths of the FDC-HSC

(d) Human-haptic conflict

Figure A.2: Results of the experiment, showing the effect of different haptic look-ahead times on several task performance variables. Plotted for participants 1 and 2.

In Figure A.3, two example time traces from the experiment are shown. The total stick deflection u and the contributions of the HO and the HSC to the stick deflection are shown (u_{HO} and u_{HSC}). The top figure, Figure A.3a shows condition H12, which is the worst performing haptic condition. Conflict occurs 86% of the time, and the HO inputs appears to be exactly the opposite of the HSC input most of the time. In fact, the participant noted here that the haptic feedback appeared to be mirrored. This can be explained by considering the forcing functions. The look-ahead time of 1.2 s is approximately half of the period of the dominant frequency in the multi-sine target signal.

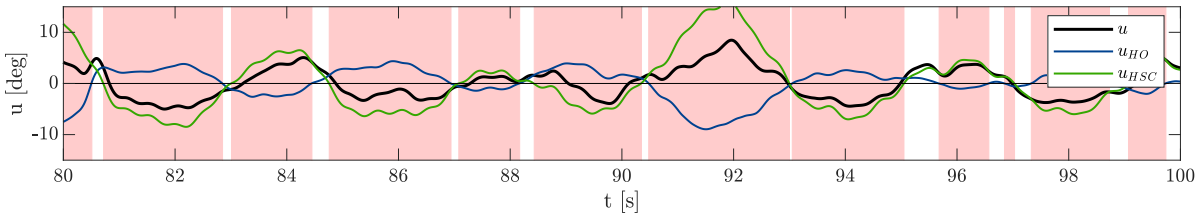

(a) Participant 2, condition H12, T_{conf} = 86.4%

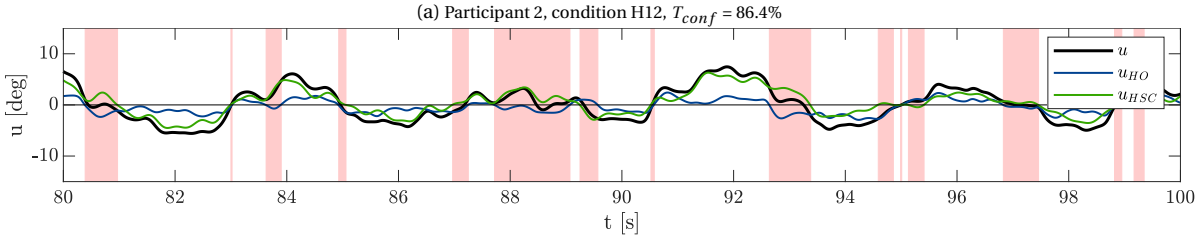

(b) Participant 2, condition H07, T_{conf} = 35.1%

Figure A.3: Two example time traces of stick deflection, including the contributions by the HO and the HSC. Conflict zones are indicated in red.

A.3.2. Van der Laan questionnaire

A Van der Laan questionnaire was filled out by the participants after each condition. This type of questionnaire can be used to rate a support system in a car driving task. The form contained 9 questions relating to how useful and satisfying the haptic support system was. From the questionnaires that were filled in by the participants, a *usefulness* and *satisfaction* score can be calculated for each condition. Figure A.4 shows the usefulness and satisfaction scores for both participants. Note that the form was filled in after each condition, including the non-haptic condition NH.

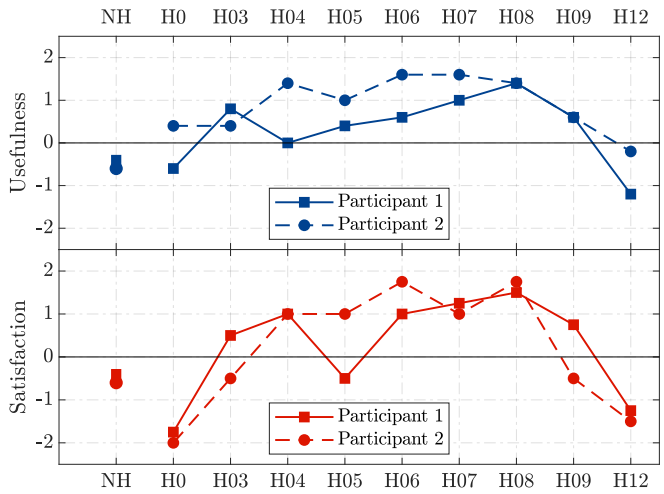

Figure A.4: Calculated usefulness and satisfaction scores from the Van der Laan questionnaires.

A.3.3. Discussion

Based on the results, the pre-experiment is considered to be successful, and the current experiment design can be used for the final experiment. The following conclusions about the experiment design can be drawn, forming the basis for the final experiment hypotheses.

- The haptic guidance is effective in improving task performance, resulting in a lower error for most haptic conditions, compared to the non-haptic condition NH.
- The haptic look-ahead time 'grid' is sufficiently dense in order to plot a relation between look-ahead time and error, control activity, and conflict. Especially the resolution of 0.1 second around the 'middle' values is useful to investigate the behavior around the minimum.
- Consistent with the simulations, an 'exchange' between the HO and HSC torques can be observed around the optimal haptic look-ahead time (see Figure A.2b). As haptic look-ahead time increases beyond the optimum, the HSC contributes more to the task, and the HO less. The opposite is true below the optimum.
- The total control activity remains constant for all conditions (u in Figure A.2b). This is the case, even as the HO and HSC inputs both increase for high and low look-ahead times (H0 and H12). The corresponding high conflict rate (see Figure A.2d) reflects this, and shows how HO and HSC inputs are mostly opposite in these conditions.
- Even for individual subjects, the Van der Laan ratings (Figure A.4) show an effect of the various conditions on *usefulness* and *satisfaction*. When averaged with multiple subjects, these scores may be compared to conflict scores. Additional meta-analysis of the conflict metric can be conducted with help of the Van der Laan scores, in order to evaluate the use of the conflict metric to describe user acceptance.

The results in this chapter are limited to time-domain analysis. Additional frequency domain analysis can be performed on the acquired test data. Identification of the HO by applying the model and the method used by Van der El [6] may reveal HO adaptation to different haptic settings. By identifying HO behavior in the non-haptic condition and training, insights can be gained on the individual differences between participants. It remains to be seen whether the relatively low amount of repetitions (3 runs) is sufficient for HO identification.

III

Paper Appendices

B

Individual Experiment Results

This appendix contains an overview of the individual results for each experiment participant, including sample time traces of three selected conditions: H0, H07 and H09.

B.1. Subject 1

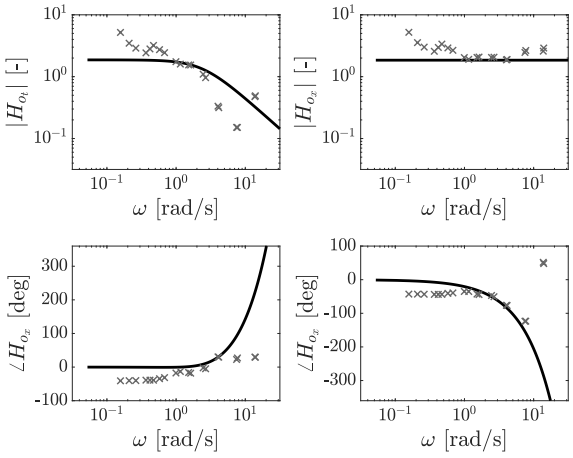

Figure B.1: Bode plots for subject 1

Table B.1: Identified parameters, subject 1

τ_{HO} [s]	K_f [-]	$T_{l,f}$ [s]	K_e [-]	τ_v [s]	VAF [%]
0.71	0.99	0.40	1.85	0.36	94.91

Table B.2: Resulting scores in sample runs, subject 1

	H0	H07	H09
RMS_e [cm]	0.23	0.16	0.19
$\text{RMS}_{T,HO}$ [N]	0.24	0.07	0.04
$\text{RMS}_{T,HSC}$ [N]	0.16	0.06	0.10
$\bar{O}_{conf}$ [%]	0.86	0.32	0.46
$\text{RMS}_\Delta T$ [N]	0.38	0.07	0.10

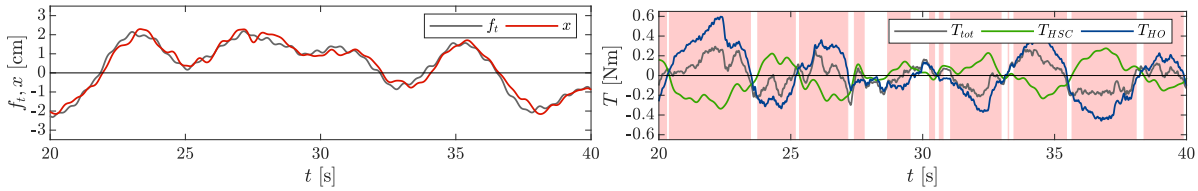

Figure B.2: Time traces for subject 1, condition H0, τ_{HSC} = 0.0 s.

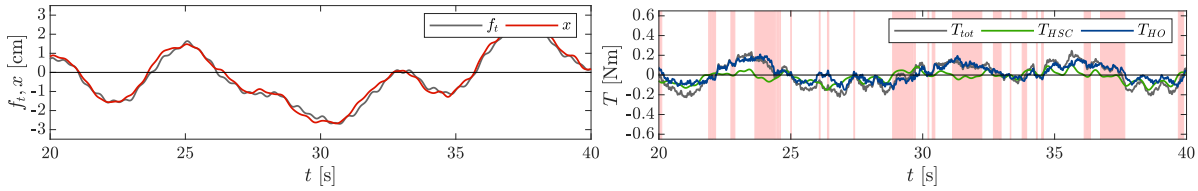

Figure B.3: Time traces for subject 1, condition H07, τ_{HSC} = 0.7 s.

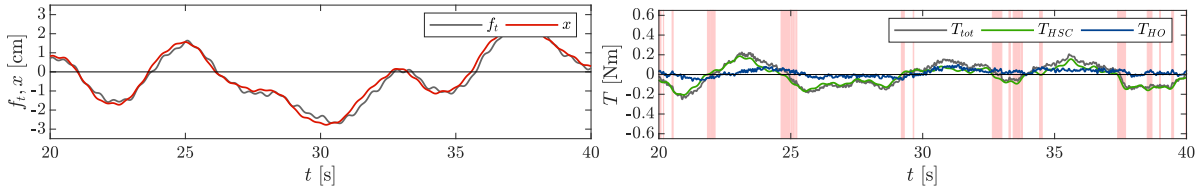

Figure B.4: Time traces for subject 1, condition H09, τ_{HSC} = 0.9 s.

B.2. Subject 2

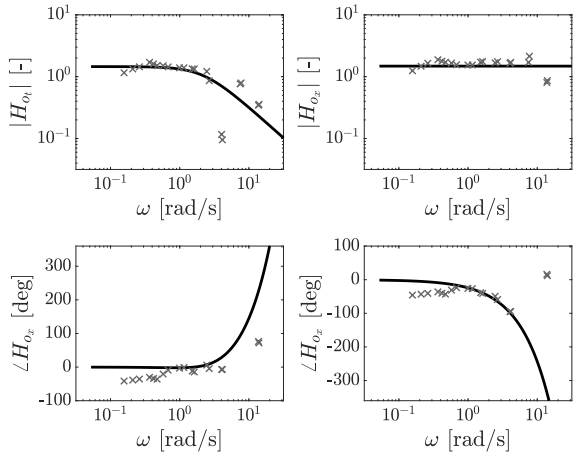

Figure B.5: Bode plots for subject 2

Table B.3: Identified parameters, subject 2

τ_{HO} [s]	K_f [-]	$T_{l,f}$ [s]	K_e [-]	τ_v [s]	VAF [%]
0.81	0.98	0.45	1.48	0.43	96.17

Table B.4: Resulting scores in sample runs, subject 2

	H0	H07	H09
RMS$_e$ [cm]	0.28	0.19	0.19
RMS$_{T,HO}$ [N]	0.23	0.05	0.04
RMS$_{T,HSC}$ [N]	0.15	0.08	0.11
$\bar{O}_{conf}$ [%]	0.88	0.37	0.61
RMS$_\Delta T$ [N]	0.37	0.08	0.13

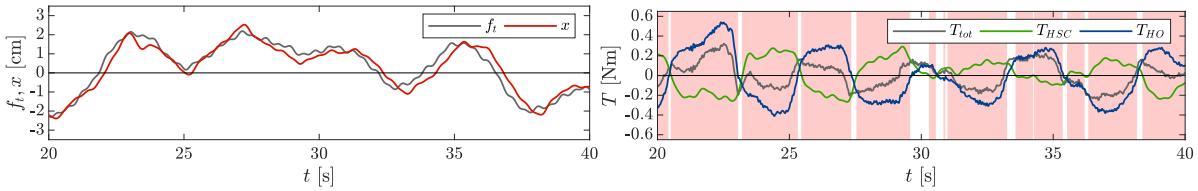

Figure B.6: Time traces for subject 2, condition H0, τ_{HSC} = 0.0 s.

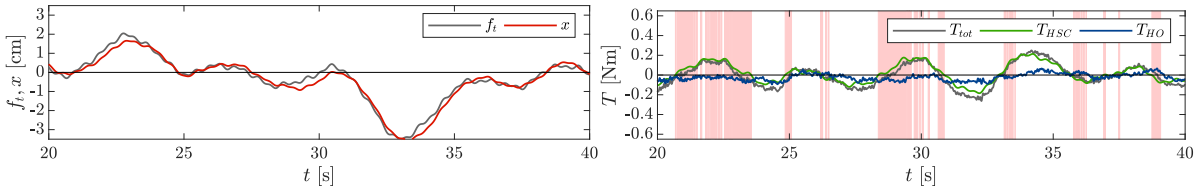

Figure B.7: Time traces for subject 2, condition H07, τ_{HSC} = 0.7 s.

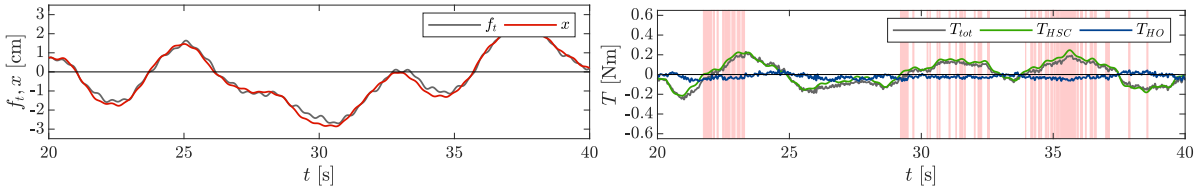

Figure B.8: Time traces for subject 2, condition H09, τ_{HSC} = 0.9 s.

B.3. Subject 3

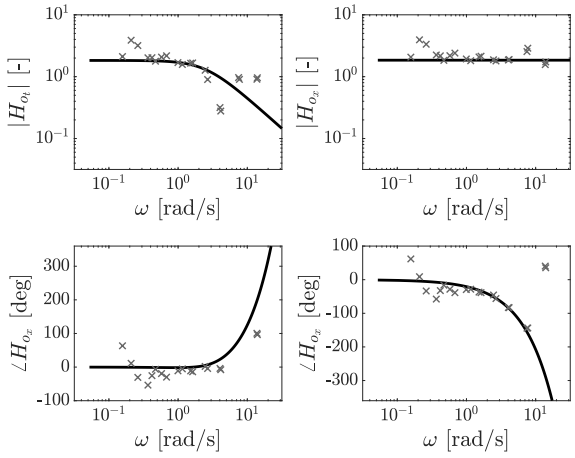

Figure B.9: Bode plots for subject 3

Table B.5: Identified parameters, subject 3

τ_{HO} [s]	K_f [-]	$T_{l,f}$ [s]	K_e [-]	τ_v [s]	VAF [%]
0.71	0.99	0.40	1.85	0.36	94.91

Table B.6: Resulting scores in sample runs, subject 3

	H0	H07	H09
RMS$_e$ [cm]	0.26	0.16	0.18
RMS$_{T,HO}$ [N]	0.25	0.06	0.03
RMS$_{T,HSC}$ [N]	0.16	0.07	0.10
$\bar{O}_{conf}$ [%]	0.86	0.28	0.52
RMS$_\Delta T$ [N]	0.40	0.06	0.11

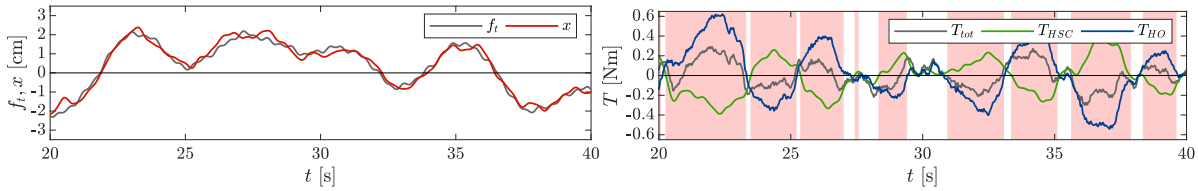

Figure B.10: Time traces for subject 3, condition H0, τ_{HSC} = 0.0 s.

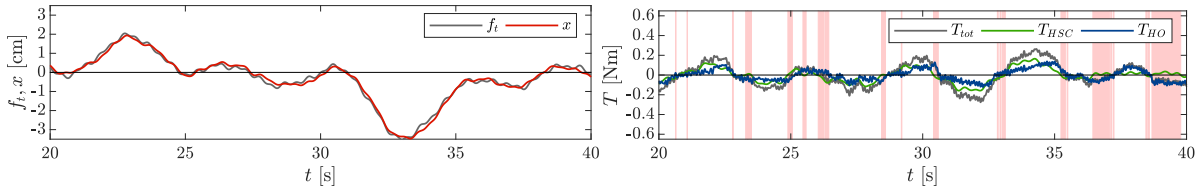

Figure B.11: Time traces for subject 3, condition H07, τ_{HSC} = 0.7 s.

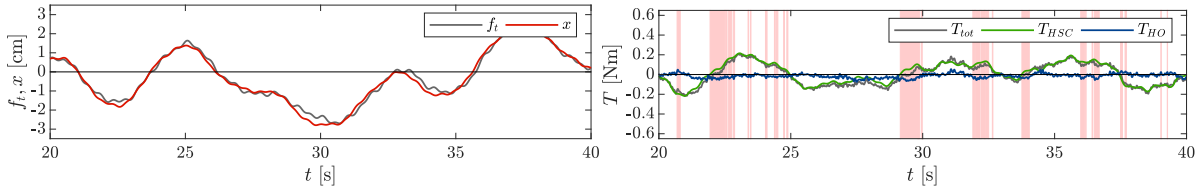

Figure B.12: Time traces for subject 3, condition H09, τ_{HSC} = 0.9 s.

B.4. Subject 4

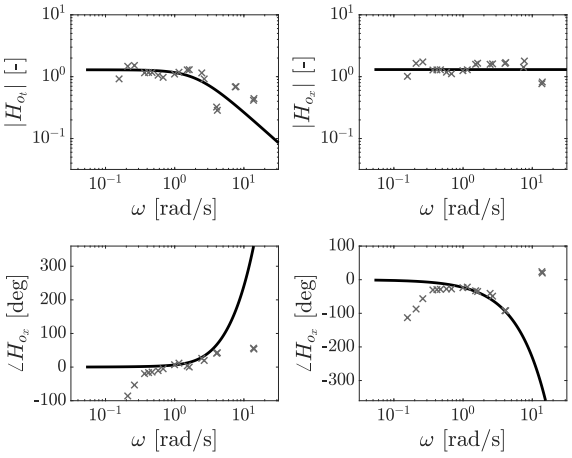

Figure B.13: Bode plots for subject 4

Table B.7: Identified parameters, subject 4

τ_{HO} [s]	K_f [-]	$T_{l,f}$ [s]	K_e [-]	τ_v [s]	VAF [%]
0.96	0.99	0.48	1.30	0.40	96.33

Table B.8: Resulting scores in sample runs, subject 4

	H0	H07	H09
RMS$_e$ [cm]	0.27	0.18	0.22
RMS$_{T,HO}$ [N]	0.25	0.06	0.04
RMS$_{T,HSC}$ [N]	0.17	0.07	0.09
$\bar{O}_{conf}$ [%]	0.87	0.31	0.40
RMS$_\Delta T$ [N]	0.41	0.08	0.08

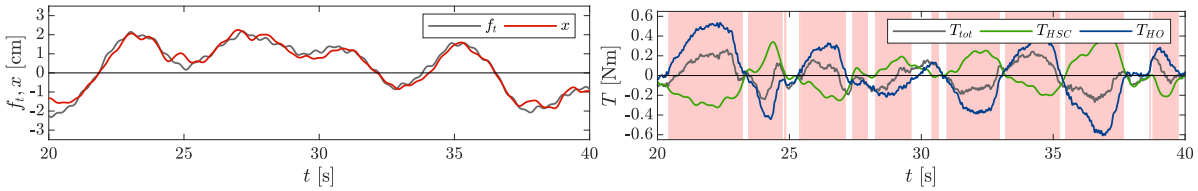

Figure B.14: Time traces for subject 4, condition H0, τ_{HSC} = 0.0 s.

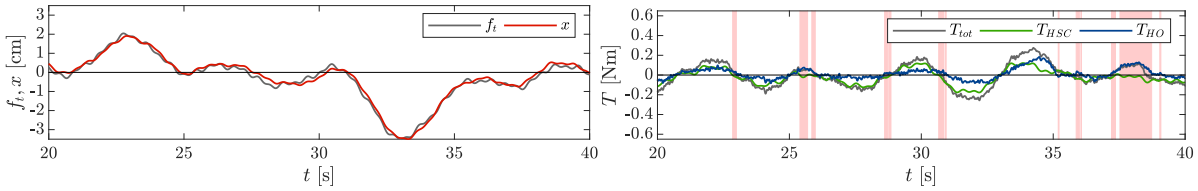

Figure B.15: Time traces for subject 4, condition H07, τ_{HSC} = 0.7 s.

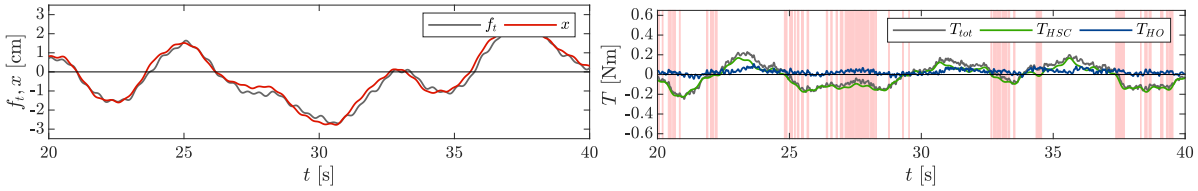

Figure B.16: Time traces for subject 4, condition H09, τ_{HSC} = 0.9 s.

B.5. Subject 5

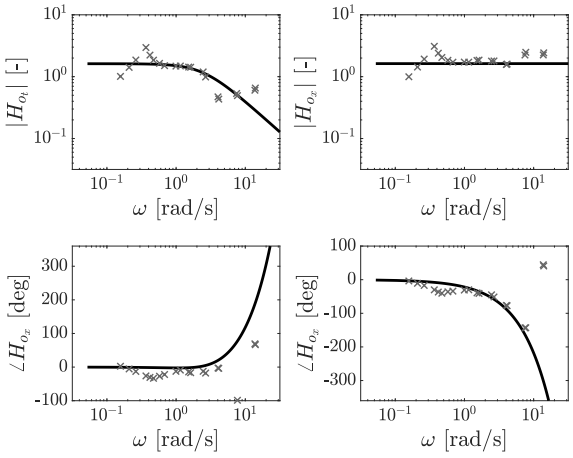

Figure B.17: Bode plots for subject 5

Table B.9: Identified parameters, subject 5

τ_{HO} [s]	K_f [-]	$T_{l,f}$ [s]	K_e [-]	τ_v [s]	VAF [%]
0.72	1.00	0.40	1.62	0.38	95.19

Table B.10: Resulting scores in sample runs, subject 5

	H0	H07	H09
RMS$_e$ [cm]	0.29	0.16	0.17
RMS$_{T,HO}$ [N]	0.21	0.06	0.04
RMS$_{T,HSC}$ [N]	0.13	0.07	0.11
$\bar{O}_{conf}$ [%]	0.86	0.31	0.56
RMS$_\Delta T$ [N]	0.33	0.07	0.12

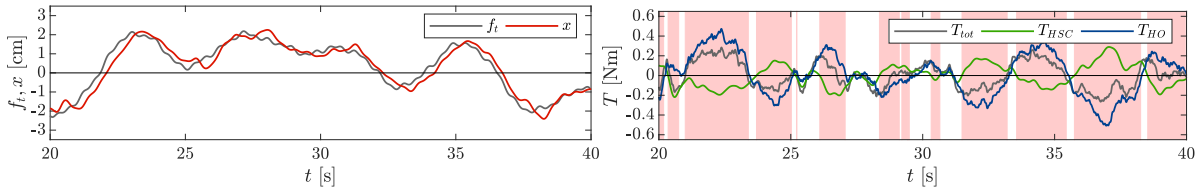

Figure B.18: Time traces for subject 5, condition H0, τ_{HSC} = 0.0 s.

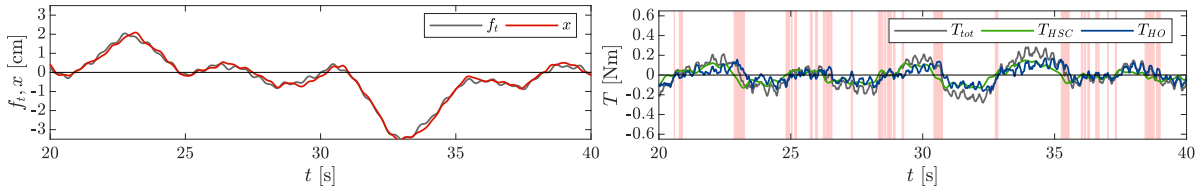

Figure B.19: Time traces for subject 5, condition H07, τ_{HSC} = 0.7 s.

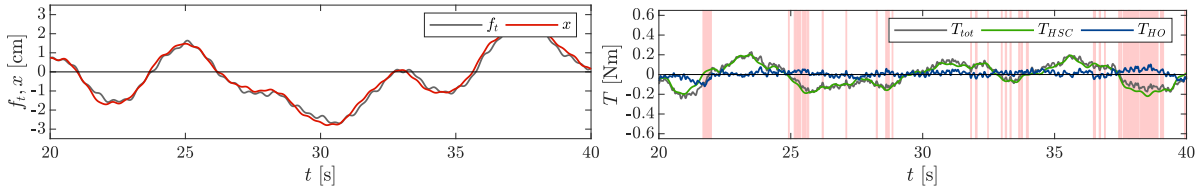

Figure B.20: Time traces for subject 5, condition H09, τ_{HSC} = 0.9 s.

B.6. Subject 6

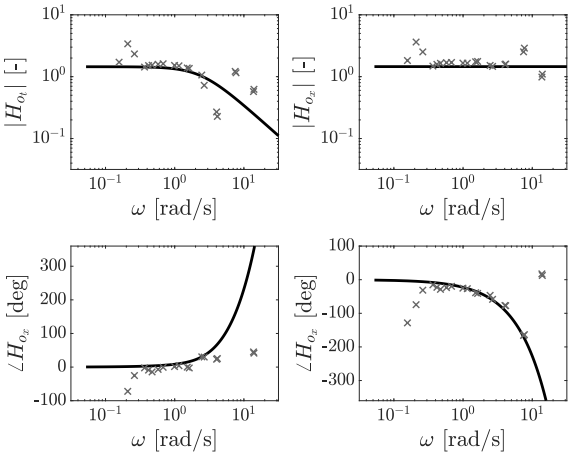

Figure B.21: Bode plots for subject 6

Table B.11: Identified parameters, subject 6

τ_{HO} [s]	K_f [-]	$T_{l,f}$ [s]	K_e [-]	τ_v [s]	VAF [%]
0.93	1.00	0.41	1.45	0.40	95.85

Table B.12: Resulting scores in sample runs, subject 6

	H0	H07	H09
RMS$_e$ [cm]	0.31	0.17	0.21
RMS$_{T,HO}$ [N]	0.21	0.07	0.04
RMS$_{T,HSC}$ [N]	0.13	0.07	0.09
$\bar{O}_{conf}$ [%]	0.84	0.34	0.41
RMS$_\Delta T$ [N]	0.33	0.08	0.09

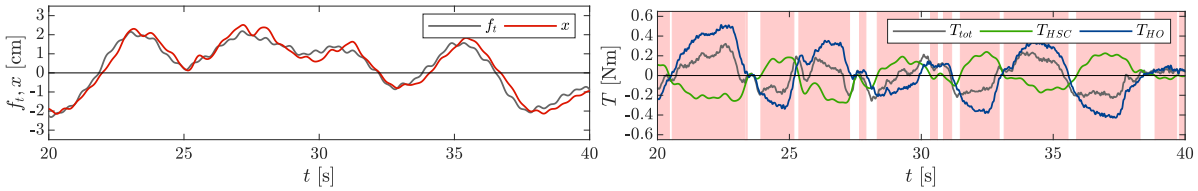

Figure B.22: Time traces for subject 6, condition H0, τ_{HSC} = 0.0 s.

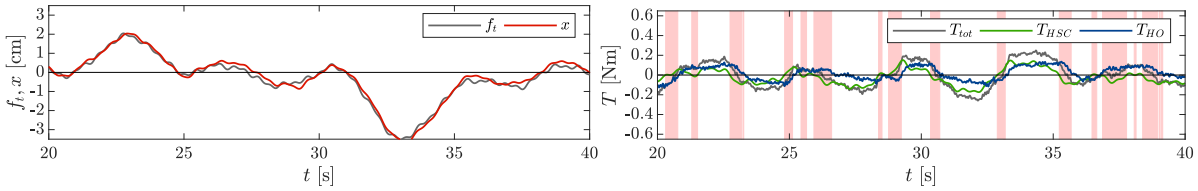

Figure B.23: Time traces for subject 6, condition H07, τ_{HSC} = 0.7 s.

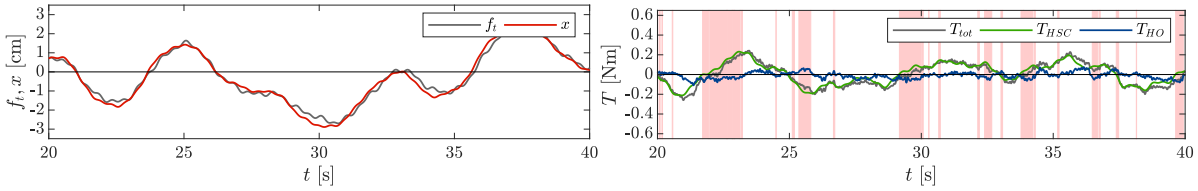

Figure B.24: Time traces for subject 6, condition H09, τ_{HSC} = 0.9 s.

B.7. Subject 7

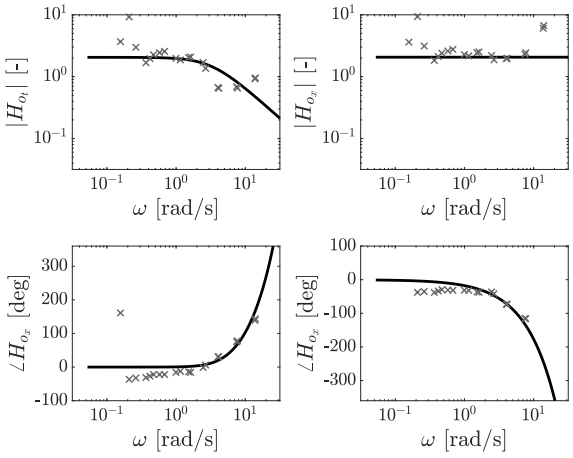

Figure B.25: Bode plots for subject 7

Table B.13: Identified parameters, subject 7

τ_{HO} [s]	K_f [-]	$T_{l,f}$ [s]	K_e [-]	τ_v [s]	VAF [%]
0.61	0.99	0.30	2.06	0.31	92.40

Table B.14: Resulting scores in sample runs, subject 7

	H0	H07	H09
RMS$_e$ [cm]	0.23	0.16	0.20
RMS$_{T,HO}$ [N]	0.26	0.09	0.06
RMS$_{T,HSC}$ [N]	0.16	0.06	0.09
$\bar{O}_{conf}$ [%]	0.84	0.33	0.40
RMS$_\Delta T$ [N]	0.41	0.08	0.09

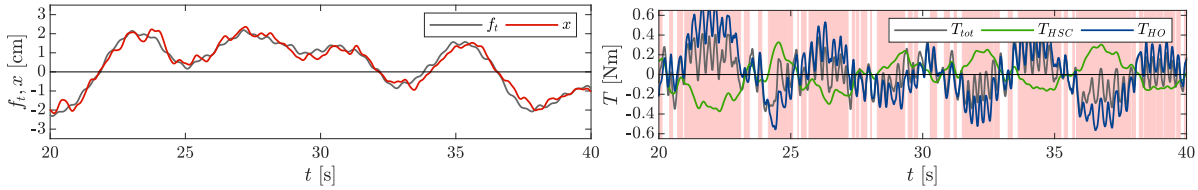

Figure B.26: Time traces for subject 7, condition H0, τ_{HSC} = 0.0 s.

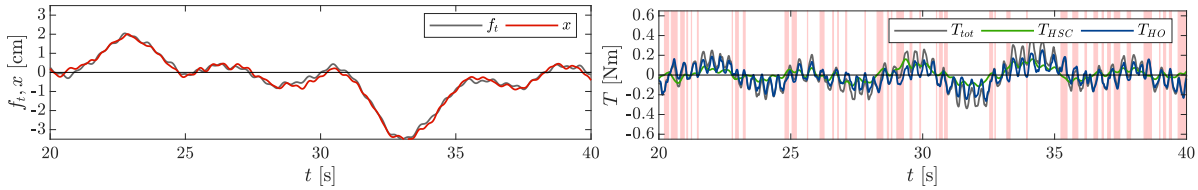

Figure B.27: Time traces for subject 7, condition H07, τ_{HSC} = 0.7 s.

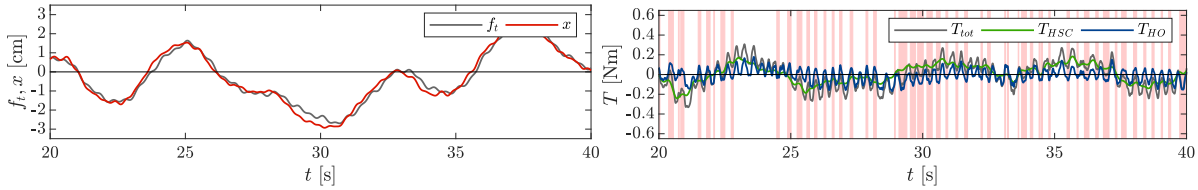

Figure B.28: Time traces for subject 7, condition H09, τ_{HSC} = 0.9 s.

B.8. Subject 8

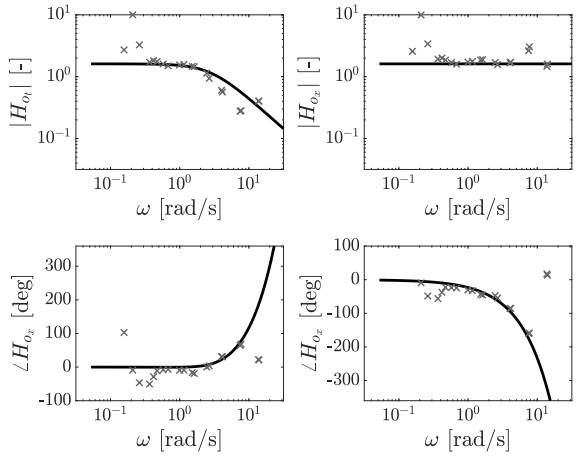

Figure B.29: Bode plots for subject 8

Table B.15: Identified parameters, subject 8

τ_{HO} [s]	K_f [-]	$T_{l,f}$ [s]	K_e [-]	τ_v [s]	VAF [%]
0.74	1.00	0.35	1.61	0.41	95.64

Table B.16: Resulting scores in sample runs, subject 8

	H0	H07	H09
RMS$_e$ [cm]	0.34	0.17	0.21
RMS$_{T,HO}$ [N]	0.22	0.07	0.05
RMS$_{T,HSC}$ [N]	0.13	0.06	0.10
$\bar{O}_{conf}$ [%]	0.84	0.34	0.44
RMS$_\Delta T$ [N]	0.34	0.07	0.10

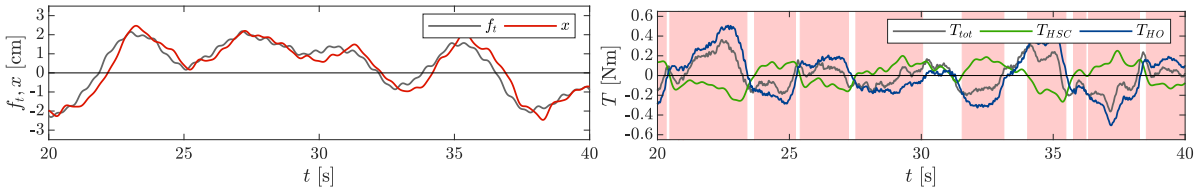

Figure B.30: Time traces for subject 8, condition H0, τ_{HSC} = 0.0 s.

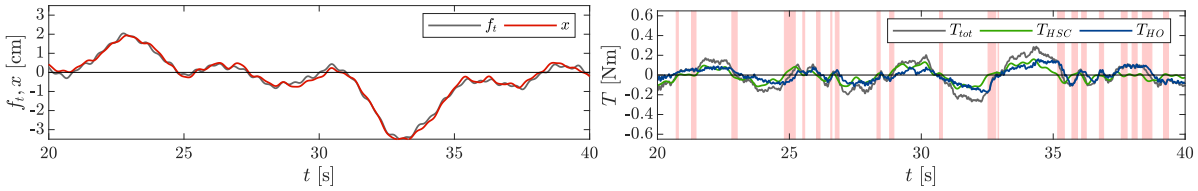

Figure B.31: Time traces for subject 8, condition H07, τ_{HSC} = 0.7 s.

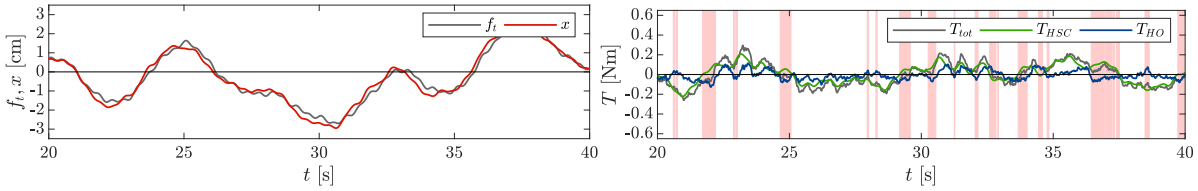

Figure B.32: Time traces for subject 8, condition H09, τ_{HSC} = 0.9 s.

B.9. Subject 9

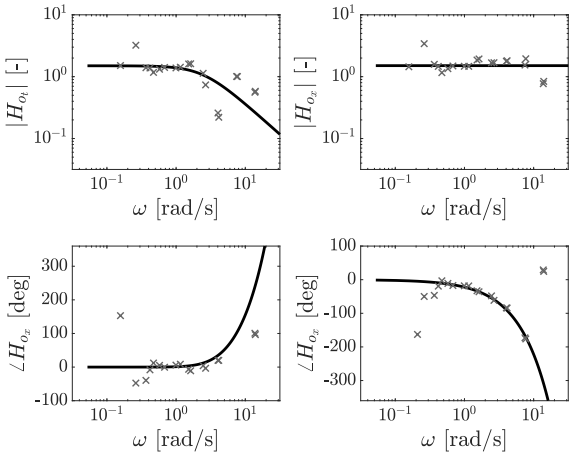

Figure B.33: Bode plots for subject 9

Table B.17: Identified parameters, subject 9

τ_{HO} [s]	K_f [-]	$T_{l,f}$ [s]	K_e [-]	τ_v [s]	VAF [%]
0.79	0.99	0.40	1.51	0.39	96.14

Table B.18: Resulting scores in sample runs, subject 9

	H0	H07	H09
RMS$_e$ [cm]	0.31	0.30	0.23
RMS$_{T,HO}$ [N]	0.23	0.12	0.05
RMS$_{T,HSC}$ [N]	0.15	0.11	0.10
$\bar{O}_{conf}$ [%]	0.87	0.26	0.43
RMS$_\Delta T$ [N]	0.38	0.09	0.10

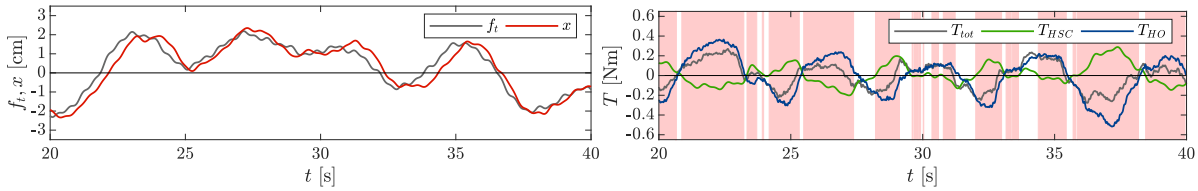

Figure B.34: Time traces for subject 9, condition H0, τ_{HSC} = 0.0 s.

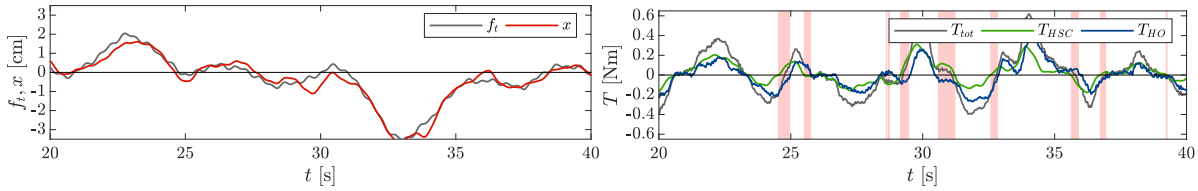

Figure B.35: Time traces for subject 9, condition H07, τ_{HSC} = 0.7 s.

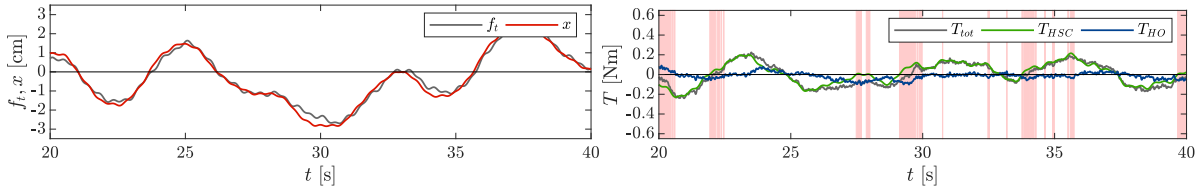

Figure B.36: Time traces for subject 9, condition H09, τ_{HSC} = 0.9 s.

B.10. Subject 10

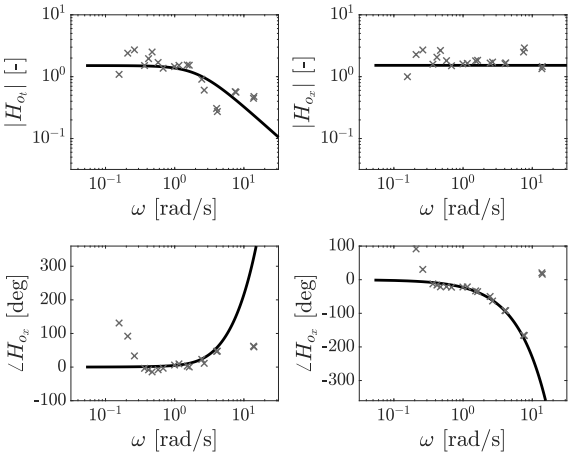

Figure B.37: Bode plots for subject 10

Figure B.38: Identified parameters, subject 10

τ_{HO} [s]	K_f [-]	$T_{l,f}$ [s]	K_e [-]	τ_v [s]	VAF [%]
0.91	0.99	0.45	1.52	0.40	96.17

Figure B.39: Resulting scores in sample runs, subject 10

	H0	H07	H09
RMS_e [cm]	0.26	0.29	0.29
$RMS_{T,HO}$ [N]	0.24	0.12	0.12
$RMS_{T,HSC}$ [N]	0.16	0.10	0.12
$\bar{O}_{conf}$ [%]	0.88	0.30	0.18
$RMS_\Delta T$ [N]	0.39	0.11	0.08

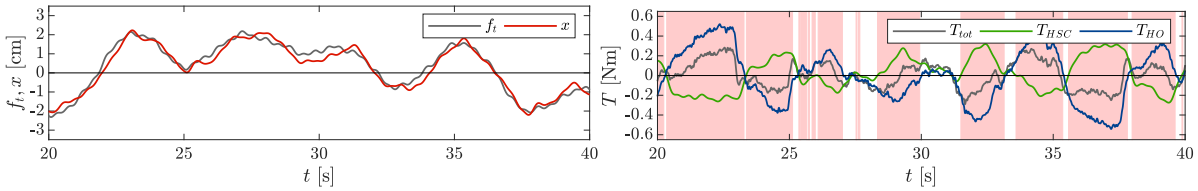

Figure B.40: Time traces for subject 10, condition H0, τ_{HSC} = 0.0 s.

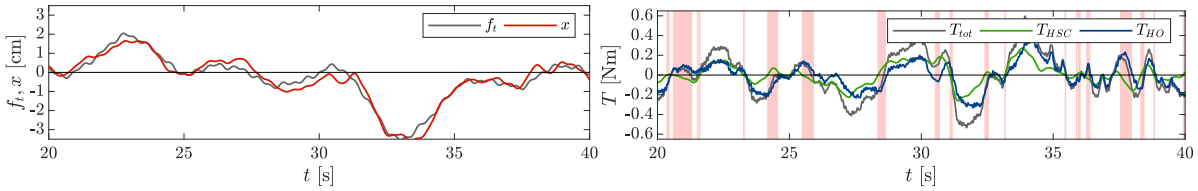

Figure B.41: Time traces for subject 10, condition H07, τ_{HSC} = 0.7 s.

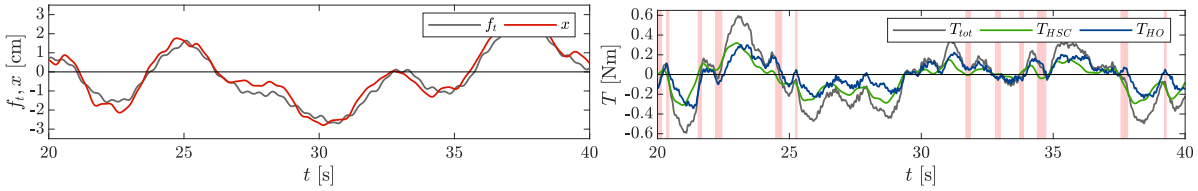

Figure B.42: Time traces for subject 10, condition H09, τ_{HSC} = 0.9 s.

C

Conflict Analysis

This appendix provides additional analysis of the conflict time, with respect to the separate feedforward (Level of Haptic Support) and feedback (Strength of Haptic Feedback) paths of the Four-Design-Choices haptic shared controller.

The occurrence of conflict, O_{conf}, is defined by Equation (C.1). For this analysis, we also consider the conflict with the separate feedforward path and the feedback path. To obtain these, T_{HSC} in Equation (C.1) is replaced by T_{LoHS} and T_{SoHF}, respectively. Here, the threshold c is set to 0 each time, which means that all conflicts are counted.

$$O_{conf} = \begin{cases} 1, & \text{if } T_{HO} \cdot T_{HSC} < 0 \\ & \text{and } |T_{HO}| > c \cdot \max|T_{HSC}| \\ 0, & \text{otherwise} \end{cases} \tag{C.1}$$

Figure C.1 shows the conflict times as a function of the haptic look-ahead time. The relation is convex, with a minimum at τ_{HSC} = 0.7 s. Figure C.1b reveals that the conflict with the SoHF torque follows a similar convex trend. However, the conflict time remains higher around the minimum, around 50% compared to 30% for the total torque conflict minimum.

The plots also show a comparison between the experiment data and the simulations. The separate LoHS and SoHF conflict times are predicted well by the simulations, especially for low look-ahead times. For high look-ahead times, the HO behavior in the experiment was different than predicted, and the conflict times are no longer predicted accurately.

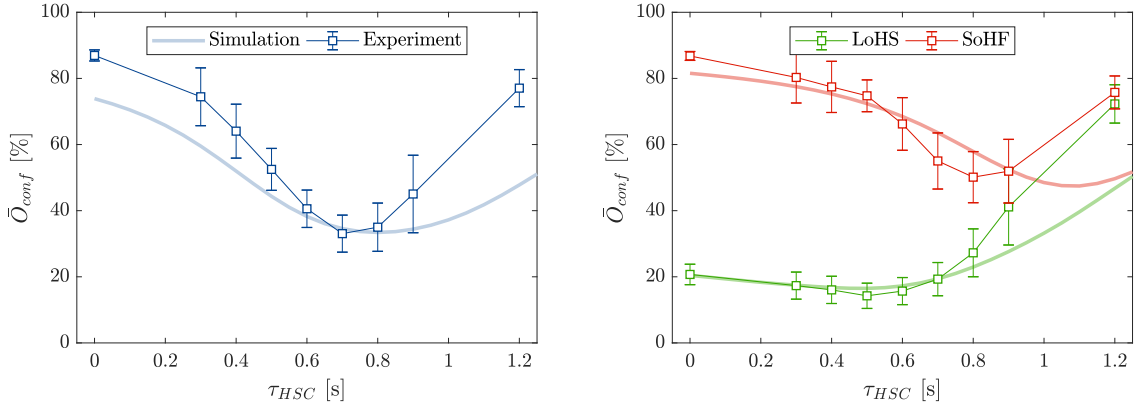

(a) τ_{HSC} vs. conflict time

(b) τ_{HSC} vs. Support/Feedback conflict time

Figure C.1: Three measures of conflict time: with the total torque (left) and with separate haptic support and feedback torques (right)

The conflict with the LoHS torque remains around 20% for haptic look-ahead times from 0 to 0.7 seconds, after which it starts increasing. It appears that for these low look-ahead times, the haptic support path is largely in line with the intentions of the HO. This is confirmed by the sample time trace shown in Appendix C, for τ_{HSC} = 0.7 s, where conflict is low. At the same time, the majority of the haptic torques is provided by the feedback path, as conflict with the SoHF torque is high.

Choosing what conflict time metric to use is not trivial. The separate torque paths of the FDC-HSC allow for separate analysis of conflict. The time traces in Figure C.2 show how each different metric results in entirely different locations of conflict, and different total conflict time. Earlier experiments suggest that conflict with the SoHF path, considered to be a 'correcting' torque, are considered more annoying by the human.

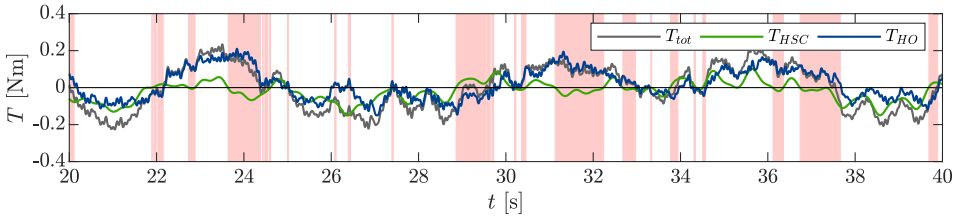

(a) Total haptic torque (T_{HSC})

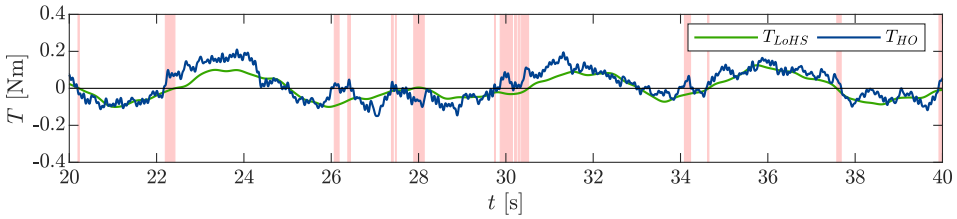

(b) Haptic Support torque (T_{LoHS})

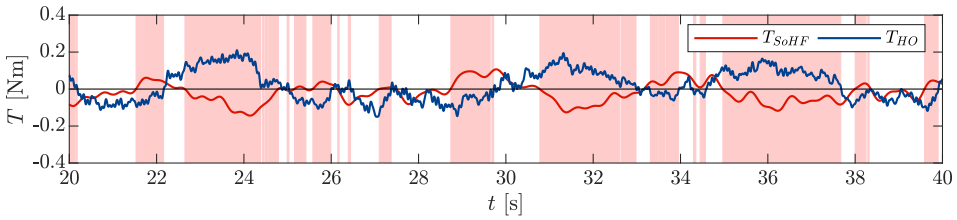

(c) Haptic Feedback torque (T_{SoHF})

Figure C.2: Time traces of the stick torques, subject 1, condition H07, τ_{HSC} = 0.7 s.

D

Experiment Briefing and Consent Form

The next pages include the experiment briefing that was sent to all participants in advance of the experiment, and the experiment consent form that was signed by all participants.

Experiment Briefing

Varying look-ahead times in a human-like haptic shared controller

Thank you for participating in this experiment! The experiment, conducted in the Human-Machine Interaction Laboratory (HMI-Lab), analyses human steering behaviour and task performance. The experiment consists of a tracking task supported by haptic force feedback. This briefing will introduce you to the experiment and what is expected of you as a participant.

Experiment Goal

In *haptic shared control*, a human operator performs a control in cooperation with an automated controller. Interaction between the human and automation is realised through force feedback on the steering wheel or stick. The goal of this experiment is to investigate participants' acceptance of haptic force feedback, and the task performance. To do this, a target tracking task with haptic force feedback is conducted. This target following task is an abstract representation of real-life control tasks such as driving a car on a road, and it allows us to analyse low-level human control behaviour in great detail. The results of the experiment should clarify what haptic settings are desirable or annoying for drivers.

Experiment Task

In this task, you will perform a target tracking task where a previewed portion of the trajectory is displayed on a screen. It is your task to track this line as accurately as possible by moving the side-stick on your right hand-side. During the task, haptic force feedback will be applied to the stick, in order to assist you in the tracking task.

Figure 1: Illustration of HMILab. The experiment will use the right side of the simulator, using the side stick and small display in front.

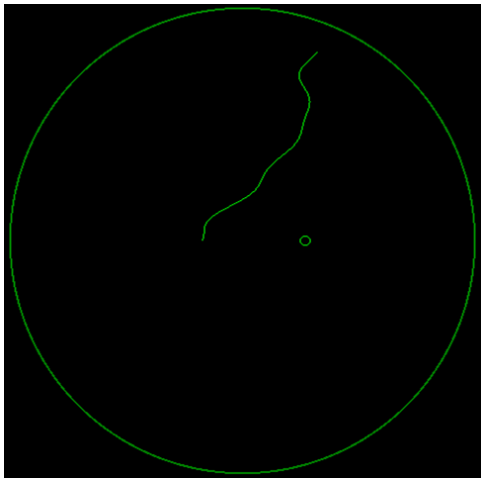

Figure 2: The display used for the experiment. The line is the target to track, the circle is the current position.

Experiment Procedures

Throughout the experiment, several different haptic guidance settings will be presented to you in a random order. You are asked to perform the tracking task to the best of your abilities each time. The researcher will keep track of your performance and will announce when the experiment has been completed. You will start the experiment by doing some practice runs *without* haptic support, to familiarise yourself with the task.

Each tracking run lasts about 120 seconds. For each haptic condition, a number of runs are conducted in direct succession. After each condition, I will ask you to fill in the questionnaire, rating the haptic

support system. Short breaks are taken after each two conditions. Including these breaks, the experiment will last at most 3 hours.

For each run, the subsequent procedure will be followed:

1. The researcher applies the settings for the next run.
2. The researcher checks whether the participant is ready to proceed and initiates the run after a countdown from 3 (3-2-1-go).
3. The participant performs the tracking task.
4. The participant will be notified of their performance in the run in terms of error score after the completed run.

COVID-19 protocol

Due to the ongoing COVID-19 ('coronavirus') pandemic, several measures are taken to reduce the risk of spreading it. First and foremost, researcher and participant will follow the guidelines as indicated on the Dutch government website[1] on the day of the experiment. Related to this experiment, the following four measures are taken:

- Both researcher and participants confirm they do not have symptoms related to COVID-19.
- 1.5 meter distance will be kept between researcher and participant at all times.
- All touched objects in the simulator will be disinfected by the researcher before and after the experiment.
- Before and after the experiment both researcher and participant will wash or disinfect their hands.

This experiment will be performed following the most recent "COVID-19 Protocols for Human Subject Experiments" of the Control and Simulation department.

Your rights

Participation in the experiment is voluntary. This means that you can terminate your cooperation at any time. By participating in the experiment you agree that the collected data may be published. Your data will remain confidential and anonymous, so only the experimenter can link the results to a particular participant. To make sure that you understand and comply with the conditions of the experiment, you will be asked to sign an informed consent form.

Contact information researcher:	Contact information research supervisor
Joeri Span	Dr. ir. Daan Pool
j.e.span-1@student.tudelft.nl	d.m.pool@tudelft.nl
+32 6 27307983	+31 15 2789611

Thank you for participating!

[1] https://www.rijksoverheid.nl/coronavirus

Experiment Consent Form

Varying look-ahead times in a human-like haptic shared controller

I hereby confirm, by ticking each box, that:

1. I volunteer to participate in the experiment conducted by the researcher (**Joeri Span**) under supervision of **Dr.ir. Daan Pool** from the Faculty of Aerospace Engineering of TU Delft. I understand that my participation in this experiment is voluntary and that I may withdraw and discontinue participation at any time, for any reason. ☐
2. I have read the experiment briefing and confirm that I understand the instructions and have had all remaining questions answered to my satisfaction. ☐
3. I understand that my participation involves performing a tracking task in a fixed-based simulator, with different settings of haptic (force) feedback on the control stick. ☐
4. I confirm that the researcher has provided me with detailed safety and operational instructions for the hardware (simulator setup, control-loaded stick, fire escape) used in the experiment. ☐
5. I understand that it is possible that I may develop some feelings of discomfort caused by focussing on the display. If this is the case, I will inform the experimenter. I also understand that the experiment may be discontinued for this reason. ☐
6. I understand that the researcher will not identify me by name in any reports or publications that will result from this experiment, and that my confidentiality as a participant in this study will remain secure. ☐
7. I confirm that the researcher has provided me with detailed safety instructions to ensure my experiment session can be performed in line with current RIVM COVID-19 regulations *at all times* and that these instructions are fully clear to me. ☐
8. I understand that also for my travel to/from the experiment session I should *at all times* adhere to current RIVM COVID-19 regulations. I confirm that I have travelled to TU Delft's Faculty of Aerospace Engineering with either my own car, by bicycle, or on foot. ☐
9. I understand that this research study has been reviewed and approved by the TU Delft Human Research Ethics Committee (HREC). To report any problems regarding my participation in the experiment, I know I can contact the researchers using the contact information below or, if necessary, the TU Delft HREC (hrec@tudelft.nl). ☐

My Signature	Date
My Printed Name	Signature of researcher

Contact information researcher:	Contact information research supervisor
Joeri Span	Dr. ir. Daan M. Pool
j.e.span-1@student.tudelft.nl	d.m.pool@tudelft.nl
+31 6 27307983	+31 15 2789611

E

Van Der Laan Questionnaire

Block 1/5

Condition 1/10

My judgements of the haptic support system are ... (please tick a box on each of the 9 lines)

1	Useful	☐	☐	☐	☐	☐	Useless
2	Pleasant	☐	☐	☐	☐	☐	Unpleasant
3	Bad	☐	☐	☐	☐	☐	Good
4	Nice	☐	☐	☐	☐	☐	Annoying
5	Effective	☐	☐	☐	☐	☐	Superfluous
6	Irritating	☐	☐	☐	☐	☐	Likeable
7	Assisting	☐	☐	☐	☐	☐	Worthless
8	Undesirable	☐	☐	☐	☐	☐	Desirable
9	Raising Alertness	☐	☐	☐	☐	☐	Sleep-inducing

Condition 2/10

My judgements of the haptic support system are ... (please tick a box on each of the 9 lines)

1	Useful	☐	☐	☐	☐	☐	Useless
2	Pleasant	☐	☐	☐	☐	☐	Unpleasant
3	Bad	☐	☐	☐	☐	☐	Good
4	Nice	☐	☐	☐	☐	☐	Annoying
5	Effective	☐	☐	☐	☐	☐	Superfluous
6	Irritating	☐	☐	☐	☐	☐	Likeable
7	Assisting	☐	☐	☐	☐	☐	Worthless
8	Undesirable	☐	☐	☐	☐	☐	Desirable
9	Raising Alertness	☐	☐	☐	☐	☐	Sleep-inducing